Chemistry Models for Major Gas Species Estimation and Tar Prediction in Fluidized Bed Biomass Gasification

by

Rajesh Sridhar

B. Tech., Mechanical Engineering & M. Tech., Product Design
Indian Institute of Technology Madras (2013)

Submitted to the School of Engineering
in partial fulfillment of the requirements of the degree of

Master of Science in Computation for Design and Optimization

at the

MASSACHUSETTS INSTITUTE OF TECHNOLOGY

February 2016

Author..... Signature redacted

School of Engineering

November 19, 2015

Certified by..... Signature redacted .....

Ahmed F. Ghoniem

Professor, Department of Mechanical Engineering

Signature redacted Thesis Supervisor

Accepted by..... .....

Nicolas Hadjiconstantinou

Professor, Department of Mechanical Engineering

Co-Director, Computation for Design and Optimization

Page left intentionally blank

Chemistry Models for Major Gas Species Estimation and Tar Prediction in Fluidized Bed Biomass Gasification

by

Rajesh Sridhar

Submitted to the School of Engineering

On TBD, 2015, in partial fulfillment of the

Requirements for the degree of

Master of Science in Computation for Design and Optimization

Abstract

The present work deals with the process of fluidized bed biomass gasification (FBBG), which is the thermochemical conversion of solid biomass into combustible synthetic gas using a fluidized bed. Fluidized bed gasifiers encounter high tar concentrations at the gasifier outlet necessitating expensive downstream cleaning equipment. Apart from the complex chemical pathways involved, tar production is also strongly dependent on the transport processes occurring inside the gasifier. Hence, the development of a detailed model to predict the variation of tar production under different operating conditions needs to include two important considerations: a comprehensive chemical kinetic sub-model and a detailed hydrodynamic sub-model. However, due to the huge computational expense associated with such a detailed simulation coupling the complex chemistry and hydrodynamics, there is a need to develop simplified models on both fronts. The first part of this work presents a detailed discussion on the chemistry models for biomass gasification: after introducing the existing state-of-the-art reaction mechanisms (both detailed and compact), two new global chemistry models, incorporating a global primary tar cracking reaction, for air-blown gasification and steam-blown gasification conditions are developed. The major gas species and total tar concentrations predicted using the global models in reactor network simulations of the gasifiers are compared with the corresponding predictions obtained using the detailed CRECK mechanism for biomass gasification, as well as with the available experimental observations. On the hydrodynamics front, an improved reactor network model based on the two-phase theory has been developed to better capture the mixing inhomogeneities in the bubbling fluidized bed, including mass transfer considerations between the bubble and emulsion phases. Finally, the predictions of various tar class concentrations and major gas species concentrations, obtained using the improved reactor network model in conjunction with the detailed CRECK kinetic reaction mechanism, for both air-blown gasification and steam gasification, are presented.

Key words: Biomass gasification, Fluidized beds, Chemical reactor network modeling, chemical kinetics, chemistry mechanism reduction, Global chemistry model

Thesis Supervisor: Ahmed F. Ghoniem
Title: Ronald C. Crane (1972) Professor, Department of Mechanical Engineering

Acknowledgements

I would like to express my sincerest gratitude to Prof. Ghoniem for his continued guidance throughout the project work. His experience in guiding students and a clear understanding of the subject matter helped me in the difficult times during the project.

I would like to thank Randall Field (MIT Energy Initiative) for the research feedback and guidance during the course of the project. I am also highly indebted to the other BP-sponsored researchers in the group (Addison, Christos, Richard and Akhilesh) for their insightful discussions. I am much obliged to Katherine for proof-reading the thesis.

I would also like to thank all the other RGD labmates for their support during the last 2 years.

I am very grateful to BP for their financial support to the project.

Table of Contents

List of Figures

List of Tables

Page left intentionally blank

1 Introduction

Over the last few decades, there has been a growing concern over the dangers of greenhouse gas emissions from the widespread use of fossil fuels for generating electricity and producing transportation fuels. In a bid to address this critical problem, there have been several research efforts aimed at developing sustainable energy solutions that could, in the short term, help us reduce our dependency on the fossil fuels and eventually replace them over the next few decades. A recent study by McGlade and Ekins [1] revealed that significant amounts of the existing fossil fuel reserves in the world would have to be left in the ground if we are to meet the target of restricting the average global temperature rise to 2°C above the temperatures that existed during the pre-industrial years.

There have been continued efforts towards developing and commercializing various renewable energy technologies such as solar, wind, biomass and geothermal, that could fuel the ever growing energy demand in the future. Amongst these technologies, biomass is considered a very attractive option because of its versatility in being applicable to both static energy production needs such as electricity generation as well as portable energy needs such as those encountered in transportation. While biomass could be used to produce electricity through the incineration and gasification technologies, biomass pyrolysis and gasification could produce fuel grade drop-in biofuels that could be used for transportation applications. In addition, biomass energy conversion technologies could be used as an efficient means of waste management for processing the disposed agricultural and forestry waste as well as municipal solid waste.

1.1 Introduction to Biomass

Biomass is a general term used to describe any kind of non-fossilized plant-derived material, including animal manure, which is essentially a processed form of plant material [2]. Biomass, in some sense, can be thought of as a natural energy storage system whereby the solar energy incident upon the plant leaves is converted into chemical energy through photosynthesis and stored as chemical bonds in the plant.

Table 1-1: Percentages of fossil fuels (highlighted) that need to be left unutilized to meet the global warming temperature goals (reproduced from McGlade and Ekins [1].

	2 °C with CCS						2 °C without CCS					
	Oil		Gas		Coal		Oil		Gas		Coal	
Country or region	Billions of barrels	%	Trillions of cubic metres	%	Gt	%	Billions of barrels	%	Trillions of cubic metres	%	Gt	%
Africa	23	21%	4.4	33%	28	85%	28	26%	4.4	34%	30	90%
Canada	39	74%	0.3	24%	5.0	75%	40	75%	0.3	24%	5.4	82%
China and India	9	25%	2.9	63%	180	66%	9	25%	2.5	53%	207	77%
FSU	27	18%	31	50%	203	94%	28	19%	36	59%	209	97%
CSA	58	39%	4.8	53%	8	51%	63	42%	5.0	56%	11	73%
Europe	5.0	20%	0.6	11%	65	78%	5.3	21%	0.3	6%	74	89%
Middle East	263	38%	46	61%	3.4	99%	264	38%	47	61%	3.4	99%
OECD Pacific	2.1	37%	2.2	56%	83	93%	2.7	46%	2.0	51%	85	95%
ODA	2.0	9%	2.2	24%	10	34%	2.8	12%	2.1	22%	17	60%
United States of America	2.8	6%	0.3	4%	235	92%	4.6	9%	0.5	6%	245	95%
Global	431	33%	95	49%	819	82%	449	35%	100	52%	887	88%

FSU, the former Soviet Union countries; CSA, Central and South America; ODA, Other developing Asian countries; OECD, the Organisation for Economic Co-operation and Development. A barrel of oil is 0.159 m^3; %, Reserves unburnable before 2050 as a percentage of current reserves.

Various authors classify biomass in different ways. The most commonly used approach, proposed by Demirbas [2], classifies biomass resources as,

1. Wastes, including agricultural wastes, crop residues, urban organic wastes
2. Forest products such as wood and wood residues, barks from forest clearings
3. Energy crops, comprising starch and sugar crops, oilseed crops and grasses
4. Aquatic plants, such as algae and water hyacinth

The desire to extract the stored chemical energy in the biomass and convert it into a form that can be readily used in the existing applications for electricity generation and transportation forms the basis of biomass conversion processes. The conversion processes can be broadly classified into four basic categories: Direct combustion processes, thermochemical processes, biochemical processes and agrochemical processes [2]. For each of these conversion processes, certain types of biomass are more suitable than others. For example, in the case of thermochemical conversion, energy crops and forest products are preferred over aquatic plants and manure as a result of their lower moisture content and hence, proportionally smaller energy requirements for drying.

The energy crops and forest products can be further categorized as [3],

1. Sugar and starchy crops
2. Lignocellulosic biomass
3. Oilseed crops

Sugars and starchy biomass, such as sugarcanes in Brazil and corn in the United States, are used to produce ethanol and are currently the dominant type of biomass to be used in the bio energy industry. Bio-oils, extracted from the oilseed crops, are used in the production of biodiesel and form only a small fraction of the entire bio-energy industry. On the contrary to both the edible sugary crops and oilseeds, Lignocellulosic biomass, such as wood wastes and agro residues, are non-edible and prove to be an ideal biomass feedstock for energy production [4].

Lignocellulosic biomass consists of three major components: cellulose, hemicellulose and lignin. While cellulose is composed of long straight chains of glucose, hemicellulose is made up of tightly bound branches of different polysaccharides such as xylose, mannose and glucose. Lignin, on the other hand, does not have a regular polymeric structure and is made up of three primary phenyl-propanoids that have zero, one or two methoxyl groups attached to the ring respectively.

Depending on the source of the plant, these three phenyl propanoids – p-hydroxyphenyl, guaiacyl and syringol, are present in varying proportions ([3], [5]). A list of the cellulose, hemicellulose and lignin proportions for different biomass feedstock is given in Table 1-2.

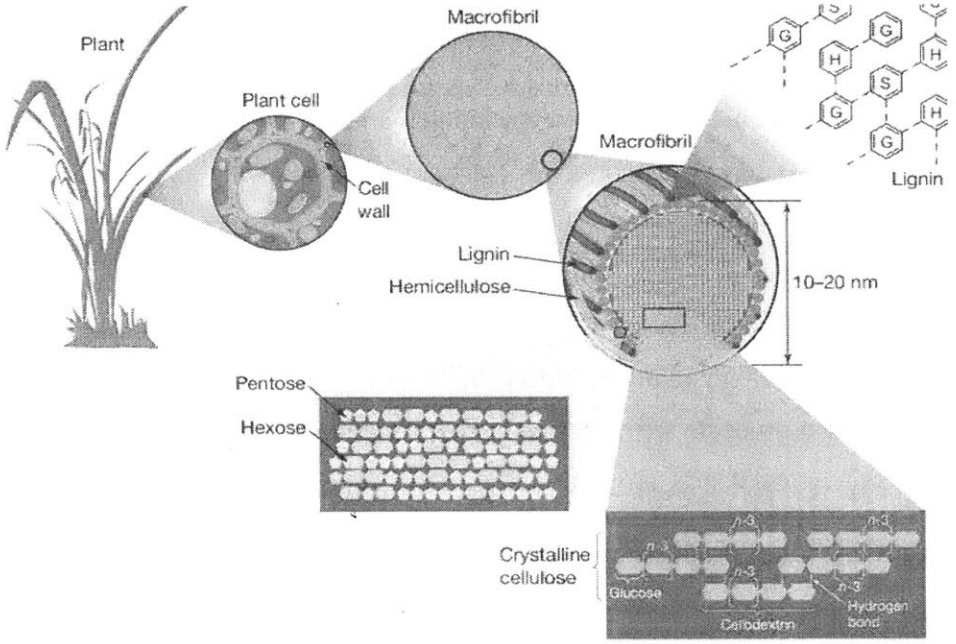

Figure 1-1: Cross-sectional view of a plant cell structure showing the regional distribution of the various biomass constituents: cellulose, hemicellulose and lignin (Source: undbiomass.blogspot.no)

Table 1-2: Compositions of different biomass feedstocks, indicating significant variations in the cellulose, hemicellulose and lignin fractions with the feedstock characteristics [101]

Feedstock	Cellulose (wt%)	Hemicellulose (wt%)	Lignin (wt%)	Ash (wt%)
Reference Pine	39.46	23.92	31.27	0.39
Oak	--	--	--	0.37
Hardwood	--	--	--	0.60
Switchgrass	34.88	27.83	17.32	3.84
Corn Stover	36.34	28.48	16.80	4.30
Tulip Poplar	42.73	22.03	26.72	0.44
Hybrid Poplar	45.31	17.51	25.95	0.69
Pine Blend	39.44	20.65	31.93	0.48
Blend 1	38.95	23.49	25.38	1.56
Blend 2	41.42	19.61	29.92	0.56

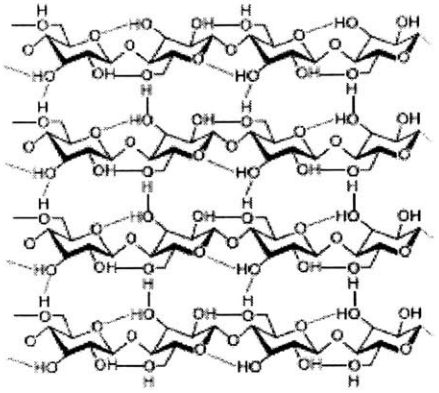

Cellulose

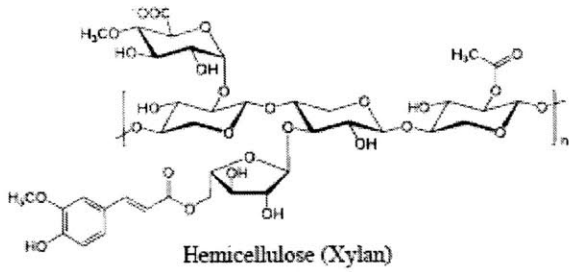

Hemicellulose (Xylan)

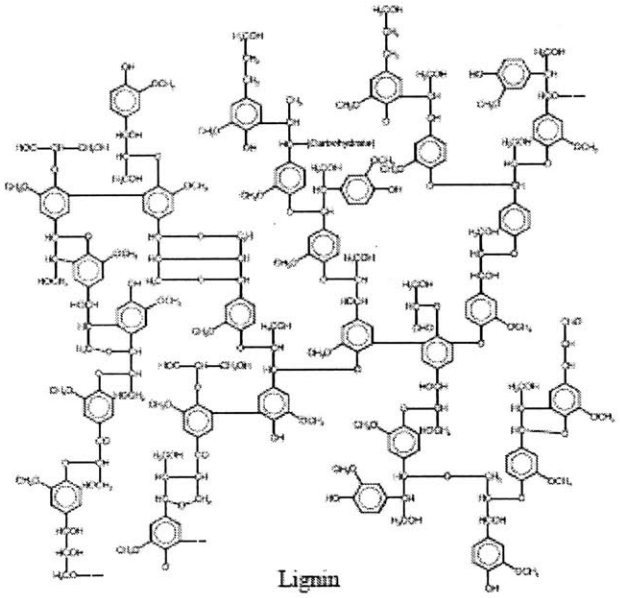

Lignin

Figure 1-2: Chemical structures of the three primary building blocks of Lignocellulosic Biomass – Cellulose, Hemicellulose and Lignin [3]

1.2 Biomass Gasification

As mentioned previously, biomass conversion processes deal with breaking down the chemical bonds in the biomass to form more stable products. Biomass conversion processes can be broadly classified as,

1. Biochemical processes such as fermentation and biological digestion,
2. Thermochemical processes such as pyrolysis, liquefaction and gasification

Biochemical processes aim to break down the biomass feedstock using microbes such as yeast and bacteria (both in the presence of oxygen or an inert atmosphere) and are typically used in the applications of high moisture biomass feedstock. However, they have large freshwater requirements and also suffer from severe scaling limitations. On the other hand, thermochemical conversion uses heat and chemical processes to obtain useful energy from the biomass feedstock. While the thermochemical processes of pyrolysis and liquefaction deal with converting the solid biomass into liquid products, gasification is used to produce high heating value gases, starting from the same biomass feedstock. In the case of direct combustion processes, biomass combustion is used to generate heat that could be used in a steam cycle to generate electricity. When the biomass feedstock is combusted, the chemical bonds (between carbon, hydrogen and oxygen molecules) in the biomass are broken down and new stable bonds formed, releasing chemical energy as heat. The present work considers the thermochemical conversion process of biomass gasification.

Biomass Gasification is the process of converting a solid biomass feedstock into a mixture of gases, with a high heating value, in a partially oxidized atmosphere at moderately high temperatures (usually > 500 °C). The product gas, rich in CO and H_2, could then be used to generate electricity using a gas turbine, or it could also serve as the starting base for the production of fertilizers and other chemicals used in the processing industries. Gasification is a multi-stage process: the solid biomass first undergoes devolatilization to release the volatile gases and also produces some residual char. These devolatilization products then undergo further secondary gas phase reactions in the presence of the gasifying agent to produce a final gas mixture that is rich in CO and H_2. Depending on the operating conditions, the char produced in the initial devolatilization process might react with the gases to produce CO, CO_2 and H_2, or gets elutriated out of the gasifier.

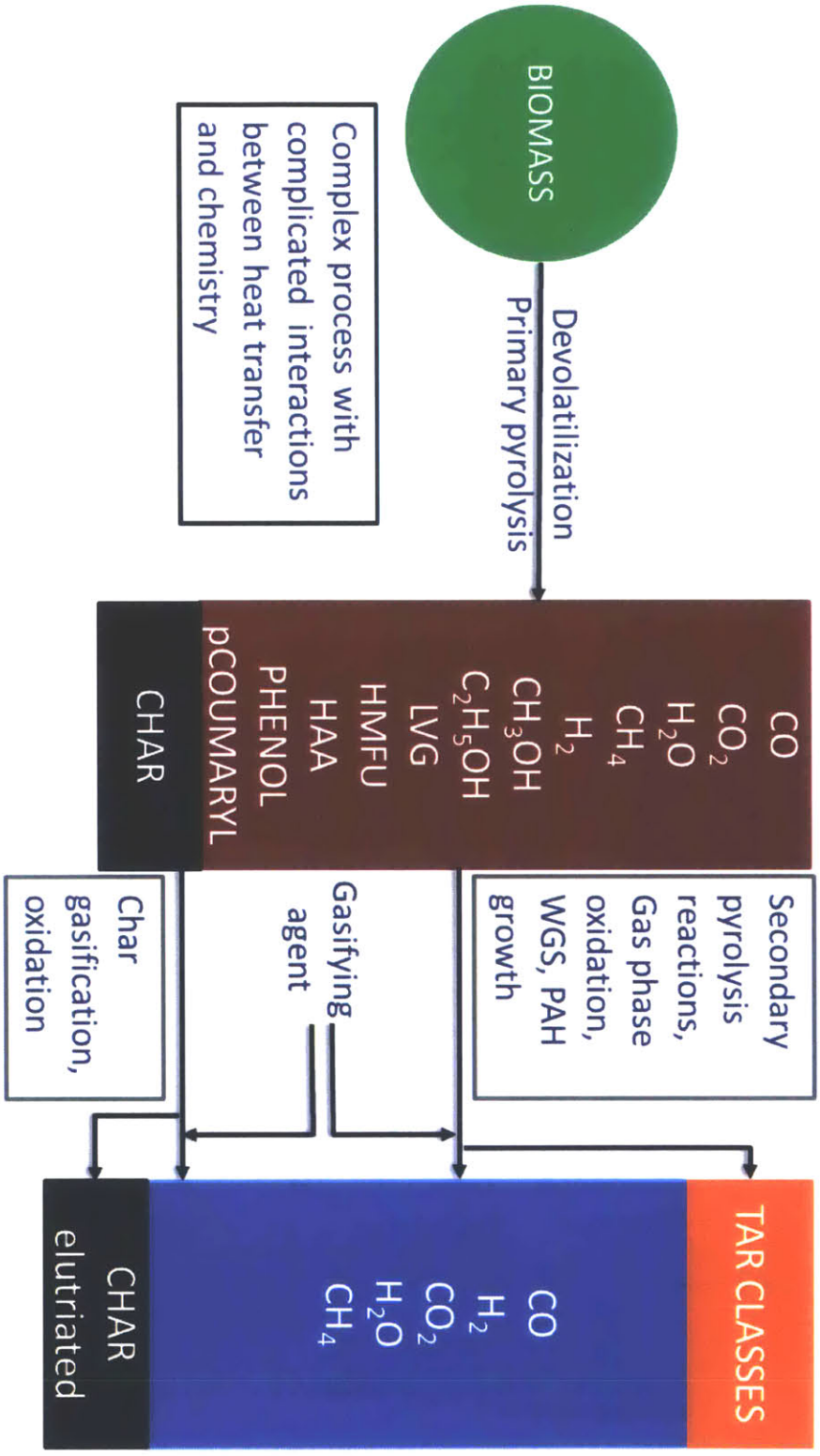

Figure 1-3: Overview of the Biomass Gasification process, describing the different sub-processes determining the end product composition

The most commonly found biomass gasifiers fall within the following categories,

1. Fixed bed gasifiers – Updraft and downdraft configurations
2. Fluidized bed gasifiers – Circulating and Bubbling Fluidized beds
3. Entrained Flow gasifiers

Fixed bed gasifiers have distinct temperature regions where the different sub-processes of gasification such as drying, pyrolysis and combustion take place. Fluidized bed gasifiers typically use an inert bed material that is fluidized by the gasifying agent and have better mixing and heat transfer characteristics. Entrained flow gasifiers operate at high temperatures and require small biomass particle sizes, hence achieving lower tar content in the output synthetic gas.

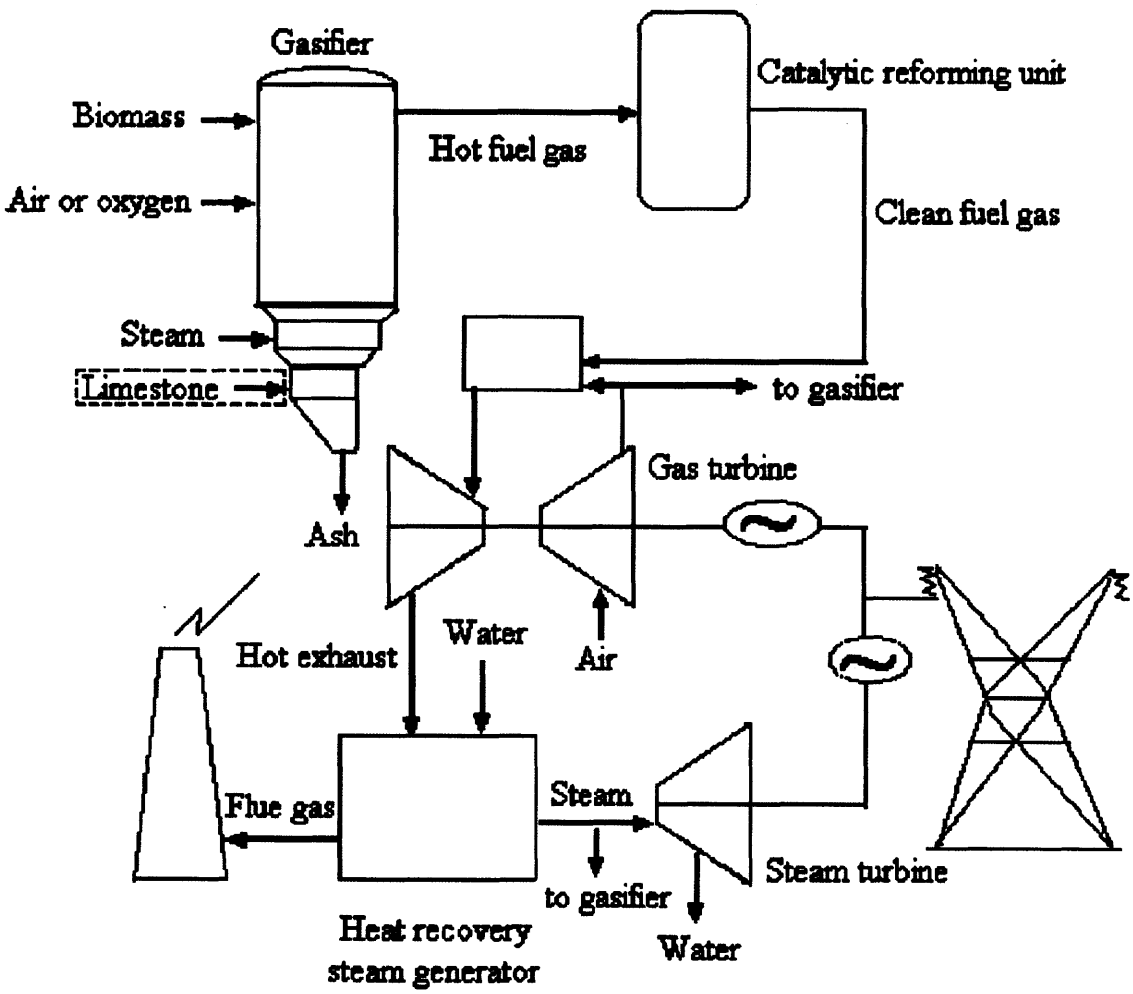

Figure 1-4: Schematic of an industrial Biomass gasifier for electricity generation (reproduced from [6]). Synthetic gas generated from the biomass gasifier is fed to a combined cycle power plant to produce electricity

Fluidized bed gasifiers have a number of significant advantages over fixed beds and entrained flow gasifiers for the application of biomass gasification. Since fluidized beds have good mixing and heat transfer characteristics, they do not suffer from any scaling limitations unlike fixed beds. In addition, fluidized bed gasifiers do not have the requirement of finely ground feedstock for operation, as in the case of entrained flow gasifiers. On the contrary to coal, grinding biomass to very fine sizes is difficult and hence, very expensive. However, due to the low operating temperatures and short residence times, fluidized beds encounter significant amounts of tar compounds at the outlet that necessitate expensive downstream cleaning equipment.

Table 1-3: Comparison of the advantages and disadvantages of different biomass gasifier configurations

Gasifier	Advantages	Disadvantages
Fixed – Updraft	High carbon conversion and High Thermal efficiency	Large amounts of tar, small feedstock size
Fixed - Downdraft	Lower Tar production	Limited scale-up, not fuel flexible
Fluidized Bed	Flexible composition, uniform temperature	Significant amounts of tar at the outlet
Entrained Flow	Low amounts of tar, flexible feedstock	Feedstock needs to be ground

1.3 Introduction to Tars and Tar classification

While there is no standard definition for the term "tars" in the literature, tars are generally considered to be the condensable high molecular weight hydrocarbons (including oxygenated compounds) with generally one or more aromatic rings, such as benzene and naphthalene. A detailed discussion on the different operational definitions used for tar was presented by Milne [6]. Apart from their refractory nature and hence, the resultant difficulty in removing them, tars also have low condensation temperatures and tend to condense along the gas pipelines clogging them. To prevent this, sophisticated gas cleanup systems to crack the tar at high temperatures using

expensive catalysts need to be retrofitted to the gasifier. Additionally, some of the tar compounds are highly soluble in water, necessitating expensive wastewater treatment and disposal systems downstream to handle the toxic wastewater.

The serious problems associated with having even small amounts of "tar" in the gasifier outlet synthetic gas was best summarized by Tom Reed [6],

"While a great deal of time and money has been spent on biomass gasification in the last two decades, there are very few truly commercial gasifiers, operating without government support or subsidies, day in, day out, generating useful gas from biomass. The typical project starts with new ideas, announcements at meetings, construction of the new gasifier. Then it is found that the gas contains 0.1-10% 'tars.' The rest of the time and money is spent trying to solve this problem. Most of the gasifier projects then quietly disappear. In some cases the cost of cleaning up the experimental site exceeds the cost of the project! Thus 'tars' can be considered the Achilles heel of biomass gasification. (In the gasification of coal, a more mature technology, the 'tars' (benzene, toluene, xylene, coal tar) are useful fuels and chemicals. The oxygenated 'tars' from biomass have only minor use. With current environmental and health concerns, we can no longer afford to relegate 'tars' to the nearest dump or stream"

Based on their water solubility characteristics and condensation temperatures, tars had been classified into five different classes [7]. The list of the characteristic properties that differentiate these different tar classes as well as some of the representative chemical species belonging to each of the classes is listed in Table 1-4.

Table 1-4: Tar classification: Characteristic properties of the various tar classes and representative compounds belonging to each of them

Tar Class	Class Name	Characteristic Properties	Example compounds
1	GC undetectable	Undetectable by GC, very heavy compounds	N/A
2	Heterocyclic aromatics	Highly water soluble compounds with hetero atoms	Phenol, Cresol, Naphthol, Syringol, pCoumaryl
3	Light aromatics (1-ring)	Not as soluble in water as class 2 tars and do not condense easily unlike other tars	Benzene, Toluene, Xylene, Styrene
4	Light PAHs (2-3 rings)	Condense at low temperatures at low concentrations	Naphthalene, Phenanthrene, Biphenyl, Anthracene
5	Heavy PAHs (4-7 rings)	Condense at high temperatures even at low concentrations	Pyrene, Corannulene and isomers

1.4 Thesis goals

The main focus of this work has been to develop simplified models that could be used to predict the variation of tar production as well as the major gas species concentrations in biomass gasification under different operating conditions. Apart from the complex chemical reaction pathways involved, the total tar production at the gasifier outlet is also strongly dependent on the transport processes occurring inside a gasifier. However, the simulation of a detailed gasification model that couples the complex fluid hydrodynamics inside a fluidized bed gasifier with the

complicated chemical reaction pathways, inherent to biomass conversion, is computational very expensive and simplifications both in the chemistry sub-model as well as the hydrodynamic sub-model need to be considered.

The early part of this work introduces the different chemical reaction mechanisms for biomass gasification: after a detailed discussion on the existing mechanisms available, various mechanism reduction strategies to develop compact reaction mechanisms are presented. With the aim to be used in the computational fluid dynamic (CFD) simulations of biomass gasification in the future, two separate global chemistry models, incorporating a global primary tar cracking reaction based on an existing CFD chemistry model [3], for air-blown and steam-blown gasification conditions, are proposed. A global primary tar cracking reaction is developed by studying the decomposition product composition of the most abundant primary tars, produced in the devolatilization process.

On the fluid hydrodynamics front, an improved reactor network model for Fluidized Bed Biomass Gasification is developed, based on the two-phase theory of fluidization. Starting with the original reactor network model (RNM) considered in [8], the improved model uses a combination of reactors to model the fluid hydrodynamics in the bubbling bed, including mass transfer considerations to improve the model predictions for the different tar class concentrations. The detailed chemical kinetic mechanism developed by the Chemical Reaction Engineering and Chemical Kinetics (CRECK) group at Politecnico di Milano for pyrolysis, oxidation and combustion of biomass is employed [9], for both air-blown and steam-blown gasification conditions.

1.5 Thesis Outline

The second chapter gives a comprehensive overview of the different chemistry models for biomass pyrolysis, gasification and combustion. Starting from global models used in the earlier studies on the topic, we introduce detailed chemistry mechanisms and discuss about the advantages and limitations of these detailed mechanisms.

In chapter 3, details on the development of the global chemistry models for air-blown and steam-blown gasification conditions are presented, with emphasis on the global primary tar cracking reaction development. Finally, the accuracy of the global model predictions are studied in comparison with experimental results.

Chapter 4 deals with the development of an improved chemical reactor network model for FBBG based on the two-phase theory. After a brief overview of the existing literature in the subject, we discuss the methodology and the associated correlations used in the present study. The predictions from the improved RNM are then compared with experimental results.

The final recommendations and conclusions are presented in the last chapter.

2 Biomass Chemistry Models

An accurate simulation of the biomass gasification process requires an appropriately detailed chemistry model to capture the various chemical processes inside the gasifier. These complex chemical processes include biomass devolatilization, describing the conversion of solid biomass into char, gas and primary tars, secondary homogenous reactions of the primary pyrolysis gases, gasification of the char produced during primary pyrolysis and evolution of the various tar compounds, comprising primary tar cracking reactions and secondary tar growth, inside the gasifier [10]. It is essential that the gasification model describes the pyrolysis step in sufficient detail, since gasification always has to go through the pyrolytic stage [11]. In addition to these complex reactions, gasification is also significantly affected by the process conditions such as biomass feedstock heating rate, mixing inhomogeneities inside the gasifier and char residence times in the reactor.

The main chemical processes in biomass gasification are,

1) Primary Pyrolysis or Devolatilization
2) Secondary Homogenous reactions
3) Char gasification and combustion
4) Tar cracking and PAH growth

In literature, most biomass gasification models used simplified chemistry models to describe these chemical processes. Devolatilization was typically assumed to be instantaneous and the product composition at the end of devolatilization was used as the starting condition for modeling further chemical processes in the bed. While heterogeneous char reactions were not considered in many studies, models that included char gasification used char reactivities obtained for coal or from TGA experiments operated at low heating rates. Additionally, the change in char reactivity during conversion was not considered. Tars were usually modeled as one or two lumped species undergoing oxidation, thermal cracking and steam reforming with the corresponding kinetic parameters evaluated empirically through experiments. The effect of in-bed catalysts on the kinetics of the various reactions had also been modeled using ad-hoc correction parameters that restricted their applicability [12].

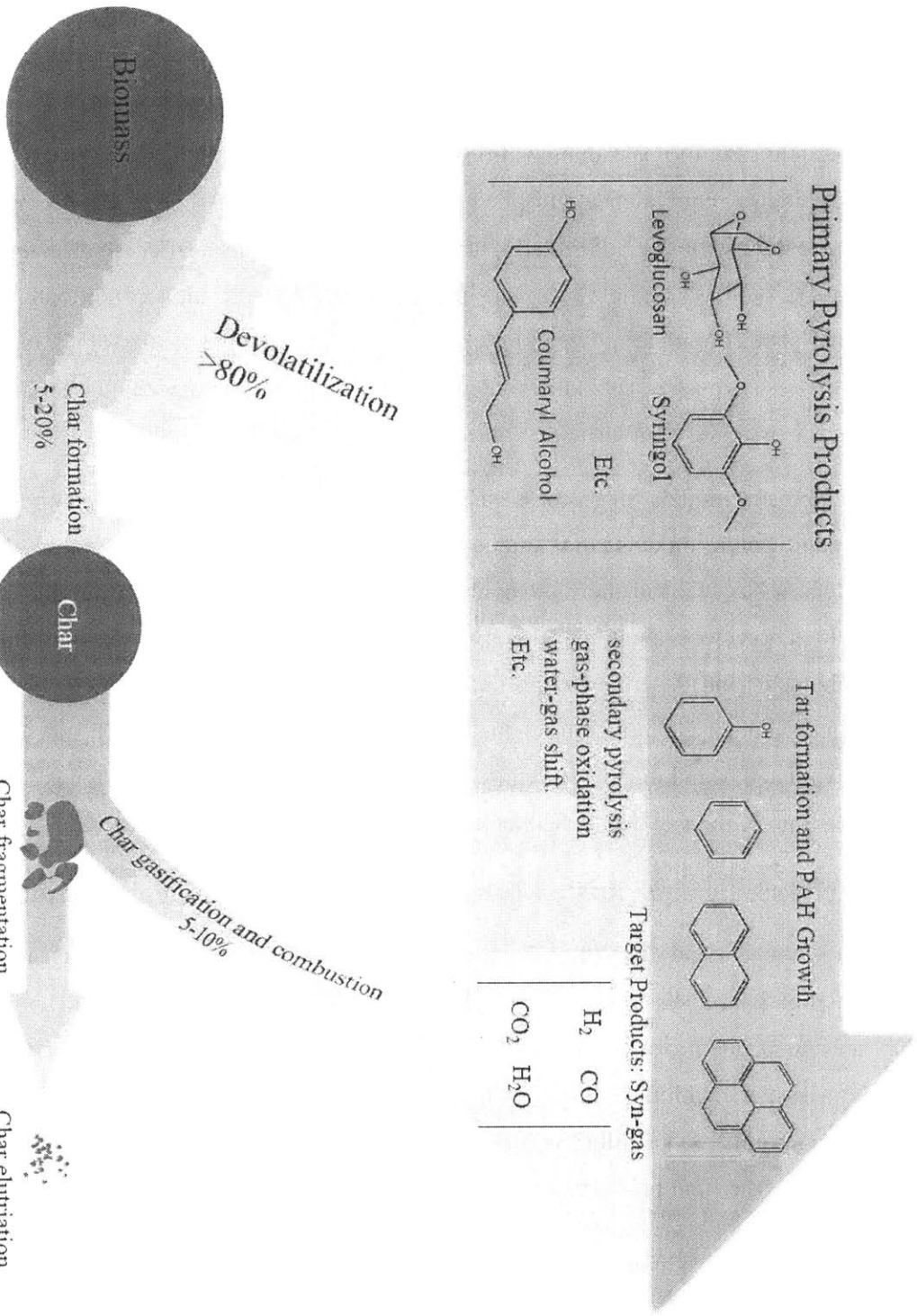

Figure 2-1: Overview of the biomass devolatilization process [3]. More than 80% of the solid biomass is converted to volatiles and gases, while the remaining fraction produces char

Each of these sub-processes are greatly influenced by the process conditions, and hence, both the final tar concentration and synthetic gas composition at the outlet of the gasifier are sensitive to the operating conditions. While the pyrolysis product composition depends on biomass particle heating rate, particle size, biomass composition, ash and moisture content, secondary gas phase reactions are affected by equivalence ratio, bed material, gas residence time and the temperature distribution inside the gasifier [13]. Similarly, tar concentrations in the gasifier are affected by the biomass feedstock, biomass particle size and heating rate and fluidization conditions. A good chemistry model should be able to accurately predict and quantify the effects of these various operating parameters such as the moisture content, air fuel ratio, reactor temperature and pressure on the output gas composition and heating value of the output synthetic gas [10].

The different chemistry models for biomass gasification available in the literature can be broadly classified as equilibrium models and kinetic models. Equilibrium models assume that the gasification process has reached thermodynamic equilibrium during the operation and employ equilibrium calculations to evaluate the final product composition. Kinetic models, on the other hand, are mechanistic and describe the gasification process through a set of chemical species interacting with each other via numerous chemical reactions. The evolution of each species inside the gasifier is evaluated from kinetic rate expressions and the end product composition is a function of the residence time of the gas inside the gasifier.

2.1 Thermodynamic equilibrium-based models for biomass gasification

Several researchers had developed thermodynamic equilibrium based chemistry models to describe the gasification process ([13]-[21]). The main advantage with the equilibrium approaches is that they are independent of the gasifier design and hence, are very suitable for system level studies of biomass gasification. Unlike kinetic models, equilibrium models have much lower computational requirements. Equilibrium approaches assume that the equilibrium state has been reached and evaluate the final product composition through minimization of Gibbs free energy of the system.

Equilibrium approaches can be classified as stoichiometric ([14], [15]) or nonstoichiometric ([16], [17]), depending on the presence of a definite reaction mechanism governing the interactions between the species. Nonstoichiometric approaches dealt with minimization of the Gibbs free energy based on the input elemental composition of the feed without considering the reaction steps. On the other hand, stoichiometric approaches defined equilibrium constants for reactions by

selecting the most energetically favorable species having the lowest free energy of formation and hence, present in large quantities in the reaction mixture. However, the stoichiometric and non-stoichiometric approaches had been shown to be essentially equivalent by Jarungthammachote et al. [15]. A third quasi-equilibrium temperature (QET) approach had also been proposed ([18], [19]). QET approaches corrected for the non-equilibrium operating regime of gasifiers by evaluating the equilibrium composition of the gasifier at a lower process temperature than the actual one.

Equilibrium models employed a number of simplistic assumptions to describe the complex gasification process [20]. While heat losses in the gasifier were neglected in most studies, perfect mixing conditions and uniform temperature distribution inside the gasifier were also assumed. Additionally, gas residence times were considered to be long enough and the reaction rates fast enough for the mixture to reach equilibrium. These assumptions were found to be more suitable for certain gasifier configurations than others. Villanuvea et al. [21] had shown that the equilibrium approaches were better suited for entrained flow gasifiers and downdraft fixed-bed gasifiers with high operating temperatures and long residence times. On the other hand, the equilibrium approaches were found to result in significant errors for updraft fixed bed and fluidized bed gasifiers. Equilibrium models for fluidized bed gasifiers predicted significantly higher hydrogen and CO, while they also under-predicted methane, CO2 and tars ([21], [22]).

In conclusion, it can be said that even though the equilibrium approaches are not accurate for modeling the chemical processes inside fluidized bed gasifiers since these gasifiers do not reach thermodynamic equilibrium during their operation due to the relatively low operating temperatures and short residence times ([10], [23], [23][24][14], [15]). Additionally, equilibrium models do not provide any information on the intermediate species concentrations or the various reaction pathways, since they evaluate only the steady state composition. However, some authors had achieved reasonable agreement between equilibrium predictions for the major gas composition and experimentally measured values ([14], [19], [24]–[26]). It should also be noted that equilibrium approaches provide a general idea of the thermodynamic bounds or limits for the different species concentrations in the gasifier.

A more detailed review of the different equilibrium models used for biomass gasification applications could be found in the review publications by Puig-Arnavat [10], Gomez-Barea [23] and Baruah [27].

2.2 Kinetic Models for Biomass Gasification

While equilibrium approaches produced reasonably accurate results for downdraft gasifiers that operate close to equilibrium conditions, they yielded significantly erroneous predictions for fluidized bed gasifiers. Stark et al.[3] compared the equilibrium concentrations of the major gas species and tars for an air-blown fluidized bed gasifier with the experimentally measured values. Equilibrium calculated predicted that methane was entirely consumed by the outlet of the gasifier and the presence of heavy tar compounds was also found to be negligible in the synthetic gas. However, experiments observed significant concentrations of both methane and tars at the gasifier outlet. In addition, the equilibrium approaches under-estimated the CO_2 concentrations and over-predicted the H_2 and CO yields. In order to address the significant errors associated with the equilibrium approaches, detailed kinetic models had been employed to describe biomass gasification. This section presents a brief overview of the various kinetic models employed in literature for biomass gasification.

Unlike equilibrium approaches, Kinetic models described the biomass gasification process mechanistically using a set of relevant chemical species interacting with each other via chemical reactions and employed kinetic rate expressions to evaluate the species evolution inside the gasifier. Therefore, kinetic models were more accurate than the equilibrium approaches, especially when the operating state of the gasifier was far off from equilibrium, as in the case of fluidized bed gasifiers.

As mentioned earlier, biomass gasification consists of a number of different chemical processes occurring concurrently inside the gasifier. Therefore, the kinetic model should include a component that describes the transformation of solid biomass into the primary pyrolysis/devolatilization products. It should also contain a set of relevant chemical species and reactions to represent the secondary homogenous reactions of the primary pyrolysis products. This part of the mechanism would include the gas phase oxidation reactions, tar cracking and PAH (polycyclic aromatic hydrocarbons) growth reactions as well as the water gas shift reaction. An additional component of the mechanism should describe the heterogeneous oxidation and gasification reactions of the char produced during biomass devolatilization.

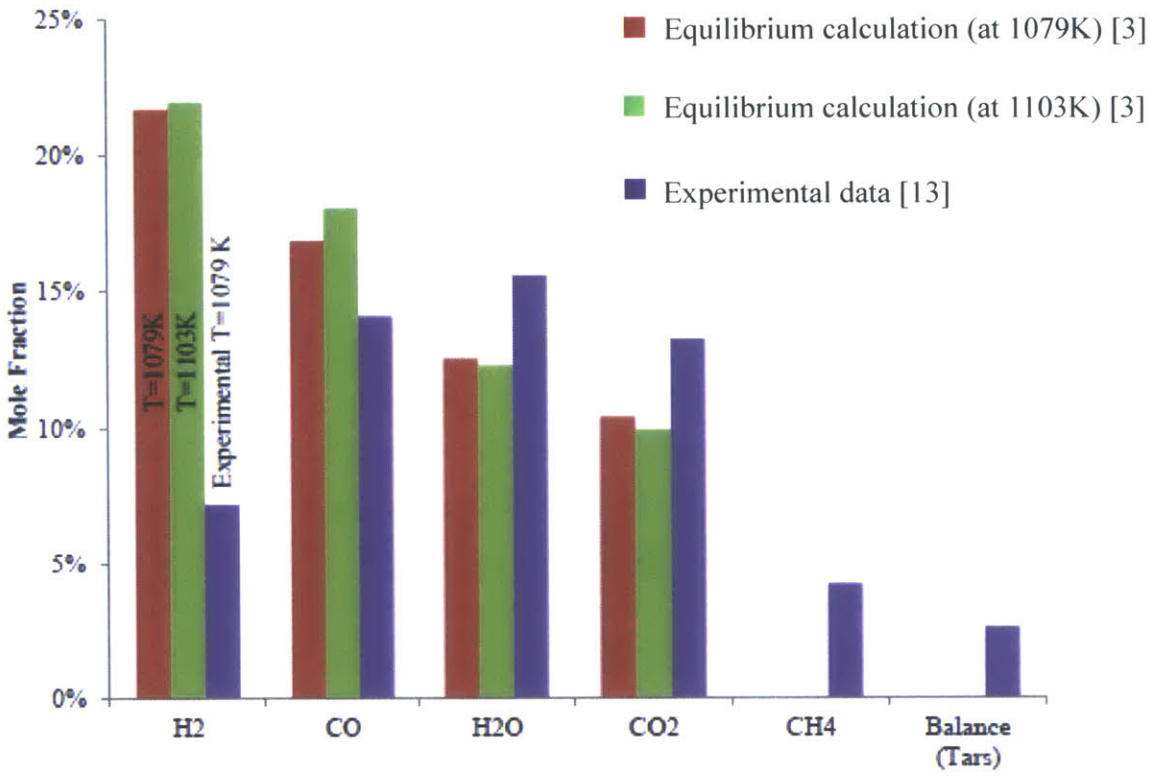

Figure 2-2: Comparison of the equilibrium concentrations of the major gas species (H_2, CO, H_2O, CO_2, CH_4) and tars with the experimental observations ([3], [13])

2.2.1 Global Models

Biomass devolatilization, which is the degradation of solid biomass into volatiles, gases and char, is an important process in biomass gasification. As noted by Gerber et al. [28], the final product gas composition and tar concentration at the gasifier outlet depend significantly on the biomass devolatilization product composition. This was because, a large fraction of solid biomass is converted to volatile gases during devolatilization and the composition of these volatiles affect the output synthetic gas composition. Hence, biomass devolatilization had received significant attention over the years. A number of different models had been proposed to accurately describe biomass devolatilization.

Biomass devolatilization models could be broadly classified as,

1. One component mechanisms
2. Multi component mechanisms

One step mechanisms described the biomass devolatilization process as the degradation of a single biomass pseudo-species under the assumption that all the different biomass constituents (cellulose, hemicellulose and lignin) degraded at the same rate. This assumption was valid under fast heating rates when the decomposition curves of the different biomass components tend to merge. The one-step mechanisms were further classified as [29],

1. One step global models
2. One stage multi-reaction models
3. Two stage semi global models

One step models used a single step first order reaction to describe the degradation of solid biomass into volatiles, light gases and char. Volatiles are the large organic compounds such as levoglucosan that typically condense at room temperatures, and play a significant role in the gasification process as tar precursors. In one step multi-reaction models, the biomass degradation process was modeled through a set of simultaneous and competing first order reactions, as proposed by Shafizadeh and Chin [30]. Two stage semi-global models considered biomass pyrolysis as a two-stage process, employing a first order reaction to describe the initial biomass break-up followed by an additional set of reactions to represent the subsequent evolution of the first stage products.

One step global models

$$\text{Biomass} \rightarrow (\text{Volatiles} + \text{Gases})_1 + (\text{Char})_1$$

One stage multi-reaction models

$$\text{Biomass} \rightarrow (\text{Volatiles} + \text{Gases})_1$$

$$\text{Biomass} \rightarrow (\text{Char})_1$$

Two stage semi-global models

$$\text{Biomass} \rightarrow (\text{Volatiles} + \text{Gases})_1 + (\text{Char})_1$$

$$(\text{Volatiles} + \text{Gases})_1 + (\text{Char})_1 \rightarrow (\text{Volatiles} + \text{Gases})_2 + (\text{Char})_2$$

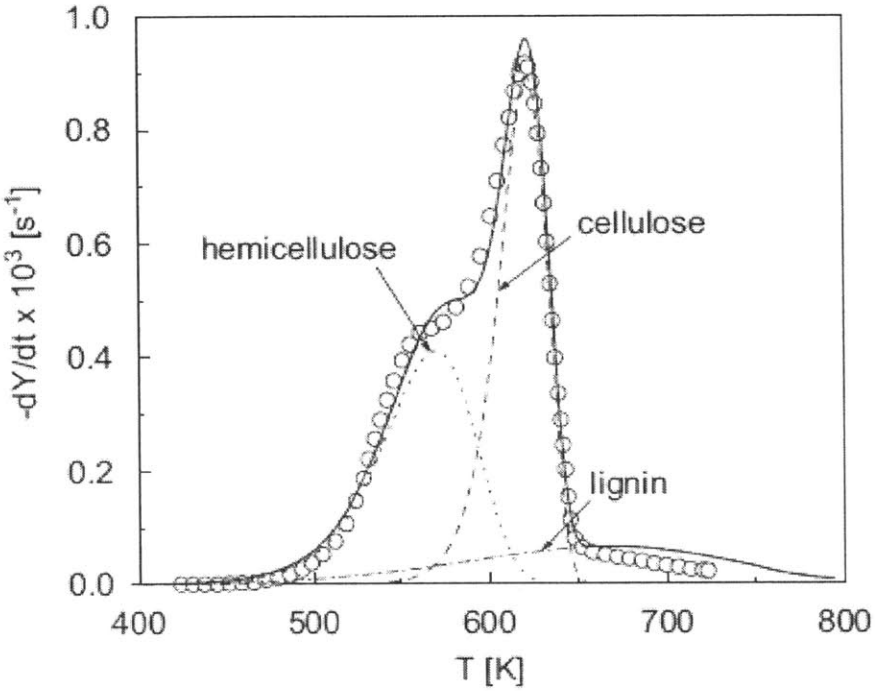

Figure 2-3: Total Biomass decomposition rate represented as the sum of individual decomposition rates of the major components: cellulose, hemicellulose and lignin [12]

Multicomponent mechanisms were more detailed and described biomass devolatilization as the combination of individual decompositions of the three biomass constituents: cellulose, hemicellulose and lignin. It was assumed that the three biomass components do not interact with each other, even though there was a considerable overlap between the individual decomposition timelines. Figure 2-3 depicts the decomposition of the solid biomass as a sum of the individual degradation of the different biomass constituents at very slow heating rates (5K/min). Hemicellulose and cellulose decomposed independent of each other, while lignin degradation was relatively slow and spread over a wide range of temperatures.

The kinetic parameters for the individual decomposition reactions were obtained from thermogravimetric experiments, and depended significantly on the particle heating rates. It was noted that there were significant uncertainties in the biomass pyrolysis kinetics due to the inherent difficulties associated with studying the phenomena [12]. During biomass devolatilization, the chemical and transport processes were found to interact strongly which made it very difficult to obtain kinetic measurements under a purely kinetic control. In addition, the effect of the secondary gas phase reactions of these devolatilization products had to be minimized. This was done either

by using smaller sample sizes or by operating the experiments at lower reaction temperatures (less than 773K) ([12], [31]).

While the initial devolatilization step played a significant role in determining the end product composition, the secondary homogenous reactions underwent by the devolatilization products were also equally important. These reactions included the homogenous reactions occurring in the vapor phase, and the heterogeneous reactions involving the char produced during devolatilization. The final tar concentrations were influenced by the different tar cracking and polymerization reactions occurring during this stage. In a majority of the studies, these reactions were typically represented by one or two global reactions, representing the conversion of the primary tar into light gases and a non-reactive condensable tarry component, as proposed by Antal ([32], [33]).

$$\text{Tars} \xrightarrow{k_1} \text{Gas}$$

$$\text{Tars} \xrightarrow{k_2} \text{Inert Tar} + H_2O$$

Unlike primary pyrolysis, the secondary reactions had not been as well studied and there was great variability in the kinetics reported by different authors. This was partly due to the widely different primary pyrolysis conditions used in the various experiments. The specific biomass feedstock used, presence of catalytic species, differences in the tar measurement equipment played an important role in the evaluation of the kinetic parameters. While most authors [12] assumed the tar cracking kinetics to be linearly dependent on the total primary tars produced in the devolatilization process, others ([34], [35]) had considered only a fraction of the primary tar to be involved in the cracking process. A few studies ([36], [37]) had also considered tar fractions with different reactivities, to compensate for the low activation energies encountered in the previous models.

A detailed review on the different physical and chemical models used for modeling the biomass pyrolysis process could be found in the review publication by Di Blasi [12].

Figure 2-4: A representative global model depicting the different reactions in biomass gasification [23]. Biomass devolatilization reaction was followed by homogenous oxidation reactions, heterogeneous char reactions and tar reforming reactions

Stoichiometry	Heat of reaction (kJ/mol)	Name	Number
Biomass → char + tar + H_2O + light gas (CO + CO_2 + H_2 + CH_4 + C_2 + N_2 + ...)	>0	Biomass devolatilization	R1
Char combustion			
$C_2 + ½O_2 \rightarrow CO$	−111	Partial combustion	R2
$C + O_2 \rightarrow CO_2$	−394	Complete combustion	R3
Char gasification			
$C + CO_2 \rightarrow 2CO$	+173	Boudouard reaction	R4
$C + H_2O \rightarrow CO + H_2$	+131	Steam gasification	R5
$C + 2H_2 \rightarrow CH_4$	−75	Hydrogen gasification	R6
Homogeneous volatile oxidation			
$CO + ½O_2 \rightarrow CO_2$	−283	Carbon monoxide oxidation	R7
$H_2 + ½O_2 \rightarrow H_2O$	−242	Hydrogen oxidation	R8
$CH_4 + 2O_2 \rightarrow CO_2 + 2\,H_2O$	−283	Methane oxidation	R9
$CO + H_2O \leftrightarrow CO_2 + H_2$	−41	Water–gas shift reaction	R10
Tar reactions (tar assumed $C_{n \text{ and } m}$)			
$C_nH_m + (n/2)\,O_2 \rightarrow nCO + (m/2)\,H_2$		Partial oxidation	R11
$C_nH_m + n\,CO_2 \rightarrow (m/2)\,H_2 + (2n)\,CO_2$		Dry reforming	R12
$C_nH_m + nHO_2 \rightarrow (m/2+n)\,H_2 + nCO_2$	Highly endothermic +(200 to 300)	Steam reforming	R13
$C_nH_m + (2n - m/2)\,H_2 \rightarrow n\,CH_4$		Hydrogenation	R14
$C_nH_m \rightarrow (m/4)\,CH_4 + (n - m/4)\,C$		Thermal cracking	R15

In an actual biomass devolatilization process, there was a strong interplay between the various chemical and the transport processes at both the level of the particle and the overall reaction environment. Complete models using varied levels of complexity for describing both the chemical process and the transport phenomena had been proposed in literature. While the detailed models ([38]–[43]) coupled the kinetics of the primary and secondary reactions for the three lumped components (char, tars and gases) with the various conservation equations for the mass, momentum and energy, many of the simplified models ([44]–[47]) used a one-step pyrolysis reaction with estimated kinetic parameters to yield a pre-defined product composition. The particle devolatilization was either simply modeled using volumetric decomposition rates or a more detailed shrinking unreacted core based approach where devolatilization was assumed to occur at an infinitely thin surface [12]. The predictive capabilities of the transport models were also limited by the accuracy of the kinetic models and the scarce experimental data available to validate them.

The main drawback with global models was their limited applicability to different operating conditions, since they had been developed specifically for a certain set of operating conditions. Additionally, global models provided very little information on the formation pathways of the different classes of tar compounds encountered during gasification. Given these inadequacies with the global kinetic models, there was a need to use more sophisticated chemistry models that would be able to capture the chemical reactions pathways more accurately. The next section describes a widely used detailed chemical kinetic mechanism that had been proposed by Ranzi et al. [48] for biomass pyrolysis, oxidation and gasification.

2.2.2 Detailed Kinetic Mechanisms

While the simplest models considered only a handful of reactions involving the major gas species and a global reaction to describe the tar evolution in the gasifier, detailed chemistry reaction mechanisms consisting of hundreds of different chemical species and thousands of elementary-type reactions to describe their interactions had also been proposed. Unlike the global kinetic models or thermodynamic equilibrium models, detailed kinetic models could be applied over a wide variety of operating conditions for different types of gasifier configurations because of their mechanistic nature. In this section, the detailed kinetic mechanism developed for biomass gasification by the Chemical Reaction Engineering and Chemical Kinetics (CRECK) group at Politechnico di Milano is considered. A detailed discussion on the development of the mechanism is given below.

As mentioned already, while hydrodynamics and heat transfer played a critical role in the product gas composition and tar concentrations, the chemistry model had to be accurate as well. Since commercial gasifiers are required to be able to accommodate a variety of biomass feedstock, the simulation model should be able to account for the variations in the input biomass composition. Hence, biomass characterization is a significant aspect of a detailed chemical mechanism, since it forms the basis for all the processes inside a gasifier. Next, the mechanism should be able to describe both the biomass pyrolysis/devolatilization as well as the secondary gas phase reactions in appropriate detail since the final product composition and the tar concentrations follow as a result of these processes. Finally, heterogeneous char oxidation and gasification reactions are also important, especially in the case of gasifiers operating at low to moderate superficial velocities where the contribution of char gasification reactions becomes considerable.

The CRECK mechanism used the standard three component characterization of biomass, describing the biomass composition in terms of cellulose, hemicellulose and lignin. In line with experimental observations [12], the three biomass constituents were assumed to evolve independent of each other.

The pyrolysis model of the CRECK mechanism was based on the multi-component devolatilization model described in the previous section. The biomass degradation process was described in terms of the individual decomposition of the biomass "pseudo-components" cellulose, hemicellulose and lignin. Due to the complex structure of lignin, it was described by a mixture of reference components: LIG-C, LIG-H and LIG-O. Depending on the biomass feedstock used, the proportions of these components were adjusted. While levoglucosan and hydroxy-acetaldehyde (HAA) were the dominant products of cellulose decomposition, phenol and other phenoxy species were formed from lignin decomposition. The mechanism included lumped pseudo species such as GCO2, GCO and GCOH2 to represent the trapped gas species in the solid biomass that would eventually be released as gases at appropriate rates. The ash content in the biomass was assumed to remain inert and its catalytic effects were neglected. The rate parameters were obtained from both thermogravimetric experiments and an existing semi-detailed kinetic scheme [49].

The secondary gas phase reactions of the devolatilization products were described using an extended reaction mechanism that was originally developed for the pyrolysis and oxidation of hydrocarbon species [50]. Typically, these large chemical kinetic mechanisms are developed in a hierarchical manner, starting from a small standardized set of species and reactions that forms the

core of mechanism. In the case of hydrocarbon combustion mechanisms, the $CO-H_2-O_2$ mechanism forms the base set from which the mechanism is built upwards.

Starting with the base $CO-H_2-O_2$ mechanism, the CRECK hydrocarbon combustion mechanism was built up by adding larger chemical species in a hierarchical manner. In the first stage, all the relevant chemical species having a single carbon atom (except those already included in the base mechanism) were added. Once these chemical species were included, the set of reactions describing the evolution of these species to the species already existing in the mechanism, were added to the overall reaction set. These primary propagation reactions were essentially the radical initiation reactions and hydrogen abstraction reactions. In the next stage, chemical species with two carbon atoms and their corresponding reactions were added. This process continued until all the species of interest were included in the mechanism. To extend the applicability of the hydrocarbon mechanism to biomass applications, biomass specific species (e.g. levoglucosan) were added to the original mechanism and the corresponding propagation reactions were also included. The kinetics rate parameters for these reactions were obtained from experimental values reported in the literature.

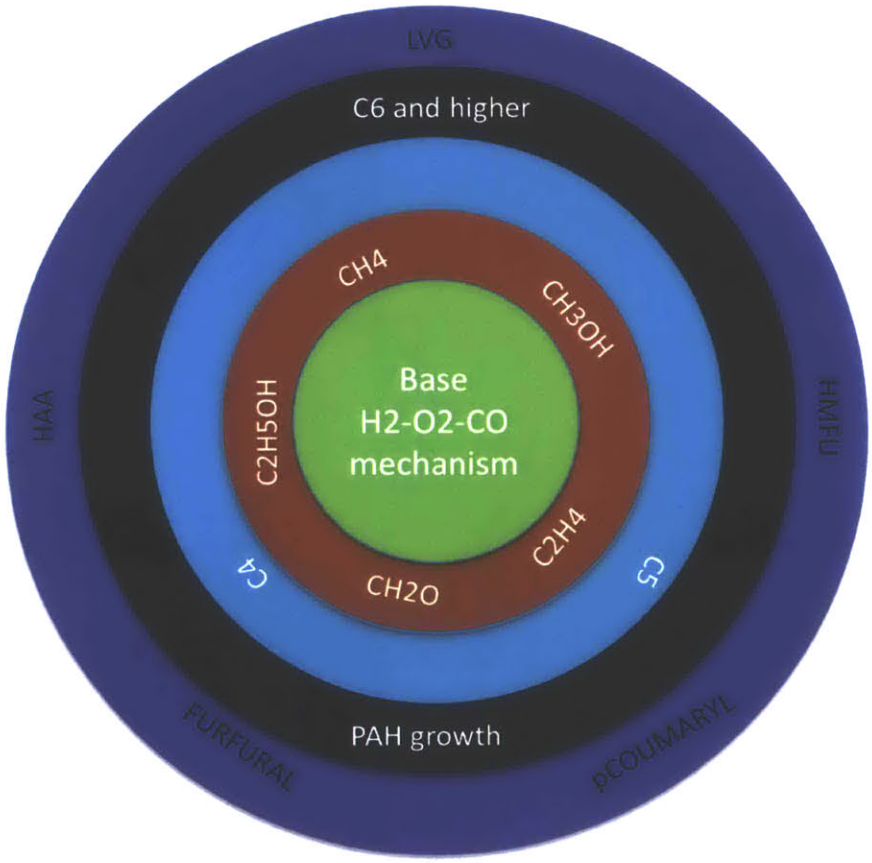

Figure 2-5: Hierarchical representation of the CRECK secondary gas phase reaction mechanism for biomass gasification. Starting with the base mechanism, additional species and the corresponding reactions are added stage by stage

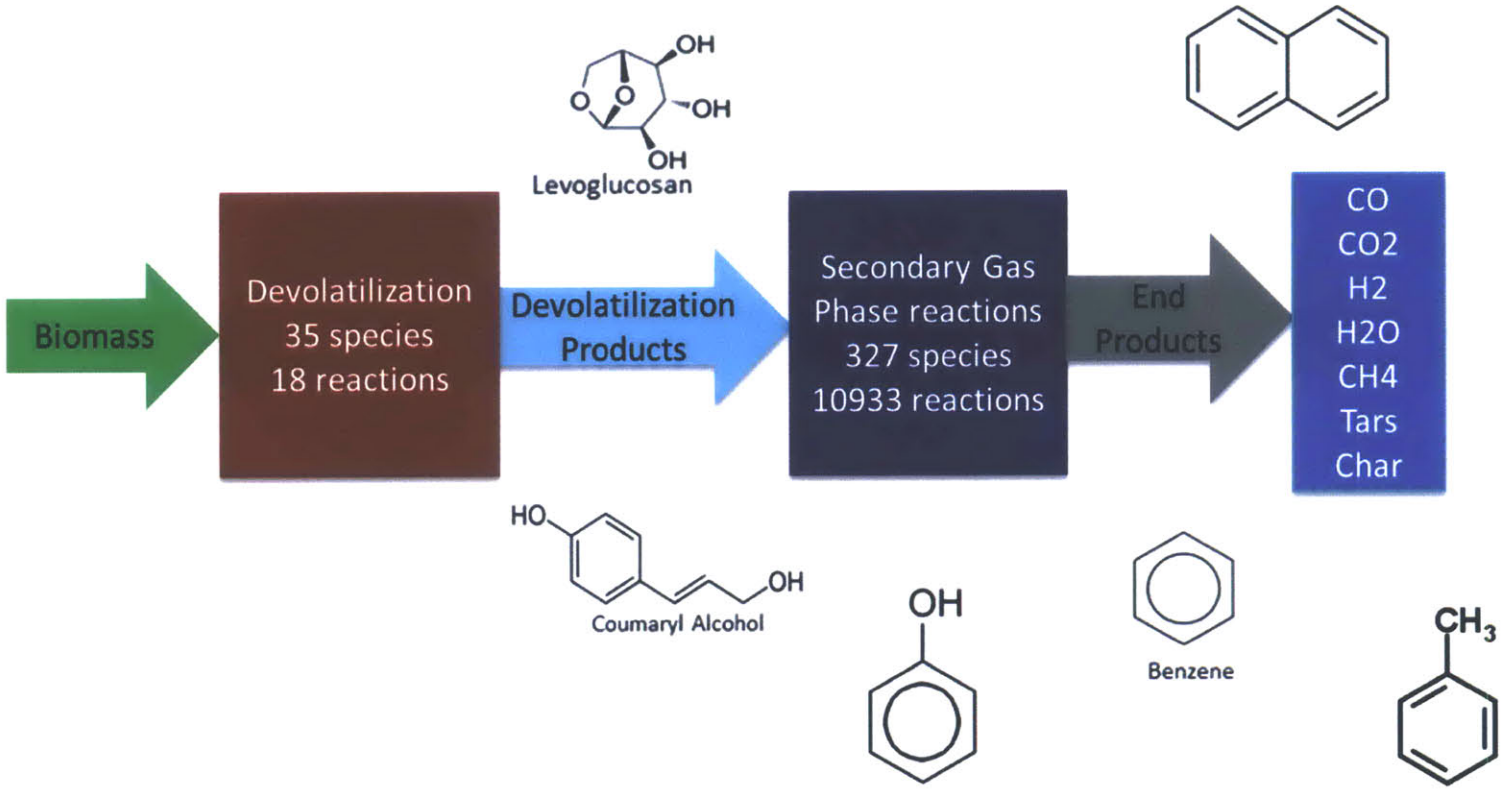

Figure 2-6: Flowchart describing the conversion of biomass to synthetic gas using the detailed CRECK mechanism. Biomass Devolatilization is described using 35 species and 18 reactions and the secondary homogenous reactions of primary pyrolysis products are represented using 327 species and 10933 reactions

While these large mechanisms are detailed and accurate, the huge computational needs associated with solving hundreds of ODE's for each species in a CFD setup is a major drawback. This has resulted in the development of reduced order chemistry mechanisms that can reliably predict the gas concentrations with a smaller number of species and reactions. Stagni et al. [51], reported that the overall CPU time to compute the reaction steps, transport properties and the transport steps increased by $\sim N^{2.3}$, where N is the number of species in the chemical mechanism. Individually, the computational time for the reaction step increased by $\sim N^{2.4}$, and that for the transport step evaluation increased by $\sim N^{2}$. It was observed that the computational time to calculate the reaction step, during which the uncoupled, stiff ODE's representing the species evolution were integrated over the time step, consumed almost 80-85% of the total computational time.

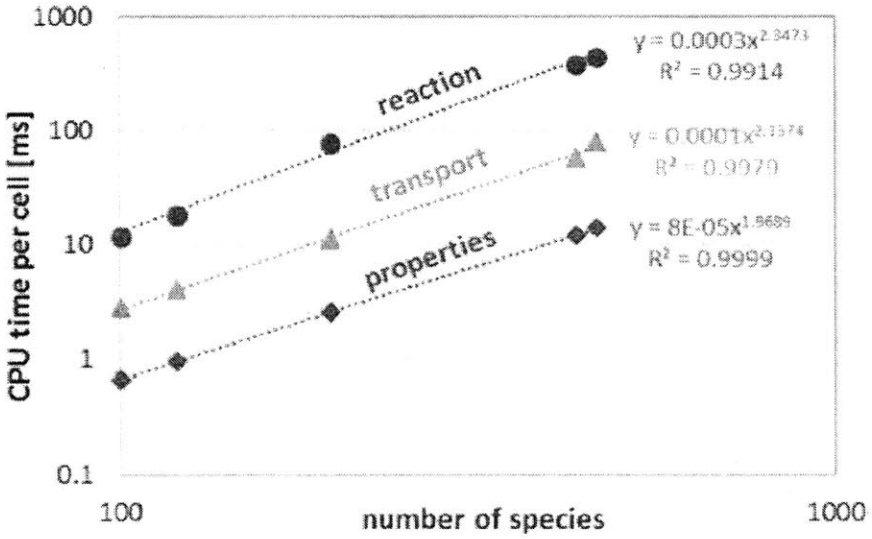

Figure 2-7: Computational time variation with the size of the kinetic mechanism, showing almost a quadratic dependence of the computation time on the number of species in the mechanism [51]

In addition to the computational demands involved, the extensive level of detail in a comprehensive mechanism might actually be too excessive, when there are significant uncertainties over the hydrodynamic model's accuracy. As a result, several mechanism reduction techniques have been developed that could be used to obtain significantly smaller mechanisms with fewer number of species and reactions, while at the same time, retaining most of the important kinetic information required for the specific application. The next section gives a brief overview of various mechanism reduction techniques proposed in literature.

2.3 Mechanism Reduction Techniques

Automatic generation of reaction networks has resulted in the development of a large number of detailed reaction mechanisms to describe the complex chemical processes in reacting systems such as combustion, pyrolysis and thermal cracking ([52]–[58]). An efficient usage of these complex reaction networks in simulations has to address a number of obstacles [59]. First, these large mechanisms are generally very difficult to solve because: 1) The sheer size of the mechanism with a large number of species and reactions has proportionately large computational requirements [51] and 2) the stiff nature of the system, due to the presence of species that evolve over a wide range of timescales, renders the Jacobian matrices ill-conditioned. In addition, the kinetic parameters used in these complex nonlinear models are not very reliable and are also difficult to obtain. The difficulties with the detailed schemes become even more magnified when they are coupled with computational fluid dynamic models of the reacting system, giving rise to the need to develop compact reaction mechanisms that could be used in simulating industrial scale systems.

Over the last few decades, several researchers had developed various mechanism reduction methodologies that could be used in reducing the size of these detailed mechanisms while retaining all the important characteristics of the complex reaction networks. At the highest level, mechanism reduction techniques can be broadly classified as physics, or rather chemistry based approaches and purely mathematical approaches. Physics based approaches require a good understanding of the underlying chemical processes and extensive knowledge and experience with the underlying chemistry behind the process. On the other hand, mathematical reduction approaches had been developed by looking at the reaction system from a purely mathematical point of view, independent of the chemical characteristics of the system.

2.3.1 Physical mechanism reduction approaches

The physical reduction approaches could either be based on skeletal reduction methods, mechanistic reduction techniques, chemical lumping approaches or a combination of these procedures. Skeletal reduction approaches reduced the size the mechanism by eliminating all the unimportant species identified using sensitivity analysis ([60], [61]), directed relation graphs ([62]–[64]) or path flux analysis [65]. Mechanistic reduction approaches such as quasi steady state analysis (QSSA), computational singular perturbation (CSP) ([66], [67]) and intrinsic low dimensional manifold (ILDM) [68] separated the species based on the different timescales over

which they evolve. The rate equations for the reactions involving the very fast (and the very slow) time-scale species were then rewritten assuming that the fast time-scale species had already reached steady-state.

Lumping approaches reduced the dimension of the system by combining a set of species into a single lumped pseudo-species. There are essentially two basic lumping approaches: chemical lumping and mathematical lumping. While physical lumping approaches would be discussed in this section, the mathematical approaches would be considered in the next section on the mathematical reduction techniques. Irrespective of the approach, all the lumping methods have to address certain fundamental issues [69]: 1) Determination of the original species that have to be lumped, 2) Definition of the lumping transformation representing the contribution of each original species to the lumped pseudo-species and 3) Estimation of the kinetic parameters for the new set of reactions involving the lumped species. Mechanism reduction through the lumping approaches had been successfully achieved for a variety of applications such as combustion, pyrolysis and atmospheric chemistry ([50], [51], [69]–[72]). Lumping approaches had also been employed in automatic generation of large reaction mechanisms to limit the total number of species used in these comprehensive chemical models [73].

While the chemical lumping methods lumped the species based on their chemical structure (isomer lumping) or reactivity, mathematical lumping techniques defined formal rules for the lumping transformation and generated lumps based on these set of rules. It is quite apparent that chemical lumping procedures require extensive chemistry knowledge and experience to be able to accurately define these lumps.

Stagni et al. [51] used a multi-stage reduction strategy incorporating the chemical lumping procedures and a skeletal reduction method based on the rate of production analysis to develop reduced kinetic models for n-heptane and n-dodecane oxidation. Different lumping strategies were used to group species based on the temperature regime of operation. It was noted that, from a theoretical standpoint, the large alkyl radicals in the combustion system interact with the reacting mixture through hydrogen abstraction, unsaturated bond addition and recombination at high temperatures. However, in reality, these interactions were found to be very weak and therefore, all the large alkyl radicals higher than C_4 were directly substituted by their primary isomerization and decomposition products. This approach eliminated a substantial number of intermediate radicals and their corresponding reactions and helped to drastically reduce the final size of the mechanism.

In the case of the low temperature mechanism, different classes of intermediate radicals (alkyl, peroxy, hydroperoxyalkyl and hydroperoxyalkylperoxy) that were formed at low temperatures, as well as the isomers of the primary products (alkenes, cyclo-ethers and carbonyl hydroperoxides) were grouped into a single lumped pseudo-species, representative of each class.

As Pepiot pointed out [73], there were two important considerations that need to be taken into account while these lumps were defined. While a proper description of the lumps was of the highest priority, it was also important that the lumping scheme allowed for a reasonably accurate estimation of the individual contributions of these original species to the lumped pseudo-species. Various authors had developed different approaches to evaluate the lumping transformations. Huang et al [69] used a numerical criterion to identify the species to be lumped and applied the scheme successfully in the simulation of isothermal conversion of methane. The numerical criterion was defined based on the initial concentrations of the original species in the mechanism and also on the ratio of their local production rates. The production rate ratio was evaluated at each time step and depending on the accuracy required, the numerical criterion was relaxed accordingly.

Chemical isomer lumping approaches had also been used for the automatic generation of reaction mechanisms [74]. Starting with a base mechanism, the mechanism was built up in a hierarchical manner by adding increasingly longer species and the corresponding reactions involving them. However, to limit the size of the overall mechanism, some of the isomer species were lumped into a single pseudo species representing all the corresponding isomers in the primary mechanism, since they had similar reaction pathways both during formation and decomposition.

2.3.2 Mathematical reduction approaches

Earliest research on mathematical reduction techniques were carried out by Wei and Kuo, who developed exact and approximate linear lumping schemes for monomolecular reaction systems ([74], [75]). The concentrations of the lumps were represented as certain linear combinations of the original species concentrations. Depending on the absence or presence of errors in defining these lumps exactly, the lumping scheme was considered exact or approximate. Li and Rabitz ([76]–[78]) extended these earlier works and proposed necessary and sufficient conditions for the exact and approximate linear lumping for arbitrary nonlinear differential equations, representative of the chemical kinetic equations. The overly restrictive nature of the linear lumping transformations and its failure to achieve low enough reduction in certain cases motivated the authors to expand their analysis to include nonlinear lumping transformations ([79]–

[81]). Non-linear lumping approaches defined the lumps as nonlinear combinations of the original species and they had been successfully applied for diverse chemical systems such as biochemistry [80] and combustion [81], petroleum cracking [82], catalytic cracking [83].

Huang et al [69] developed an approximate linear lumping scheme incorporating a numerical criterion to decide on the species to be lumped and applied the scheme successfully in the simulation of isothermal conversion of methane. The numerical criterion was defined based on the initial concentrations and the ratio of the local production rates of the original species. The production rate ratio was evaluated at each time step and depending on the accuracy required, the numerical criterion was relaxed accordingly. The reduced mechanism was compatible with standard chemistry solvers and the contributions of each species to the lump were a function of time and space.

However, it has to be noted that these mathematical lumping schemes are very restrictive in that they require the differential equation system to satisfy a number of mathematical constraints for the lumping scheme to be applicable. Additionally, the mathematical computation of these lumping schemes is, in general, not readily apparent and has to be treated on an individual basis, exploiting the specific properties of the original system. Overall, it can be concluded that, even though the nonlinear mathematical lumping procedure would produce the largest reduction, there does not exist a systematic procedure to obtain an optimal lumping transformation ([79]–[81]).

2.3.3 Multi-stage reduction approaches

While the individual mechanism reduction approaches produced significantly smaller mechanism compared to the original mechanism, it was still too large to implement in a detailed fluid hydrodynamic setup. In an effort to produce even smaller mechanisms, many researchers had used a combination of multiple mechanism reduction strategies. Lu and Law [84] employed a combination of DRG, isomer lumping and QSSA to develop a reduced mechanism for n-heptane oxidation. Starting with the original Westbrook's mechanism with approximately 550 species and 2500 reactions, they developed a final reduced mechanism with just 55 species and 51 global steps. The reduced mechanism was validated for homogenous ignition and flame speed applications.

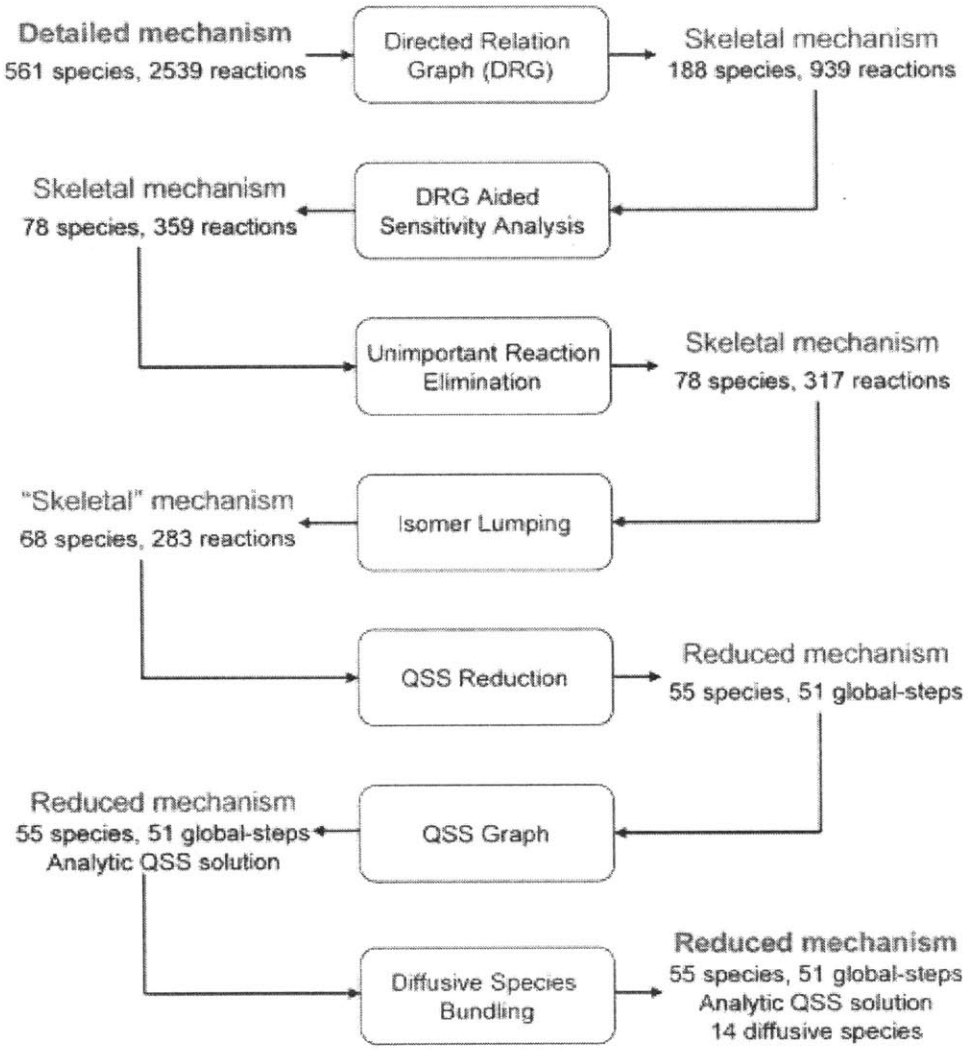

Figure 2-8: Combination of different mechanism reduction approaches (Directed Relation Graph, Lumping and Quasi Steady State Approximations) used to obtain a ten-fold decrease in the size of the n-heptane oxidation mechanism [84]

In conclusion, it has to be noted that the final selection of the overall mechanism reduction procedure should reflect the broad applicability of the procedure across the different conditions of interest, the ability to analyze the procedure at each level of the reduction approach and finally, the capability to understand the modeling errors associated with the procedure [59].

2.4 Compact Mechanisms for Biomass gasification

While the oversimplified global models provide little information on the different tar classes, the detailed mechanisms have the disadvantage of being too complex for CFD simulations. As a result, there have been efforts to develop compact kinetic models for biomass gasification with the aim to be able to accurately predict the major gas species and tars. In this section, two different compact biomass gasification that have been developed by Palma [85] and Pepiot [86] would be presented.

2.4.1 Palma Model for Biomass Gasification

Based on a review of the different chemical reaction pathways proposed in the literature for tar formation inside a biomass gasifier [87], this mechanism was developed to predict the concentrations of the major gas species and the different tar compounds belonging to the various classes. Unlike the detailed mechanisms that involve hundreds of species and thousands of reactions, this mechanism used a small set of species and reactions (~30 reactions and ~40 species) to represent the gasification process in a fluidized bed biomass gasifier.

The primary decomposition of the biomass feedstock was represented using two separate reactions, one describing the decomposition of the lignin fraction and the other, for the decomposition of the rest of the biomass components. The kinetics for these reactions were obtained from weight loss curves and yield measurements of three products (gas, char and tar) and were valid for fast particle heating rates. While the lignin decomposition reaction resulted in the production of the primary tar precursors, the other reaction produces light gases (CO, CO_2, H_2O, H_2, CH_4) and char. Lignin was assumed to be the sole contributor for tar formation, and lignin pyrolysis products that were found to be the most abundant from experiments - catechol, guaiacol and vanillin, were used as the primary tar precursors. The subsequent evolution of these primary devolatilization products were represented using secondary reactions that were deemed the most favorable, based on thermodynamics, among the set of reactions presented in the review.

The compact mechanism was used to predict the major gas species concentrations and tar production for the experimental conditions employed by van Paasen and Kiel [13] and the predictions were compared with the experimental observations for two different equivalence ratios [85]. While the kinetic model has been shown to significantly over predict the class 2 tars, the class 4 tars predictions were found to be much smaller than the experimentally measured values. Class

5 tars were not included in the compact mechanism. In addition, there were also significant discrepancies in the prediction of the light gas concentrations. Estimates of the methane and steam concentrations at the gasifier outlet were significantly lower than the experimental observations. However, the predictions for carbon monoxide, carbon dioxide and hydrogen were in good agreement with the experiments. Figure 2-9 lists the predicted and experimentally measured concentrations of the different major gas species and tar classes.

	units	exp. data	kinetic model	exp. data	kinetic model
ER		0.25	0.25	0.26	0.26
biomass feeding rate	kg/h	1	1	1	1
CO	vol %	14.09	12.9	14.20	13.4
CO_2	vol %	13.25	13.7	13.18	13.5
H_2	vol %	7.17	9.1	7.10	8.8
N_2	vol %	43.04	57.5	43.94	58.4
CH_4	vol %	4.22	0.54	4.23	0.37
H_2O	vol %	15.6[a]	5.4	15.5[a]	4.9
SPA total tar	g/m^3	10.0	21.0	7.6	13.7
class 2	mg/m^3	1089	17255	471	10 909
class 3	mg/m^3	1359	1871	756	1481
class 4	mg/m^3	5495	1876	5024	1342
phenol	mg/m^3	1015	555	425	339
class 5	mg/m^3	311		354	
temperature bed	K	1079	969	1103	965
temperature freeboard	K	1049	910	1073	918
temperature of air	K	298	960	298	967
carbon conversion	%	97–99	96.7	97–99	97.0

Figure 2-9: Comparison of the predictions of major gas species and tar classes using the Palma mechanism with experiments [85]. Palma mechanism predicts significantly different concentrations of the major gases and the tars, compared to the experimentally measured values

2.4.2 Pepiot mechanism for biomass gasification

This section presents the compact biomass gasification kinetic mechanism developed by Perinne Pepiot at Cornell University [86]. After assembling and validating a semi-detailed chemistry base model for both the devolatilization and secondary gas phase reactions, several stages of reduction using the different mechanism reduction procedures were used to obtain final

compact mechanism. While the lumped devolatilization mechanism developed in the CRECK model [9] was used as the base mechanism for devolatilization, a semi-detailed kinetic model developed by Pepiot for hydrocarbon combustion applications, was used for the secondary gas phase reactions of the devolatilization products. Biomass devolatilization was described in terms of the three components: cellulose, hemicellulose and lignin. Unlike the CRECK model that used three different species to describe lignin decomposition, only one component of lignin was considered. Lignin decomposition kinetics were also modified to better fit the experimental data obtained by Shin [88]. Since biomass gasification involved certain chemical species that were specific to biomass, the semi-detailed model was extended to include the biomass specific components using the detailed secondary gas phase reaction mechanism in the CRECK model.

The size of the semi-detailed mechanism was first reduced by eliminating all the chemical species and reactions using the Direction relation graph approach. The importance of a chemical species or a reaction on the prediction of the target species was quantitatively defined and all those species and reactions that had an importance index below a specified value were removed from the mechanism. In the next step, isomer lumping techniques were used to lump the different chemical isomer species together. Quasi steady state (QSS) approximations were then applied to eliminate all those species that evolve very fast (and very slow). In order to further reduce the size of the mechanism, the decomposition of different products were lumped to obtain a smaller set of reactions involving lumped pseudo-species.

Reduced chemical mechanisms are typically developed for a specific set of operating conditions, and hence, it is important to understand their range of applicability. This compact mechanism was developed for gasification under an inert nitrogen atmosphere at operating temperatures between 1050-1250K, for particle heating rates around 1000K/s.

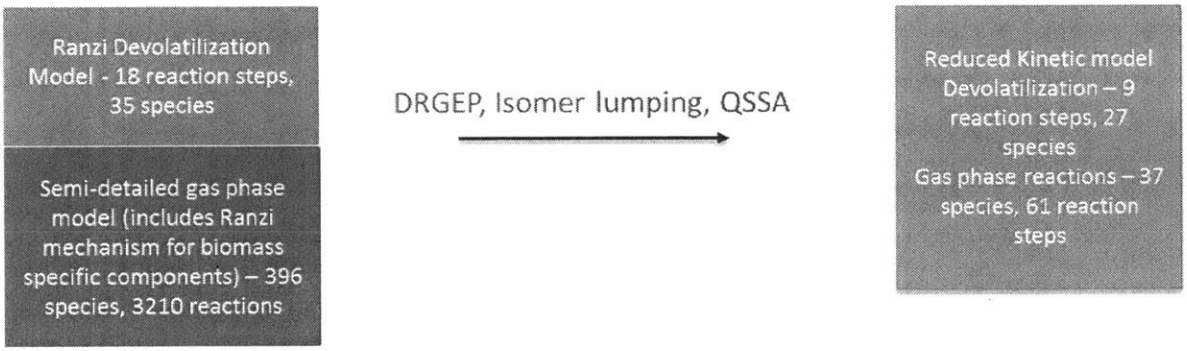

Figure 2-10: Combination of different mechanism reduction techniques (DRGEP, Isomer Lumping, QSSA) were employed by Pepiot to obtain a reduced model for biomass gasification [86]

2.5 Conclusions

This chapter presented the various chemistry models available in literature to describe biomass gasification. After a brief overview on the advantages and disadvantages of thermodynamic equilibrium-based models, a detailed discussion of the various kinetic models was presented. The earliest kinetic models were the empirically developed global models that consisted of a small number of chemical species and reactions to describe the various sub-processes in biomass gasification. The global models were followed by detailed kinetic mechanisms and details on the development of the CRECK mechanism for biomass gasification was discussed. The need for compact kinetic mechanisms was introduced followed by a brief discussion of the various mechanism reduction techniques. Finally, the methodology and development of two existing compact kinetic models for biomass gasification were presented.

3 Global Chemistry Model development for Biomass Gasification

The significant computational challenges associated with using detailed chemistry mechanisms in computational fluid dynamics (CFD) prompted the development of simplified global chemistry models with significantly smaller computational requirements. Several global chemistry models aimed at describing the biomass gasification process using a small number of chemical species and reactions, typically on the order of ~10 chemical species and ~10 reactions, have been proposed ([10], [23]). The global models were developed empirically, using lumped pseudo-species to describe the chemical species present in biomass gasification such as the different tar compounds (primary, secondary and tertiary tars).

The structure of these global models follow a similar pattern: the initial pyrolysis step was described using 1-3 competitive global reactions (an additional drying reaction was included at lower temperatures), followed by a secondary tar cracking reaction to account for the tar evolution towards the gasifier outlet, and then a few homogenous reactions to describe the secondary gas phase oxidation reactions. These secondary homogenous reactions also included the water-gas shift reaction, which plays a very important role in the major gas species estimation, especially under steam gasification conditions. In addition, a set of reactions to represent the heterogeneous char reactions of the biomass char produced during the devolatilization process is included. The kinetic parameters for the reactions were typically obtained empirically from experiments for a specific set of operating conditions.

In this chapter, two different global chemistry models have been developed for biomass gasification under air-blown gasification and steam-blown gasification conditions. After a brief discussion of existing global biomass gasification models that have been developed by Stark for use in CFD [3], a detailed discussion on the development of the proposed global models is presented. The proposed global models are then used in conjunction with the appropriate reactor network model of the gasifiers to estimate the major gas species concentrations and tar production. For each set of gasification conditions, the major gas species and total tar concentrations predicted by the global model are compared with the corresponding predictions evaluated using the detailed CRECK chemical kinetic mechanism in the same reactor network model of the gasifier as well as the experimentally measured values.

3.1 Motivation

Biomass gasification is a very complex process involving a number of different interacting sub-processes, each of which is modeled using the appropriate sub-model. The biomass devolatilization model describing the conversion of solid biomass feedstock into the primary pyrolysis/devolatilization products is an important constituent of the modeling framework. The subsequent evolution of the devolatilization products into the output synthetic gas is modeled using a reactor network model of the gasifier. In addition, the highly carbonaceous char produced in the devolatilization process undergoes gasification reactions with H_2O and CO_2, and combustion in the presence of oxygen and an appropriate heterogeneous char conversion model is essential to model these reactions. An accurate chemistry model, describing each of these processes in appropriate detail, is an essential component of all these sub-models and hence, it plays a very significant role in the accurate prediction of the end product composition.

Gerber [28] observed a significant variation in the end product compositions, depending on the choice of the secondary pyrolysis chemistry model. The devolatilization process was modeled using three competitive reactions, representing the conversion pathways of biomass into gases, char and primary tars. The secondary reactions undergone by these primary tars species were described using two different secondary pyrolysis models, as depicted in Figure 3-1. The first model considered only a single primary tar pseudo-species and assumed a fixed fraction of the primary tar to remain inert, while the remaining fraction degraded into light gases, with the values of the two fractions obtained from experiments. Similar to the first model, the second pyrolysis model considered a fixed fraction of inert tar products. However, the degradation of the remaining tar fraction was modeled using two different primary tar pseudo-species. The two reactive tar fractions represented the varying decomposition properties of the primary tar compounds produced at different temperatures and hence, were modeled to decompose at different kinetic rates into a mixture of light gases of different compositions.

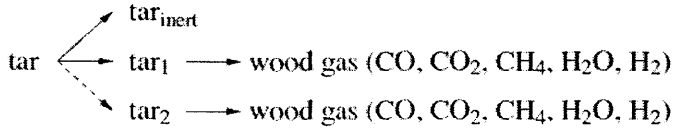

Figure 3-1: Two different secondary pyrolysis models considered by Gerber et al [28] to model tar production in biomass gasification (Pathway to Tar_2 applies only to the second model)

While the major gas species (CO, CO_2, H_2, H_2O and CH_4) concentrations were significantly impacted by the secondary pyrolysis model used, the effect on the inert tar concentrations was relatively small. This trend was observed because both the models shared the same primary pyrolysis model. Figure 3-2 shows the variation of the different major gas species and inert tar concentrations for the two secondary pyrolysis models used in the study.

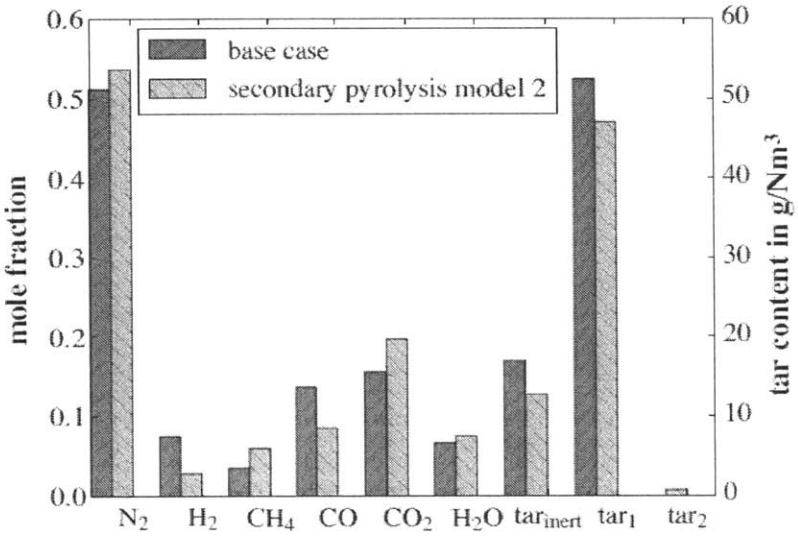

Figure 3-2: Variation of the outlet gas composition with the secondary pyrolysis model employed (reproduced from Gerber et al [28]). Inert tar fraction and the major gas concentrations were significantly affected by the choice of the secondary pyrolysis model

The secondary pyrolysis models used by Gerber were developed for a specific set of experimental conditions and assumed a constant inert tar fraction at the outlet. However, a number of different operating conditions such as fluidizing agent, temperature, residence times and bed material could affect the outlet tar concentrations, limiting the applicability of these models to other conditions. Various ad-hoc measures have been used in literature to account for the dependence of tar concentrations on operating conditions. Kaushal et al [89] used a correction factor, ranging between zero and one (depending on the operating conditions), for the tar cracking reaction kinetics in their secondary pyrolysis model. As reported in the review publication on biomass pyrolysis mechanisms by di Blasi [12], there has been little work on developing accurate secondary pyrolysis models in literature. Even amongst the existing pyrolysis models, there is a wide range of kinetic parameters employed and there are still significant uncertainties associated with the applicability of each of these models to varying operating conditions.

3.2 Stark global chemistry model

The details of the global biomass gasification model used by Stark [3] for CFD simulations of lab scale gasifiers is presented in this section. The list of reactions used in the model is given in Table 3-1.

Devolatilization was represented using a simple primary pyrolysis mechanism proposed by Di Blasi [90], that consisted of three concurrent reactions, each describing the conversion of solid biomass into light gases, tar and char respectively. The di Blasi devolatilization mechanism was developed empirically from experiments using beech wood powder under fast heating rates (1000K/min) at temperatures in the range of 573-708 K. Although the primary tars produced during actual devolatilization experiments comprise a number of different volatile compounds, a single pseudo-species named "Tar_1" was used in this mechanism to represent the primary tars. Tar_1 was modeled as benzene, since benzene was the most prevalent tar compound under the gasification conditions considered. An additional drying reaction was included to represent the evaporation of moisture stored inside the biomass particles and the related kinetic parameters were obtained from literature.

The primary pyrolysis products underwent further secondary gas phase reactions in the gasifier bed and freeboard to produce the final gasifier output composition. A global primary tar cracking reaction, developed by Gerber [28], based on the experimental works of Boroson et al. [34] and Seebauer [91], was used to describe the degradation of the primary tar. While a major fraction of the primary tar produced during devolatilization was assumed to degrade into light gases, the remaining fraction was assumed to stay inert. The unreactive refractory tar present at the gasifier outlet was denoted "Tar_2" and its chemical composition was modeled as benzene. Similar to other global models ([26], [91]), the secondary gas phase combustion and oxidation reactions were represented by a global gas phase reaction mechanism.

The char produced during devolatilization underwent heterogeneous oxidation with O_2 and gasification reactions with CO_2 and H_2O. The kinetic expressions for the char reactions were adapted from the mechanisms proposed by Wurzenberger [93], Di Blasi [94] and Gómez-Barea [95]. The rate equation for the combustion reaction in the model neglected the diffusive effects of the char particle under the assumption that, at typical operating temperatures of fluidized bed gasifiers, the diffusion rates of the particles were much faster than the reaction rates.

Table 3-1: Global chemistry model employed by Stark [3] for CFD simulations of biomass gasification. A three-step devolatilization mechanism was followed by homogenous oxidation reactions, heterogeneous reactions and tar cracking reaction

Reaction	Rate Expression
Devolatilization & Drying	[1/s]
$\text{Biomass} \longrightarrow \cdot 3054\,H_2 + \cdot 1854\,CO + \cdot 1687\,CO_2 + \cdot 0671\,CH_4 + \cdot 2734\,H_2O$	$4.379 \times 10^9 exp(-152700/RT)$
$\text{Biomass} \longrightarrow 0.246\,Tar_1$	$1.077 \times 10^{10} exp(-148000/RT)$
$\text{Biomass} \longrightarrow 1.602\,Char$	$3.269 \times 10^6 exp(-111700/RT)$
$H_2O_{(l)} \longrightarrow H_2O_{(g)}$	$5.13 \times 10^6 exp(-87900/RT)$
Tar Cracking	[1/s]
$Tar_1 \longrightarrow \cdot 22\,Tar_2 + 1.5709\,CO + \cdot 1970\,CO_2 + \cdot 4304\,CH_4 + \cdot 6704\,H_2$	$2.30 \times 10^4 exp(-80000/RT)$
Gas-Phase Combustion Reactions	$[mol/cm^3 s]$
$CO + H_2O \longleftrightarrow H_2 + CO_2$	$2.780 \times 10^6 exp(-1510/T)\,[[CO][H_2O] - [CO_2][H_2]/K_p(T)]$
$2\,CO + O_2 \longrightarrow 2\,CO_2$	$3.980 \times 10^{(}14) exp(-20119/T)[CO][O_2]^{1.25}[H_2O]^{.5}$
$2\,H_2 + O_2 \longrightarrow 2\,H_2O$	$2.196 \times 10^{12} exp(-13127/T)[H_2][O_2]$
$CH_4 + 2\,O_2 \longrightarrow CO_2 + 2\,H_2O$	$5.16 \times 10^{13} T^{-1} exp(-15699/T)[CH_4][O_2]$
Heterogenous Char Reactions	
$C + O_2 \longrightarrow CO_2$	$1.5 \times 10^6 exp(-13078/T) p_{O_2}[C]$
$C + CO_2 \longrightarrow 2\,CO$	$3.1 \times 10^6 exp(-215000/RT) p_{CO_2}^{.38}[C]$
$C + H_2O \longrightarrow CO + H_2$	$2.6 \times 10^8 exp(-237000/RT) p_{H_2O}^{.57}[C]$

3.3 Biomass devolatilization model

Biomass devolatilization is a complex physiochemical process, coupling the kinetics of the primary pyrolysis reactions with the external and internal heat transfer effects at the particle level. In this study, a detailed particle scale model developed by Stark [3], incorporating both the detailed chemical kinetics and the heat transfer effects, was employed to describe biomass devolatilization.

The particle devolatilization model used the primary pyrolysis reaction mechanism developed by the CRECK group [9] to describe the conversion of solid biomass to gaseous primary pyrolysis products and residual char. The CRECK primary pyrolysis mechanism represented the overall biomass degradation through the individual decompositions of the biomass constituents: cellulose, hemicellulose and lignin. The CRECK primary pyrolysis mechanism had been rigorously validated and was shown to predict the mass loss curves of cellulose, hemicellulose and lignin under different particle heating rates ([3], [96]).

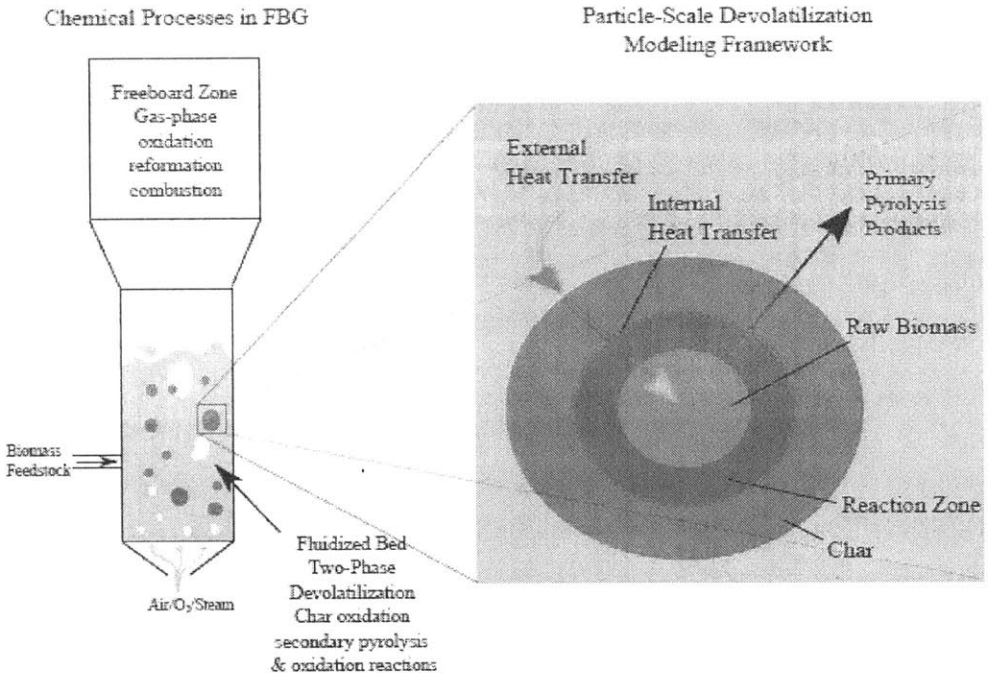

Figure 3-3: Biomass Devolatilization was described using a particle scale model developed by Stark, incorporating the heat transfer effects with detailed chemical kinetics ([3], [8])

An accurate particle scale devolatilization model is essential because devolatilization product composition is significantly impacted by the various processes occurring at the particle level. In particular, the biomass particle radius (along with the reactor temperature) plays an important role in the dynamics of the devolatilization process. Under fluidized bed gasifier conditions, primary pyrolysis is characterized by large heat transfer coefficients at high temperatures. Small biomass particles (<1mm) exhibit similar devolatilization dynamics irrespective of the reactor temperature, due to the negligible internal heat transfer effects. However, large particles behave differently under different temperatures: At low temperatures, the particle exhibits a mixed kinetic and heat transfer control. On the other hand, at high temperatures, devolatilization occurs under a purely internal heat transfer control since the onset of reactions occurs instantaneously due to the faster external heat transfer.

The devolatilization product composition obtained from the particle scale model serves as the input to the reactor network model of the biomass gasifier. Details on the reactor network modeling of biomass gasification are discussed in the next section.

3.4 Reactor Network Modeling of Biomass Gasification

While an accurate chemistry model plays a very important role in predicting the outlet gas composition, it is equally important to have a high-fidelity hydrodynamic model to describe the transport processes inside the gasifier. This section gives a brief description of the reactor network model (RNM) of the fluidized bed biomass gasifier that had been developed by Stark et al [8].

The reactor network model used a set of ideal chemical reactors to represent the different regions inside the biomass gasifier. While the dense bubbling bed region was represented as an isothermal continuously stirred reactor (CSTR), the freeboard was modeled as an isothermal plug flow reactor (PFR). The CSTR assumption was valid when the bed was well mixed and the bubbles were relatively small. When the freeboard had low solids concentration due to negligible axial mixing, the PFR assumption applied as well. The isothermal assumption for the reactors was valid when the temperature distribution inside the gasifier remained uniform due to external heating.

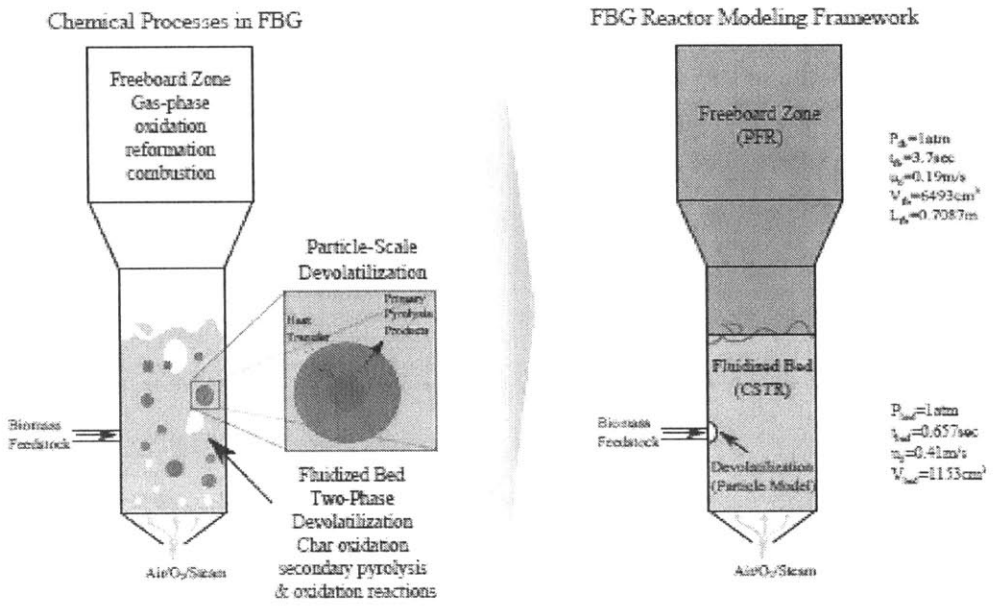

Figure 3-4: Fluidized bed biomass gasifier, represented as a network of ideal chemical reactors. Bubbling bed was represented using a continuously stirred reactor and the freeboard was modeled as plug flow reactor (reproduced from Stark et al. [8])

The biomass devolatilization products, obtained from the single particle model, and the incoming gasifying agent served as the input conditions to the CSTR and the CSTR conservation equations were solved to obtain the gas composition at the top of the bubbling bed. The output gas composition from the CSTR served as the input to the PFR, and the PFR equations were then solved to evaluate the outlet product composition. Either a detailed secondary homogenous gas phase reaction mechanism such as the detailed CRECK kinetic scheme or the homogenous gas phase reactions from the global CFD chemistry model could be employed to evaluate the chemical source terms (production/destruction of species due to the chemical reactions) in the conservation equations.

To account for the catalytic effects of the bed material and char on the water-gas shift (WGS) reaction in the bed, the CSTR used faster WGS kinetic rate parameters from experiments under similar conditions ([23], [97]).

Depending on the operating conditions, the heterogeneous char reactions were modeled using the char conversion model described in the next section.

3.5 Char conversion model

This section gives a brief description of the char gasification model, developed by Bates et al.[98]. In fluidized bed biomass gasification, the input biomass feedstock undergoes devolatilization to produce primary pyrolysis products as well as residual char, composed mostly of carbon. The evolution of char particles inside the fluidized bed involves two important physical/chemical processes. While the char particles undergo attrition inside the bed to produce fines that eventually get elutriated out of the gasifier, they also react with steam and CO_2 in the gasifier environment to produce syngas. These processes are interdependent on each other: the weakening in the char structure due to the gasification reactions results in the breakup of char particles. The attrition of the char particles results in the production of significant amounts of fines that get elutriated out of the gasifier. This results in shorter residence times for the particles to undergo gasification reactions with steam/CO_2, and subsequently results in lower char conversion.

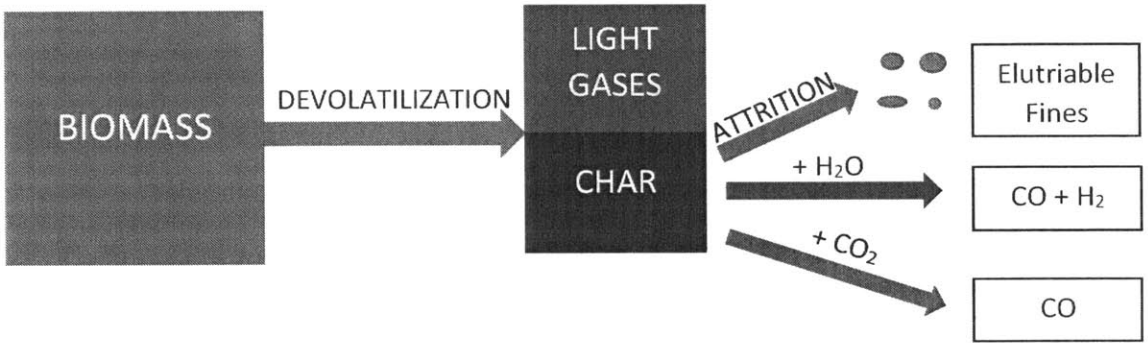

Figure 3-5: Schematic of the char gasification model, considering the gasification assisted attrition phenomena, developed by Bates et al. [98]. Char produced during devolatilization underwent gasification reactions with steam and CO_2, and attrition to produce char fines that was elutriated out of the gasifier

A good char conversion model is essential for an accurate simulation of the gasifier, since it affects several important operating performance metrics such as the overall carbon conversion, the energy content of the output syngas and the net cold gas efficiency of the gasifier. In this work, the steady-state char gasification model is employed for the steam gasification simulations.

The transient char gasification model, developed by Bates et al. [98], evaluated the reacting fraction of char, after accounting for the gasification assisted attrition phenomena using a conversion-dependent structural function. The steady state values of the char gasified for a continuously fed system were obtained using residence time averaging of the transient model

results. The transient gasification model assumed that the internal and external mass transfer effects were much faster compared to chemical kinetics. In addition, the char fines were assumed to be elutriated out of the gasifier as soon as they were formed. This assumption was valid under oxygen free conditions when the residence time of the char fines was much smaller than the reaction timescale for the gasification reactions.

3.6 Motivation for a better global chemistry model

In this section, the various sub-models described previously, are assembled together to study the accuracy of the Stark global chemistry in predicting the tar concentration at the gasifier outlet. A schematic of the simulation procedure is presented in Figure 3-6.

The global chemistry model proposed by Stark [3] is used in conjunction with the particle scale model of the biomass devolatilization process and the Reactor Network model to simulate the air-blown gasifier experiments carried out by van Paasen and Kiel [13]. A summary of the simulation conditions considered in this study is presented in Table 3-2.

Table 3-2: Simulation conditions employed in accordance with the van Paasen and Kiel experiments [13]

Simulation conditions	
Biomass feedstock	Beech wood (0.75-2mm)
Fluidizing medium	Silica sand (270 μm)
Fluidizing agent	Air
Bed diameter (in m)	0.074
Biomass feed rate (in kg/hr)	1
Bed temperature (in K)	973-1273
Pressure (in atm)	1
Air equivalence ratio	0.25

As emphasized previously, an accurate prediction of the tar concentrations encountered in the gasifier is critical towards the evaluation of the gasifier design using reactor network simulations. While inaccuracies in any of the sub-models could result in erroneous predictions of the tar concentration, the importance of the chemistry sub-model in achieving accurate predictions is examined here. Hence, the tar predictions obtained using the Stark global chemistry model are compared with the experimentally measured values and the tar concentration predicted using the more detailed CRECK chemical mechanism in the same reactor network model for the gasifier.

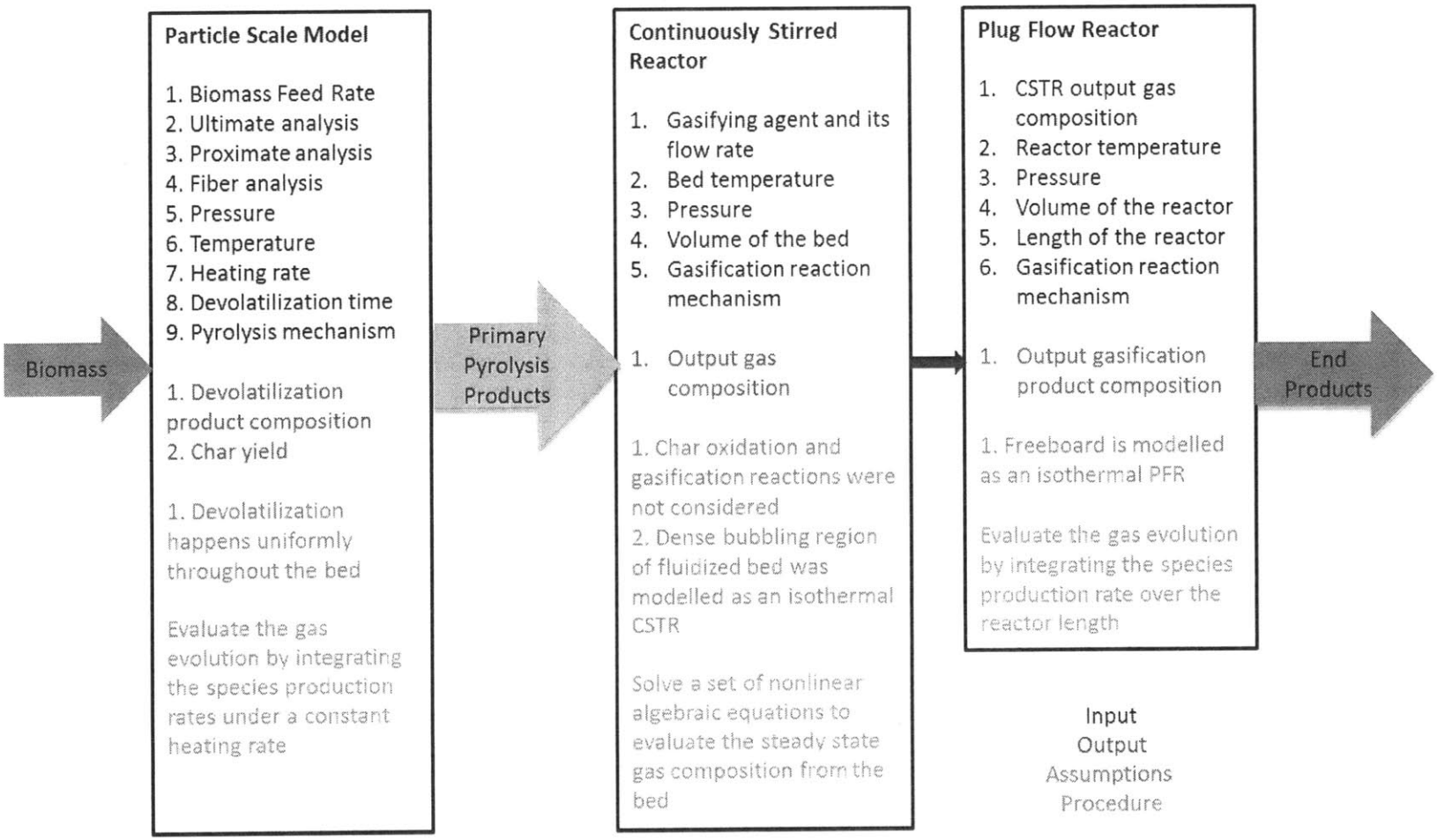

Figure 3-6: Details on the different sub-models used in the Reactor Network Simulations of the Fluidized bed biomass gasifier. The different assumptions, the solution procedure and the required input conditions for each of these sub-models are listed

The total tar concentration at the gasifier outlet is calculated as the sum of the individual concentrations of all the C_6+ species (species with more than 6 carbon atoms) in the synthetic gas. The predicted total tar concentrations using the Stark global model and the detailed CRECK mechanism for various gasification temperatures are plotted along with the experimentally measured total tar concentrations, reported by van Paasen and Kiel [13] and Narvaez et al. [99].

It can be seen from Figure 3-7 that the Stark global chemistry model over-predicts the total tar formation by almost an order of magnitude, while the corresponding predictions obtained using the detailed CRECK mechanism are in very good agreement with the experimentally measured values. In addition, the predictions of the major gas species concentrations evaluated using the Stark global chemistry model have large discrepancies with the experimentally observed values. The significant errors in the Stark global model predictions for total tar and major gas concentrations give rise to the need to develop a more accurate global chemistry model that could better predict these important quantities with higher precision.

A detailed discussion on the development of a more accurate global chemistry model is presented in the next section.

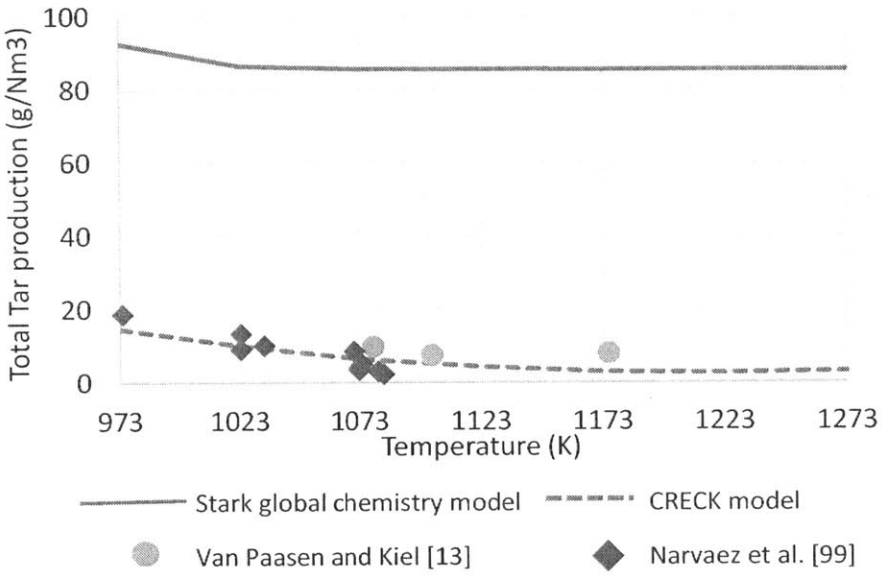

Figure 3-7: Comparison of the total tar predictions obtained using the Stark global chemistry model and the CRECK model with the experimental observations ([13], [99]). Stark global model predicts significantly higher amounts of tars than the detailed CRECK mechanism predictions and experimental values

3.7 New global chemistry model development and validation

Since an accurate understanding of the variation in the total tar concentration with gasification conditions is crucial towards operating the gasifier efficiently, a new global chemistry model is developed that better describes tar evolution inside the gasifier than the Stark global model. The global primary tar cracking reaction from the Stark global model is modified to represent the actual conversion pathways undergone by the primary tars produced during biomass devolatilization.

Depending on the gasification conditions employed, primary tars decompose along different reaction pathways to produce light gases (CO, CO_2, H_2, H_2O and CH_4) and secondary tars. Li and Suzuki [7] reported that primary tars underwent reforming reactions in the presence of steam to produce light gases and inert/refractory secondary tars. When oxygen was present in the gasifier environment, primary tars decomposed more rapidly to produce predominantly light gases and small amounts of secondary tars.

This section considers the two gasification conditions separately: a global chemistry model for air-blown gasification conditions is developed first, followed by a different global model for steam gasification. These global models are developed based on the primary tar composition in the devolatilization products for the specific set of operating conditions under consideration and hence, their applicability to other operating conditions is unknown.

3.7.1 Air-blown gasification conditions

The objective of this section is to develop a global chemistry model describing the evolution of the primary pyrolysis products inside the gasifier to produce major gases and tars at the gasifier outlet. Starting from the primary pyrolysis composition obtained using the particle scale model described in Section 3.2, a new global model based on Stark's global chemistry model is developed.

In the previous section, Stark's global chemistry model was shown to predict a significantly high amount of tar compared to the observed values in the van Paasen and Kiel experiments [13]. This is because the model was developed empirically for a specific set of operating conditions and therefore, cannot be reliably applied outside those conditions. Hence, a new global chemistry model is developed, including a more accurate primary tar cracking reaction that better describes the reaction pathways of the primary tar precursors inside the gasifier under the specific set of operating conditions under consideration.

The primary pyrolysis product composition is obtained using the particle scale model developed by Stark[3]. A particle diameter of 1mm is used in the model, representative of the biomass particle sizes used in the van Paasen and Kiel experiments. Since the CRECK pyrolysis mechanism used in the devolatilization model requires the compositions of cellulose, hemicellulose and lignin in the biomass feedstock as inputs, these are determined from the ultimate analysis for beech wood and a reported lignin fraction of 24% daf (dry ash-free basis). Moreover, a moisture content of 10.2% is considered in the model, as reported in the experiments. For the case of a bed temperature at 1073K, the devolatilization product composition obtained using the particle scale model is reported in Table 3-3.

Table 3-3: Devolatilization product composition for beech feedstock, obtained from the single particle model at temperature T=1073K

Species	**Mass Fraction**
Hydrogen	0.0056
Steam	0.0487
Carbon Monoxide	0.1398
Carbon Dioxide	0.1424
Formaldehyde	0.0585
Methane	0.0386
Methanol	0.0409
Glyoxal	0.0171
Ethylene	0.035
Acetaldehyde	0.01271
Acetic acid/HAA	0.0673
Ethanol	0.0176
Acetone	0.0267
Phenol	0.0053
5-hydroxy methyl furfural	0.0372
Levoglucosan	**0.2572**
Sinapaldehyde	0.0303

Levoglucosan (LVG) forms the largest fraction of the primary pyrolysis products in terms of mass fraction; carbon monoxide and carbon dioxide being the other major components. A number of

other compounds such as formaldehyde, Hydroxy-acetaldehyde (HAA) and ethylene are also formed. While these small aliphatic compounds degrade into light gases in the presence of oxygen, levoglucosan undergoes secondary reactions to produce light gases and small amounts of benzene and other tarry compounds. Hence, levoglucosan is selected as a model compound to represent the primary tars (Tar_1) produced during biomass devolatilization.

3.7.1.1 Global primary tar cracking reaction for air-blown gasification conditions

The global primary tar cracking reaction describing the decomposition of the primary tars is then developed by examining the decomposition of levoglucosan under similar gasification conditions. The decomposition of levoglucosan, under the van Paasen and Kiel gasification conditions described in Table 3-2, is modeled using the reactor network model presented in Section 3-4 in conjunction with the detailed CRECK chemical kinetic scheme. The input conditions used in the simulation are tabulated in Table 3-4.

The catalytic effects of the bed material, char and ash on the water-gas shift (WGS) kinetics are represented by using different WGS kinetics for the different regions of the gasifier. The faster WGS kinetics proposed by Biba et al. [97] is employed in the bed, while the original WGS kinetics (from the CRECK model) is used in the freeboard region.

No char gasification reactions are included since the motivation of this simulation is to examine the decomposition of levoglucosan under the current set of operating conditions.

Table 3-4: Input gas composition to the Reactor Network model of the air-blown gasifier for the evaluation of LVG decomposition characteristics (T=1273 K)

Species	Input Mass Fraction
N_2	0.4845
O_2	0.1304
Levoglucosan	0.3851

The mass fractions of the different products obtained from levoglucosan decomposition at temperature T=1273K are presented in Table 3-5. Consistent with the terminology used in the Stark global chemistry model, a single lumped pseudo-species is used to describe the total tars

produced and it is obtained as the sum of the concentrations of all the C_6+ species (species with more than 6 carbon atoms), including benzene.

Since the primary tar cracking reaction considers only the five major gas species and a lumped inert tar species, the mass fractions obtained for these species are normalized to ensure that the final product composition consists of only these species. The errors associated with this normalization are negligible, since the total sum of the concentrations of these species already form more than 99% of the output products. The normalized mass fractions of these species are given below in Table 3-5.

Table 3-5: Product composition of levoglucosan decomposition in the presence of air at temperature T =1273K, obtained using the Reactor Network model

Species	**Mass Fractions**
CH_4	0.0178
CO	0.2554
CO_2	0.1539
H_2	0.0106
H_2O	0.0745
Tar_2 (Secondary tars)	0.00336
N_2	0.4845

Based on these mass fractions (and the corresponding mole fractions) of each of the products, the new global primary tar cracking reaction is formulated as,

$$\mathbf{1\ Tar_1 + 1.7166\ O_2 \rightarrow 2.2071\ H_2 + 1.7412\ H_2O + 3.8392\ CO + 1.4723\ CO_2 + 0.4681\ CH_4 + 0.01809\ Tar_2}$$

Because of the lack of data on the reaction kinetics for the new reaction, the original tar cracking kinetics used in the Stark global chemistry model (obtained from Gerber et al. [28]) is employed here: this kinetic rate equation exhibits a first order dependence on the primary tar (Tar_1) concentration.

Rate Expression for the Primary Tar Cracking Reaction (from [3],[28]):

$$\frac{d[Tar_1]}{dt} = -2.30x10^4 \exp\left(-\frac{80000}{RT}\right)[Tar_1]$$

(R in J/mole-K and T in K)

Because the primary tar cracking reaction is developed in a global manner employing a single pseudo-species to represent all the secondary tar compounds, there are small errors (<2%) in the elemental balance across the global reaction. However, the overall mass balance across the reaction is conserved, as depicted in Table 3-6.

Table 3-6: Overall mass balance across the reactants and products for the global primary tar cracking reaction

Species	**Molecular Mass**	**Moles**	**Net Mass**
Tar1 (LVG)	162.14	1	162.14
O_2	31.9988	1.7166	54.92914008
Sum (Reactants)			**217.0691401**
Tar_2 (C_6H_6)	78.11364	0.0181	1.413856884
H_2	2.01588	2.2071	4.449248748
CO	28.0104	3.8392	107.5375277
CO_2	44.0098	1.4723	64.79562854
CH_4	16.04276	0.4681	7.509615956
H_2O	18.01528	1.7412	31.36820554
Sum (Products)			**217.0740833**
Relative Error (Products-Reactants)/Reactants			**2.27728E-05**

Table 3-7: Elemental balance of Carbon, Hydrogen and Oxygen across the reactants and products for the global primary tar cracking reaction

Species	Mass of Carbon	Mass of hydrogen	Mass of oxygen
Tar_1 (LVG)	72.066	10.0794	79.997
O_2	0	0	54.92914008
Sum (Reactants)	**72.066**	**10.0794**	**134.9261401**
Tar_2 (C_6H_6)	1.3043946	0.109462284	0
H_2	0	4.449248748	0
CO	46.1126312	0	61.42489648
CO_2	17.6837953	0	47.11183324
CH_4	5.6223491	1.887266856	0
H_2O	0	3.510050256	27.85815528
Sum (Products)	**70.7231702**	**9.956028144**	**136.394885**
Relative Error (Products-Reactants)/Reactants	**0.018633333**	**0.01224**	**0.010885548**

3.7.2 New global model validation

The new global chemistry model is then assembled by replacing the original global tar cracking reaction from the Stark global chemistry model with the new global primary tar cracking reaction, while the drying reaction and the secondary gas phase reactions remain unchanged. The devolatilization reaction, describing the degradation of biomass into primary tars, is modified to reflect the use of levoglucosan as the model compound for primary tars. The other devolatilization reactions describing the degradation of biomass into light gases and char remain unaffected. The newly assembled global chemistry model, listing all the reactions, is presented in Table 3-8.

Employing the particle scale model for devolatilization and the reactor network model described previously, the global model predictions are studied for the van Paasen and Kiel experimental conditions summarized in Table 3-2. The global model predictions of the major gas species and

total tar concentrations for the different gasification temperatures are then compared with the corresponding predictions using the detailed CRECK mechanism and experimentally measured values.

In these simulations, faster water-gas shift kinetics proposed by Biba et al. [97] are used in the bed region to account for the catalytic effects of the bed material, char and ash.

The char gasification reactions are not included since the average residence time of the char particles under the given reactor conditions is found to be much shorter than the characteristic for the gasification reactions. Stark et al [8] estimated the characteristic residence time for the wood-chip char particles to be ~110s. On the other hand, the characteristic time for gasification at 800 °C was found to be almost an order of magnitude higher (~1100-4000 seconds) [100].

3.7.2.1 Results and Discussion

The global model predictions for the major gas and total tar concentration are plotted in Figure 3-8, along with the corresponding predictions using the detailed CRECK mechanism and experimentally measured values. While the new global model is able to accurately predict the concentrations of methane, carbon monoxide and carbon dioxide, both hydrogen and steam are over predicted. However, in both the cases, the trends are correctly predicted for all the major gas species. There were significant uncertainties with the steam values reported in the experiments since the steam concentration was not measured directly and instead, was calculated from the concentrations of the other species. The total tar concentrations predicted by the global chemistry model are found to be in very good agreement with the experimental observations as well as the predictions obtained using the CRECK detailed chemistry mechanism, at all temperatures.

Figure 3-9 depicts the evolution of the major gases and tars inside the gasifier, evaluated using the reactor network simulations employing the new global model, for a bed temperature of 1123K. It can be seen that a large fraction (~90%) of the primary tar (Tar_1) is decomposed by the end of the bed region. The remaining fraction decomposes into the major gases and secondary tars in the initial part of the freeboard. The subsequent evolution of the major gases is governed by the water-gas shift reaction and it can be observed that the major gas concentrations remain almost constant due to the slow water-gas shift kinetics employed in the freeboard.

The development of a similar global chemistry model for the steam-blown gasification conditions is considered in the next section.

Table 3-8: Global chemistry model for air-blown gasification conditions

Devolatilization	Biomass → 7.7872 H_2 + 4.7274 CO + 4.3016 CO_2 + 1.7109 CH_4 + 6.9712 H_2O
	Biomass → 3.0249 Tar_1
	Biomass → 40.8343 Char
Drying	H_2O (l) → H_2O (g)
Primary tar cracking (new)	**Tar_1 + 1.7166 O_2 → 0.0181 Tar_2 + 3.8392 CO + 1.4723 CO_2 + 0.4681 CH_4 + 2.2071 H_2 + 1.7412 H_2O**
Secondary gas phase reactions	CO + H_2O → CO_2 + H_2
	2 CO + O_2 → 2 CO_2
	2H_2 + O_2 → 2 H_2O
	CH_4 + 2 O_2 → CO_2 + 2 H_2O

Figure 3-8: Major gas species and total tar concentrations predicted using the global chemistry model and the detailed CRECK mechanism for van Paasen and Kiel experimental conditions [13]. The model predictions for all the species (Except H_2O) are in good agreement with experiments

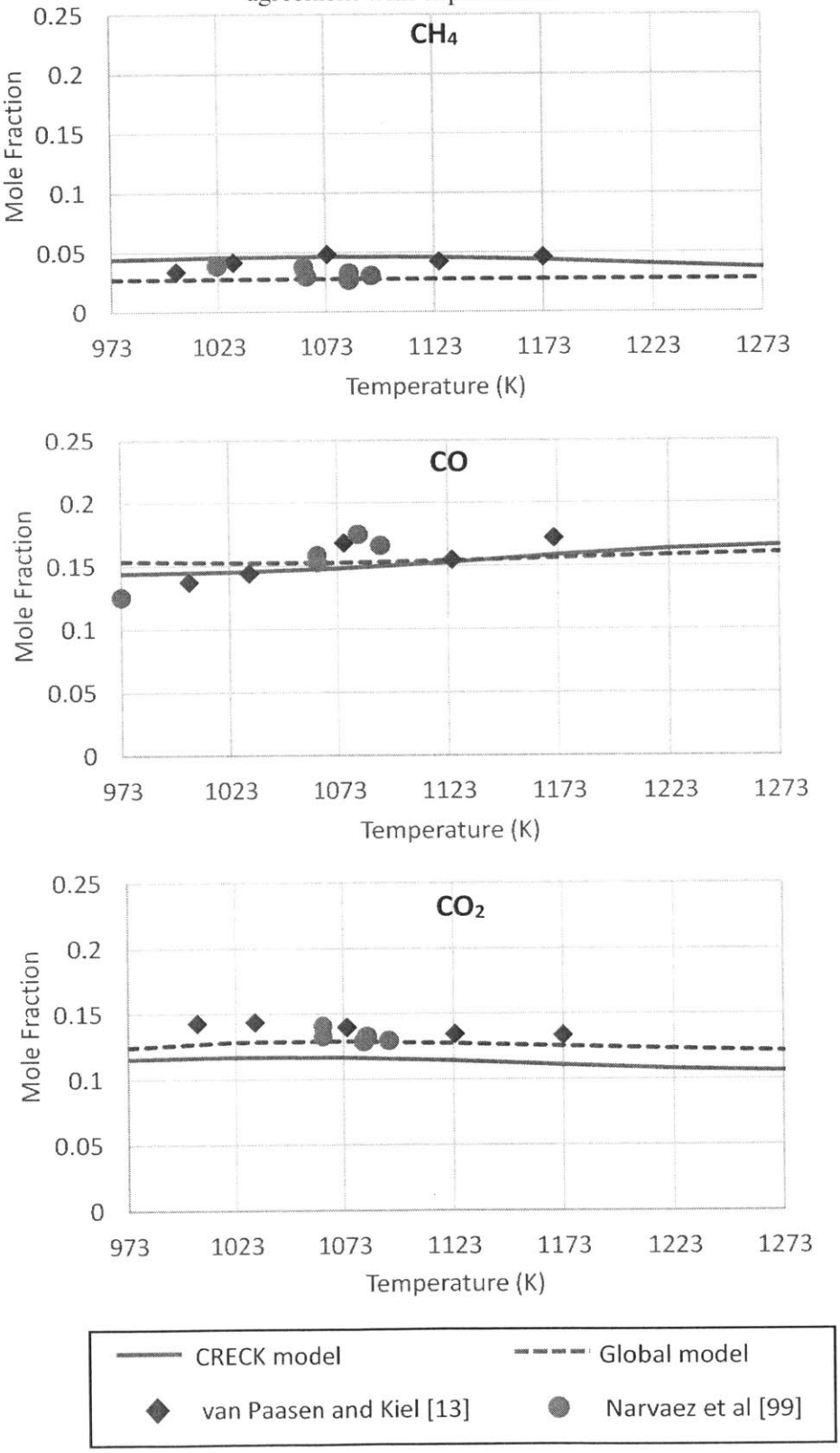

Figure 3-8 (contd.): Major gas species and total tar concentrations predicted using the global chemistry model and the detailed CRECK mechanism for van Paasen and Kiel experimental conditions [13]. The model predictions for all the species (Except H2O) are in good agreement with experiments

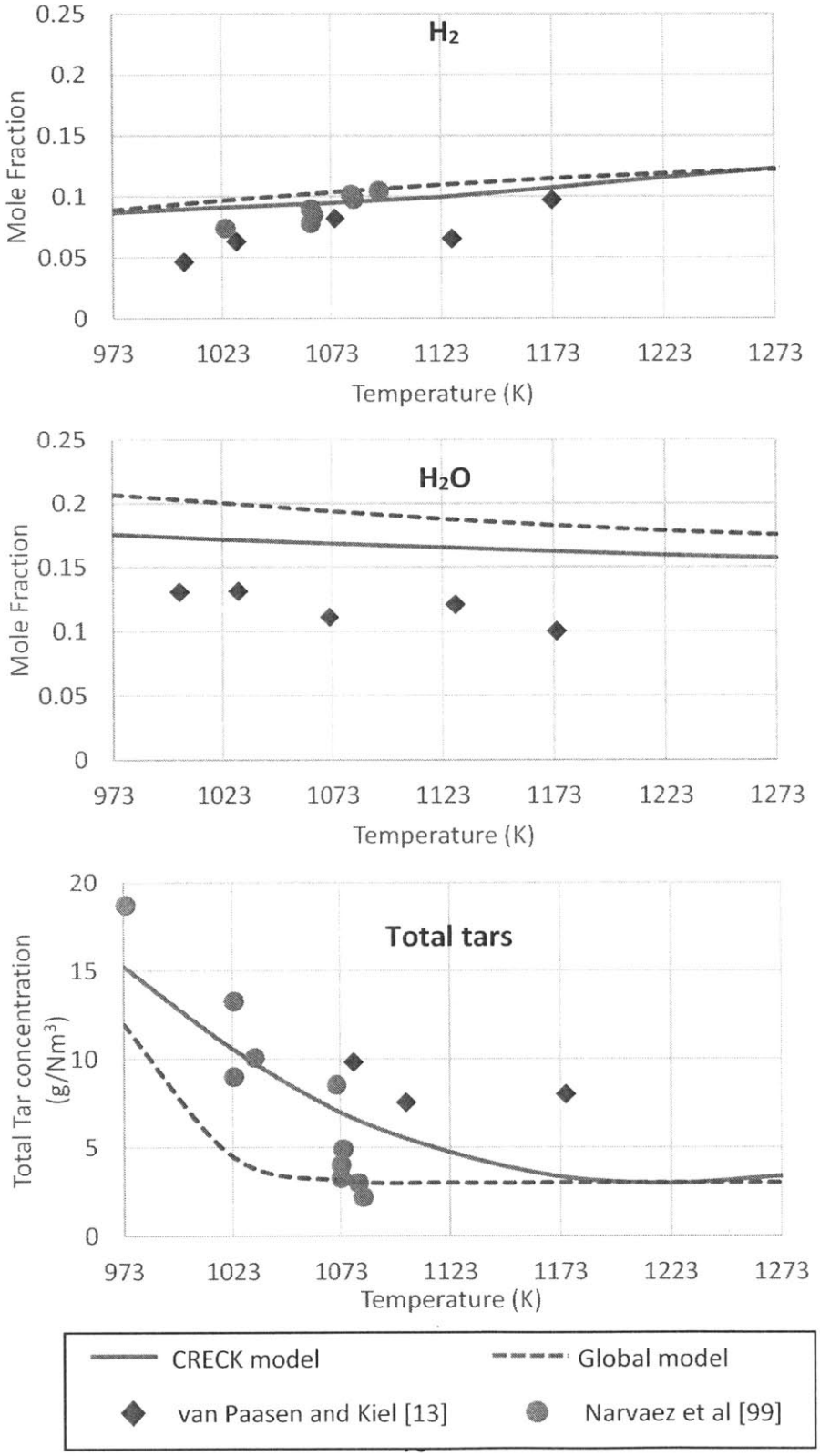

Figure 3-9: Evolution of the major gas species and tars along the gasifier at bed temperature T_b = 1123 K, evaluated using the new global chemistry model Tar_1 is completely consumed by the early portion of the freeboard

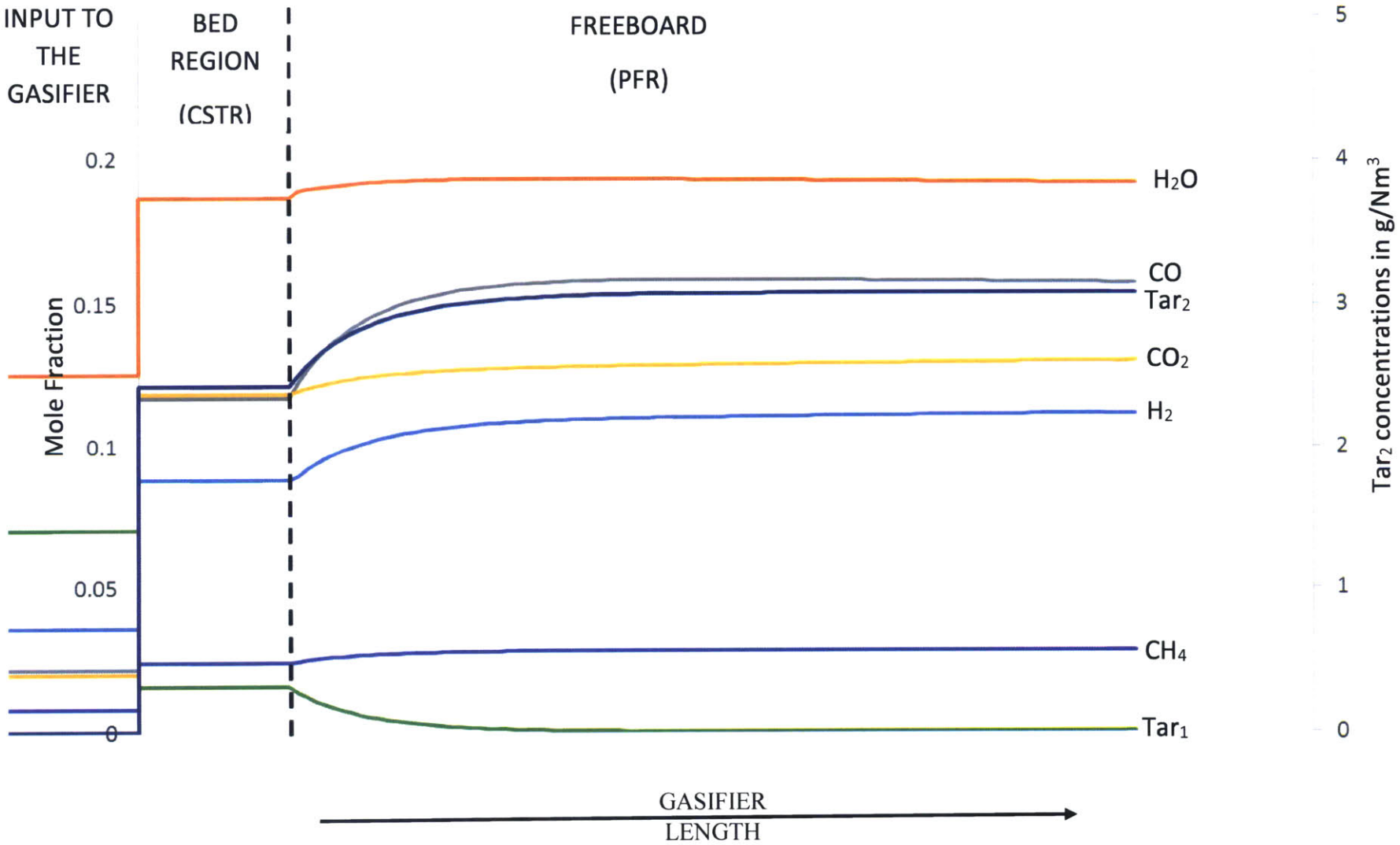

3.7.3 Steam-blown gasification conditions

This section considers the biomass gasification experiments conducted at the National Renewable Energy Laboratory (NREL) under steam conditions [101]. Details on the experimental conditions are presented in Table 3-9.

Similar to the previous section, the devolatilization product composition for the biomass is obtained using the particle scale model, described in Section 3.2. Using the ultimate analysis data for Oak, the particle scale model is run for the different bed temperatures (750°C-850°C), assuming a particle diameter of 1mm, representative of the experiments. The devolatilization product composition obtained using the particle scale model for 800°C, is tabulated in Table 3-10.

Table 3-9: Gasification conditions employed in the NREL experiments [101]

Simulation conditions	
Biomass feedstock	Oak (0.75-2mm)
Fluidizing agent	Steam
Biomass feed rate (in kg/hr)	0.8
Bed temperature (in °C)	750-850
Pressure (in atm)	1.1547
Steam flow rate (in kg/hr)	0.8

While levoglucosan (LVG) still forms a large portion of the volatiles in the devolatilization product output, there is also a significant amount of other volatile compounds present, such as 5-hydroxymethylfurfural (HMFU). While LVG predominantly decomposes into a mixture of light gases and small amounts of tarry compounds, HMFU decomposition produces carbon monoxide and significant amounts of benzene [9]. Hence, a different primary tar cracking reaction that better represents the primary tar evolution inside the gasifier, has been developed.

The volatiles, apart from the light gases, are grouped into two different categories, as depicted in Table 3-11. The first category included all the smaller volatile compounds and LVG that upon degradation, resulted predominantly in the production of a mixture of light gases, and very small amounts of tars. The secondary category is composed of the heavy volatile compounds, a major part of it being HMFU that produced significant amounts of benzene upon cracking.

In order to accurately capture the primary tar evolution in this case, the global primary tar cracking reaction should reflect the decomposition characteristics of both the categories of primary tars. Hence, the individual decomposition characteristics of the two tar categories are examined by considering the decomposition of the most significant species in each category. While levoglucosan is chosen as a model compound to represent the decomposition of Category 1 primary tars, HMFU is used to model the decomposition of Category 2 primary tars.

Table 3-10: Devolatilization product composition for Oak, obtained using the particle scale model (T = 800°C)

Species	**Mass Fraction**
Hydrogen	0.0007
Steam	0.1285
Carbon Monoxide	0.0988
Carbon Dioxide	0.1128
Formaldehyde	0.0666
Methane	0.0289
Methanol	0.0575
Glyoxal	0.031
Ethylene	0.0246
Acetaldehyde	0.0189
Acetic acid/HAA	0.1418
Ethanol	0.0074
Acetone	0.0559
Xylosan	0.0094
Phenol	0.0038
5-hydroxy methyl furfural	**0.0843**
Levoglucosan	**0.1088**
pCoumaryl alcohol	0.0083
Sinapaldehyde	0.01195

Table 3-11: List of the different devolatilization products belonging to the two primary tar groups

Category 1	**Category 2**
CH_2O (Formaldehyde)	C_6H_5OH (Phenol)
CH_3OH (Methanol)	$C_6H_6O_3$ (5-hydroxy methyl furfural)
$C_2H_2O_2$ (Glyoxal)	$C_9H_{10}O_2$ (pCoumaryl alcohol)
$C_2H_4O_2$ (Acetic acid/Hydroxy-acetaldehyde)	$C_{11}H_{12}O_4$ (Sinapaldehyde)
C_2H_5OH (Ethanol)	
C_3H_6O (Acetone)	
$C_5H_8O_4$ (Xylosan)	
$C_6H_{10}O_5$ (Levoglucosan)	

3.7.3.1 Global primary tar cracking reaction for steam-blown gasification conditions

Similar to the previous section, the new tar cracking reaction is formulated by studying the individual decomposition of the model compounds representing the primary tar species. In this case, since two model compounds are considered, the individual decompositions of both these species are separately considered.

The decomposition of levoglucosan in the presence of steam under the NREL gasifier conditions described in Table 3-12 is studied first. Using the reactor network model corresponding to the experimental conditions considered in [101], the following input conditions are used in the simulation and the detailed CRECK kinetic scheme is utilized to predict the output product composition. The water-gas shift kinetics proposed by Biba et al.[97] is used in the bed region, to account for the catalytic effects of the bed material and char.

Table 3-12: Input gas composition used to study the levoglucosan decomposition characteristics in the reactor network model of the steam-blown gasifier

Species	**Input Mass Fraction**
Steam	0.5576
Levoglucosan	0.4424

The mass fractions of the different products of levoglucosan decomposition are tabulated in Table 3-13. As noted before, levoglucosan degrades mostly into light gases, though there is a small

amount of tars that are formed. Similar to the previous sections, tars are calculated as the sum of the concentrations of all C_6+ species (species with more than 6 carbon atoms). Benzene, being the most abundant secondary tar, is used to represent the secondary tars, Tar_2, in the primary tar cracking reaction.

Table 3-13: Product composition of Levoglucosan degradation in the presence of steam for the NREL gasification conditions (T = 800° C)

Species	Mass Fractions
CH_4	0.0474
CO	0.1462
CO_2	0.3221
H_2	0.0268
Tar_2 (Secondary tars)	0.0067

Based on the output product composition presented in Table 3-11, a global tar cracking reaction to describe the degradation of levoglucosan in the presence of steam is formulated as,

$$\mathbf{1\ LVG + 2.172\ H_2O \rightarrow 4.865\ H_2 + 1.913\ CO + 2.682\ CO_2 + 1.084\ CH_4 + 0.0315\ Tar_2}$$

Similarly, the decomposition of 5-hydroxy methyl furfural is examined using the Reactor network model employing the CRECK detailed chemistry mechanism. The input conditions used in the simulation is given below in Table 3-14.

Table 3-14: Input gas composition used to study HMFU decomposition characteristics in the reactor network model of the steam-blown gasifier

Species	**Input Mass Fraction**
Steam	0.5576
HMFU	0.4424

The mass fractions of the different products of HMFU decomposition are tabulated in Table 3-15. As in the previous case, the total tar concentration is evaluated as the sum of the concentrations of all C_6+ species (species with more than 6 carbon atoms) and benzene is used as the model compound to represent the secondary tars, Tar_2. It can be seen that that HMFU decomposition results in the production of significantly higher amounts of secondary tars, unlike levoglucosan decomposition.

Table 3-15: Product composition of HMFU degradation in the presence of steam for the NREL gasification conditions (T = 800° C)

Species	Mass Fractions
CH_4	0.0095
CO	0.1176
CO_2	0.2664
H_2	0.0210
Tar_2 (Secondary tars)	0.1090

Based on these output product compositions, the global decomposition reaction of HMFU in the presence of steam is obtained as,

1 HMFU + 1.2835 H_2O → 2.971 H_2 + 1.197 CO + 1.726 CO_2 + 0.1679 CH_4 + 0.3979 Tar_2

While the individual decomposition reactions of levoglucosan and HMFU are representative of the cracking reactions of the two types of primary tars encountered in biomass devolatilization, it is desirable to use a single pseudo-species to represent the primary tars, since the devolatilization mechanism considers only a single primary tar pseudo-species.

A new global primary tar cracking reaction is then obtained by combining the Levoglucosan and HMFU decomposition reactions based on the relative mass fractions of the two primary tar categories. The calculated relative mass fractions of the primary tar categories at the three temperatures considered in the study are given below in Table 3-16. It is observed that the fractions remain almost constant across the range of temperatures, supporting the validity of a single global primary tar cracking reaction across all the gasification temperatures considered.

Table 3-16: Relative mass fractions of the two categories of primary tars in the devolatilization product composition

	750 °C	**800 °C**	**850 °C**
Category 1 tars	82.8	82.8	82.9
Category 2 tars	17.2	17.2	17.1

The new tar cracking reaction, encompassing the decomposition characteristics of both levoglucosan and HMFU in the presence of steam, is then obtained as,

1 Tar1 + 2.0995 H_2O → 4.7196 H_2 + 1.8611 CO + 2.6175 CO_2 + 0.9631 CH_4 + 0.0983 Tar_2

Where Tar_1 is represented by Levoglucosan and Tar_2 is described using benzene. The lack of kinetic data for the proposed tar cracking reaction necessitates the use of the tar cracking kinetics employed in the Stark global chemistry model.

Rate Expression for the Primary Tar Cracking Reaction (from [3],[28]):

$$\frac{d[Tar_1]}{dt} = -2.30x10^4 \exp\left(-\frac{80000}{RT}\right)[$$

(R in J/mole-K and T in K)

Similar to the air gasification case, the new global primary tar cracking reaction does not completely satisfy the elemental balance across the reactants and products even though the overall mass balance is conserved. This is because the global reaction employs a single pseudo-species with a constant chemical composition to describe all the different secondary tars produced in the gasifier. The overall mass balance and the atomic balance of the individual elements (carbon, hydrogen and oxygen) is presented in Tables 3-17 and 3-18.

The new global chemistry model for steam-blown gasification conditions is then assembled by adding the new global primary tar cracking reaction with all the other relevant reactions from the Stark global model. Biomass devolatilization is described using three concurrent reactions representing the conversion of biomass into volatiles, gases and char. Secondary homogenous reactions include only the global primary tar cracking reaction and the water-gas shift reactions, since there is no oxygen present under the considered steam-gasification conditions. The heterogeneous char gasification reactions with CO_2 and steam complete the final component of the global model. The list of reactions in the new global model for steam-gasification conditions is presented in Table 3-19.

Table 3-17: Overall mass balance across the reactants and products for the global primary tar cracking reaction

Species	Molecular Mass	Moles	Net Mass
Tar_1 (LVG)	162.14	1	162.14
H_2O	18.01528	2.0995	37.82308036
Sum (Reactants)			**199.9630804**
Tar_2 (C_6H_6)	78.11364	0.0983	7.678570812
H_2	2.01588	4.7196	9.514147248
CO	28.0104	1.8611	52.13015544
CO_2	44.0098	2.6175	115.1956515
CH_4	16.04276	0.9631	15.45078216
Sum (Products)			**199.9693072**
Relative Error (Products-Reactants)/Reactants			**3.11397E-05**

Table 3-18: Elemental balance of Carbon, Hydrogen and Oxygen across the reactants and products for the global primary tar cracking reaction

Species	Mass of Carbon	Mass of hydrogen	Mass of oxygen
Tar_1 (LVG)	72.066	10.0794	79.997
H_2O	0	4.23234006	33.5907403
Sum (Reactants)	**72.066**	**14.31174006**	**113.5877403**
Tar_2 (C_6H_6)	7.0840878	0.594483012	0
H_2	0	9.514147248	0
CO	22.3536721	0	29.77648334
CO_2	31.4387925	0	83.756859
CH_4	11.5677941	3.882988056	0
Sum (Products)	**72.4443465**	**13.99161832**	**113.5333423**
Relative Error (Products-Reactants)/Reactants	**0.00525**	**0.022367772**	**0.000478907**

Table 3-19: Global chemistry model for steam-blown gasification conditions

Devolatilization	Biomass → 7.7872 H_2 + 4.7274 CO + 4.3016 CO_2 + 1.7109 CH_4 + 6.9712 H_2O
	Biomass → 3.0249 Tar_1
	Biomass → 40.8343 Char
Drying	H_2O (l) → H_2O (g)
Primary tar cracking	Tar_1 + 2.0995 H_2O → 0.0983 Tar_2 + 4.7196 H2 + 1.8611 CO + 2.6175 CO2 + 0.9631 CH4
Secondary gas phase reactions	CO + H_2O → CO_2 + H_2
Heterogeneous char reactions	C + CO_2 → 2 CO
	C + H_2O → CO + H_2

3.7.4 New global model validation

The accuracy of the new global chemistry model in predicting the major gas species and tar concentrations is evaluated for the NREL steam gasification experiments[101]. The global model predictions are compared with the corresponding predictions using the detailed CRECK mechanism and experimentally measured values. A schematic of the simulation procedure is presented in Figure 3-10.

The devolatilization output product composition obtained using the particle scale model from Section 3.3, which employed the CRECK primary pyrolysis mechanism, is used as the input condition to the Reactor Network model of the gasifier.

The heterogeneous char gasification reactions in the bed are represented by the char conversion model, described in Section 3.5. Using the char production rates calculated from the particle scale model and the relative fractions of the produced char that reacts with CO_2 and steam, the char gasification rate is calculated. The contribution of steam gasification towards the char conversion seems to reach a threshold around a value of 0.2, while the CO_2 gasification rate increases significantly with temperature. This threshold is likely attributed to the strong inhibition effect of high hydrogen concentrations (~20-25 vol. %) on the steam gasification rate.

Inputs
Steady state gas composition in the bed
Temperature
Pressure
Superficial gas velocity

CHAR CONVERSION MODEL

Output		
Temperature	X_H_2O	X_CO_2
750°C	0.197	0.354
800°C	0.159	0.465
850°C	0.161	0.612

Figure 3-10: Steady state char gasification rates, evaluated using the char conversion model (X_H_2O and X_CO_2 represent the char fractions gasified by H_2O and CO_2) respectively)

As in the case of air gasification, different water-gas shift (WGS) kinetics are employed for the different regions of the gasifier. The faster WGS kinetics from Gomez Barea [15] is employed in the bed, while the original WGS kinetics from the CRECK mechanism is used in the freeboard region.

Figure 3-11: Schematic of the different sub-models and simulation conditions used in the NREL steam gasification simulations

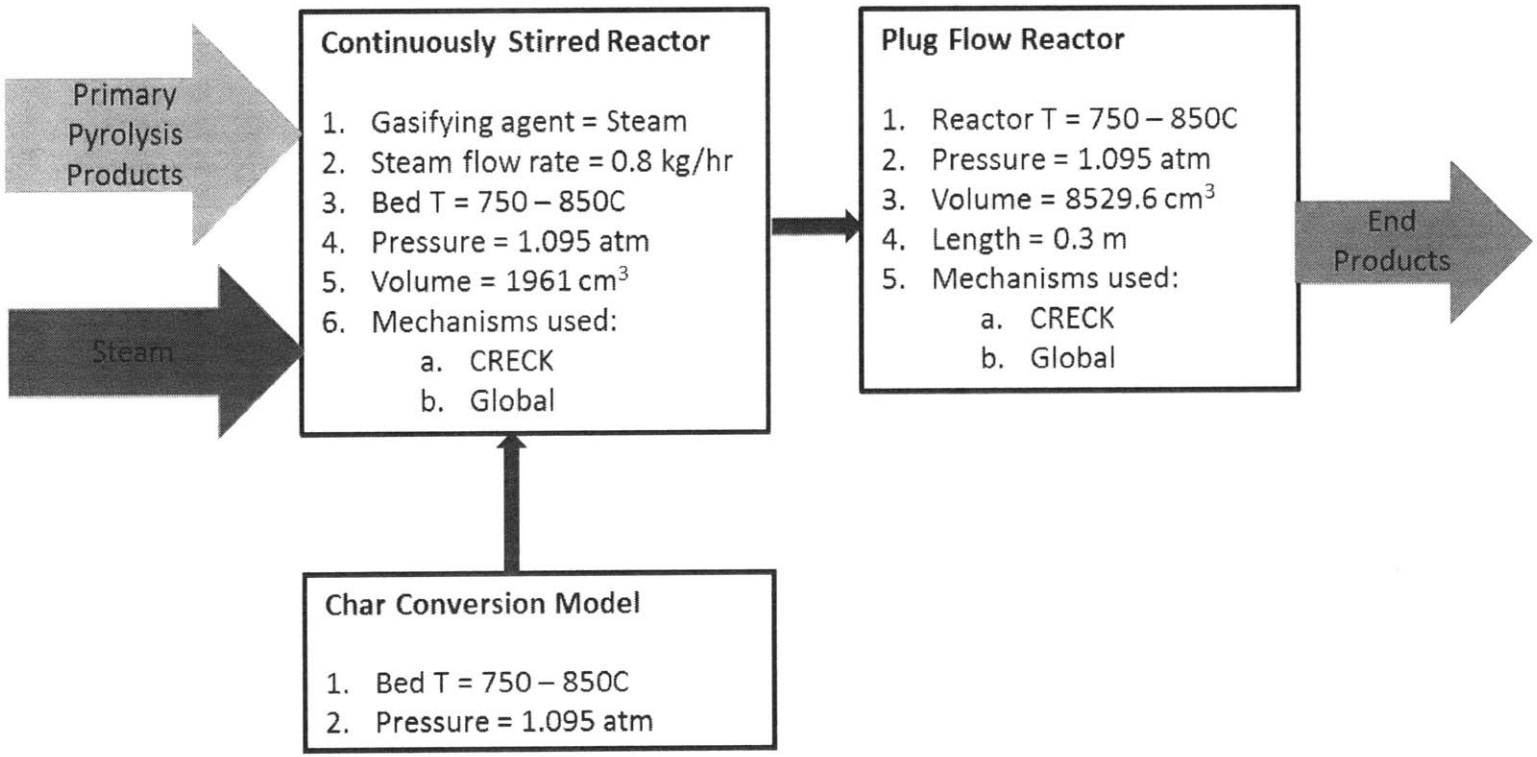

3.7.4.1 Results and Discussion

The global model predictions of the major gas and total tar concentration for the different gasification temperatures are plotted in Figure 3-12, along with the corresponding predictions using the detailed CRECK mechanism and experimentally measured values. It is observed that the global model is able to accurately predict all the major gas concentrations and the global model predictions are also in very good agreement with the detailed CRECK mechanism predictions. While both the global model and the CRECK mechanism over-predict the total tar concentrations, the trend of reduction in the tar amounts with gasification temperature is correctly captured.

Figure 3-13 and 3-14 depict the evolution of the major gas species and tars inside the gasifier, evaluated using the new global chemistry model for a bed temperature of 1073K. It can be seen that a large fraction of the primary tar decomposed within the bed region, while the remaining fraction decomposes in the freeboard. The primary tar decomposition rates are faster at higher temperatures and hence, larger amounts of light gases are produced within the bed region at higher temperatures. It is also observed that the variation in the secondary tar concentrations with the gasification temperature was very small. The variation in the major gas concentrations with the gasification temperature is due to the difference in the initial primary tar concentration from biomass devolatilization at the different gasification temperatures as well as the effect of faster water-gas shift reaction rates at higher temperatures.

Figure 3-12: Major Gas species and total tar concentrations predicted using the global chemistry model and the detailed CRECK mechanism for NREL gasification conditions [101]. Major gas species predictions are in good agreement with experiments, however the total tars are over-predicted by both the chemistry models

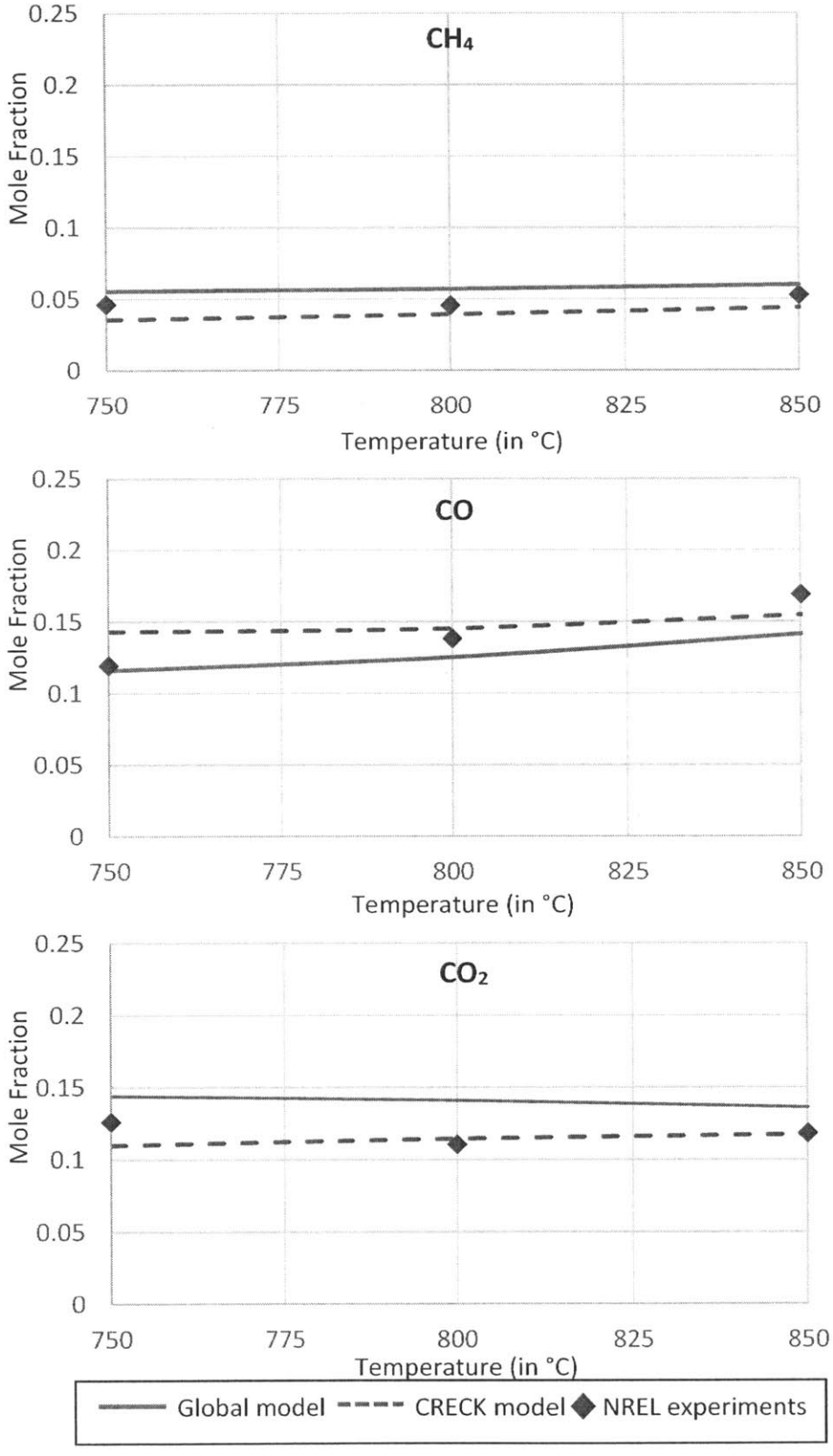

Figure 3-12 (contd.): Major Gas species and total tar concentrations predicted using the global chemistry model and the detailed CRECK mechanism for NREL gasification conditions [101]. Major gas species predictions are in good agreement with experiments, however the total tars are over-predicted by both the chemistry models

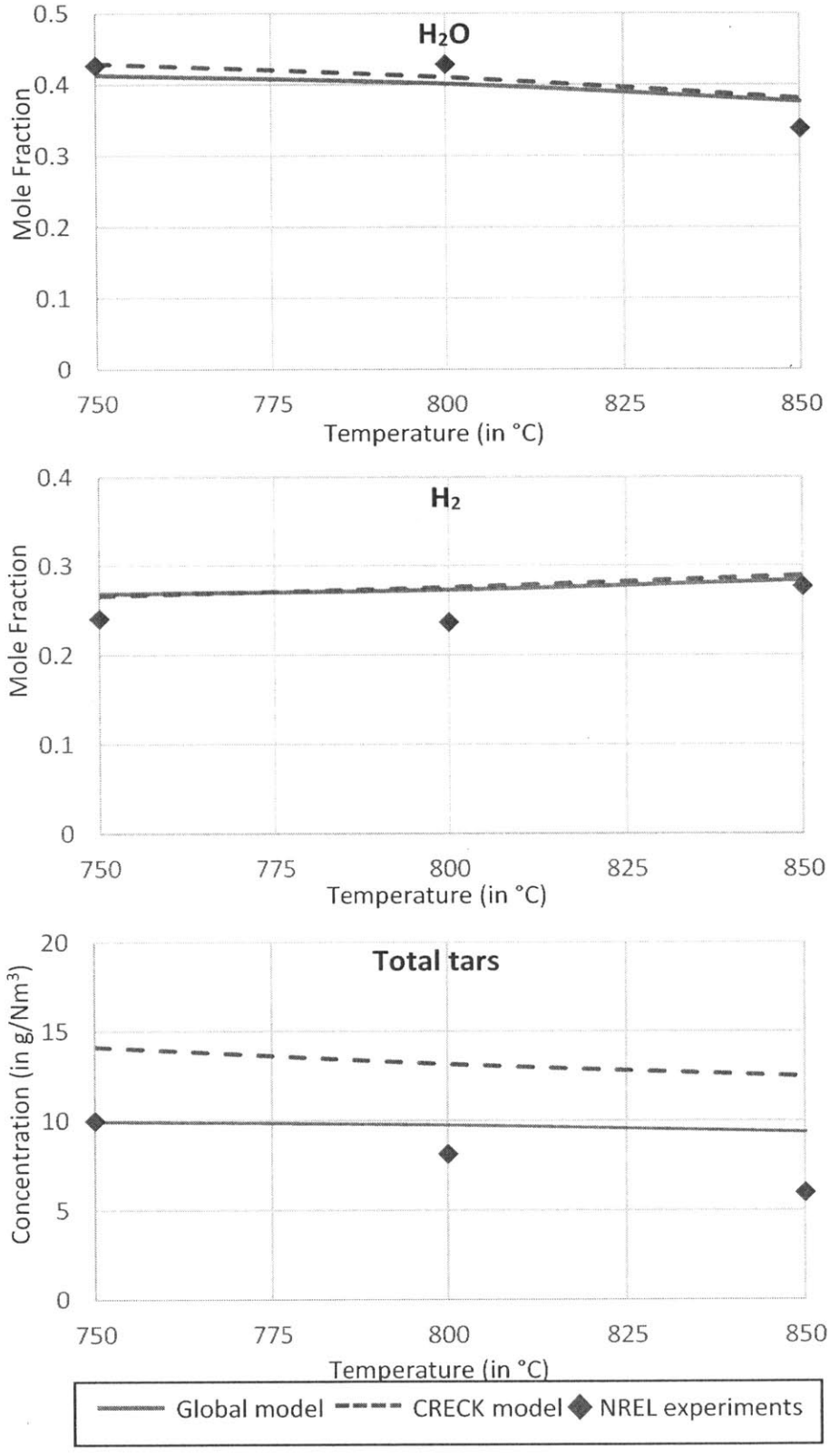

Figure 3-13: Evolution of the major gas species concentrations along the gasifier, evaluated using the global chemistry model for different gasification temperatures. The main variation in the concentrations occurs in the early part of freeboard, where the remaining primary tars are converted to light gases and secondary tars. Solid lines correspond to T=750°C, dashed lines represent T=800°C and dotted lines denote T=850°C

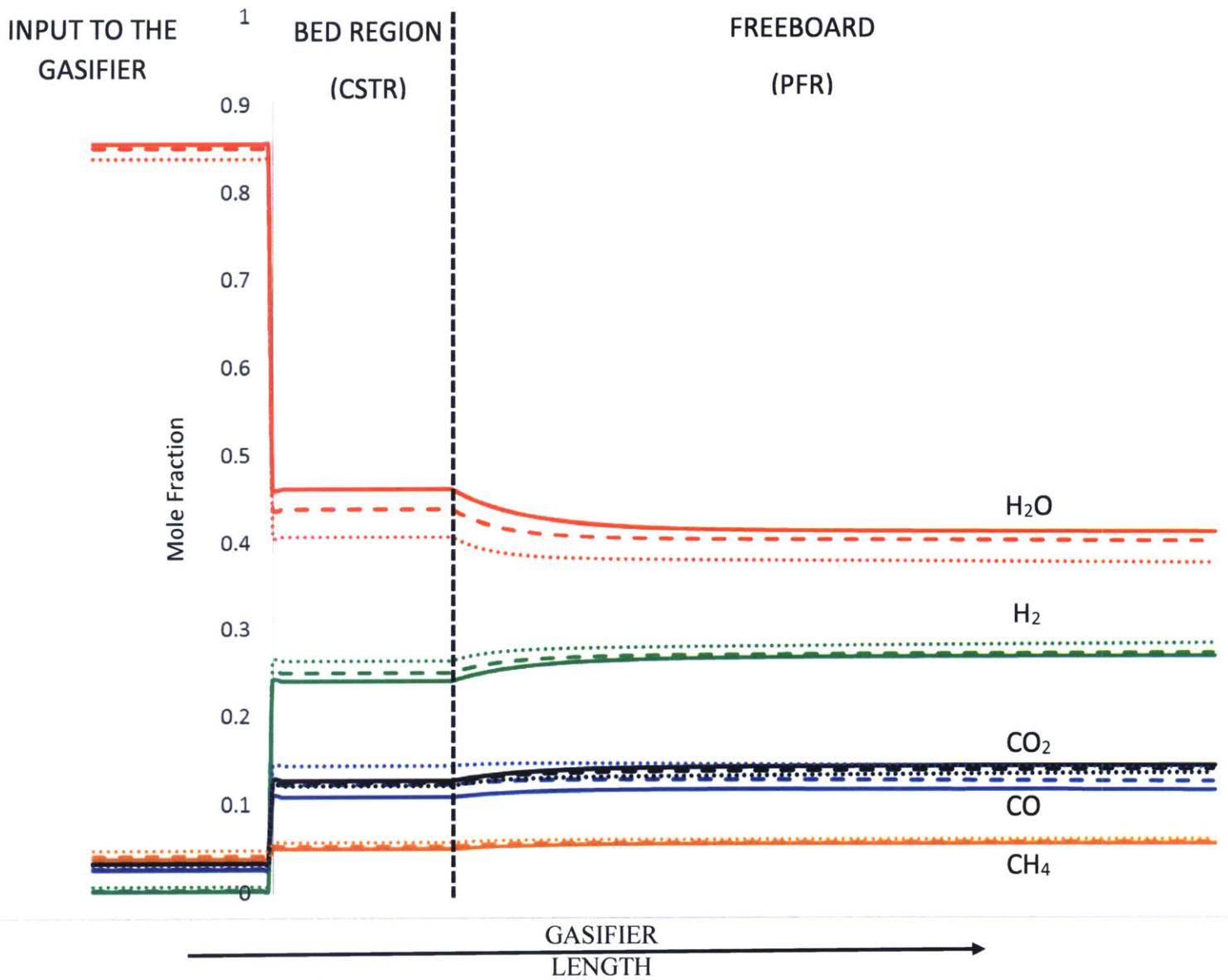

Figure 3-14: Evolution of the primary (Tar_1) and secondary tars (Tar_2) along the gasifier, evaluated using the global chemistry model for different gasification temperatures. Primary tars are completely converted by the early part of the freeboard, while the secondary tars concentrations remain almost constant throughout the freeboard. Solid lines correspond to T=750°C, dashed lines represent T=800°C and dotted lines denote T=850°C

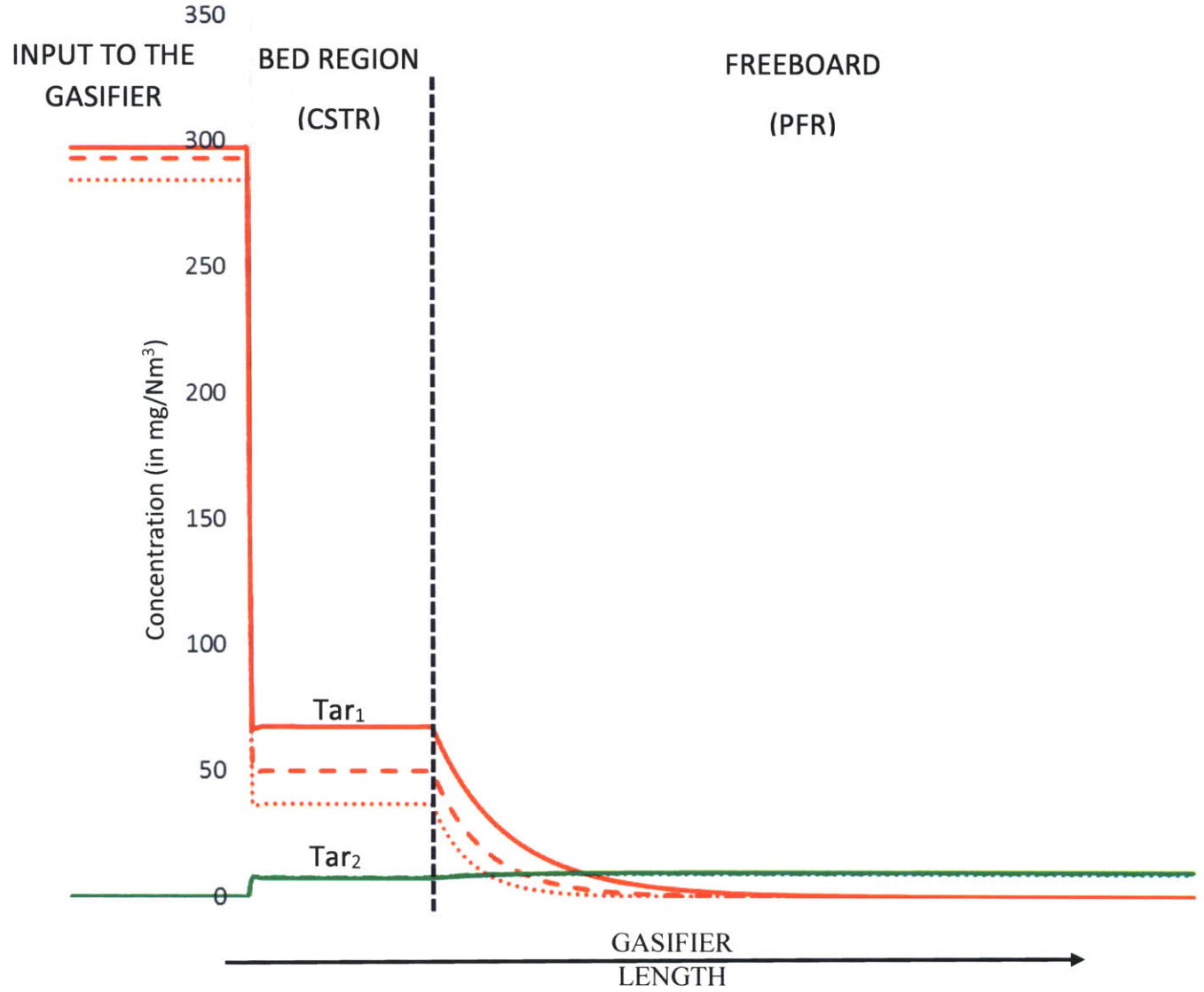

3.8 Sensitivity analysis of the modeling parameters

A number of different sub-models, describing the various physical and chemical processes in biomass gasification, have been used in the reactor network simulations of the biomass gasifier. In this section, the impact of these sub-models and the parameters employed inside these sub-models on the final simulation predictions are studied for the NREL steam-blown gasification conditions.

Since the estimation of the major gas species and tar concentrations is the overarching objective of this work, the relative sensitivities of these outputs to different controlling parameters are studied. The relative sensitivity of the species concentration X_i to parameter p is obtained as,

$$S_{i,p} = \frac{d\ln(X_i)}{d\ln(p)} = \frac{dX_i}{dp}\frac{p}{X_i}$$

Where $S_{i,p}$ is the relative sensitivity of the species i's concentration on parameter p. These sensitivities are evaluated at 800 °C, using the CRECK detailed kinetic mechanism in the reactor network model considered in Section 3.4.

3.8.1 Sensitivity of the model outputs to char conversion

The impact of the char gasification model on the output gas composition is studied for the NREL steam gasification conditions. The devolatilization model estimates that nearly 15% of the input biomass is converted to char, and hence, a good char conversion model is essential for the accurate prediction of the major gas species concentrations (i.e. CO, CO_2, H_2 and H_2O). The relative species sensitivities of the major gas species and tar concentrations to the char conversion model at 800°C are plotted in Figure 3-15.

The char conversion model has the greatest impact on the concentrations of CO, H_2, and H_2O. The impact of the char conversion model on CO_2 is small due to the stabilizing effect of the water-gas shift reaction on CO_2 concentration. Similarly, it can also be seen that the total tar concentration is weakly sensitive to the char conversion model.

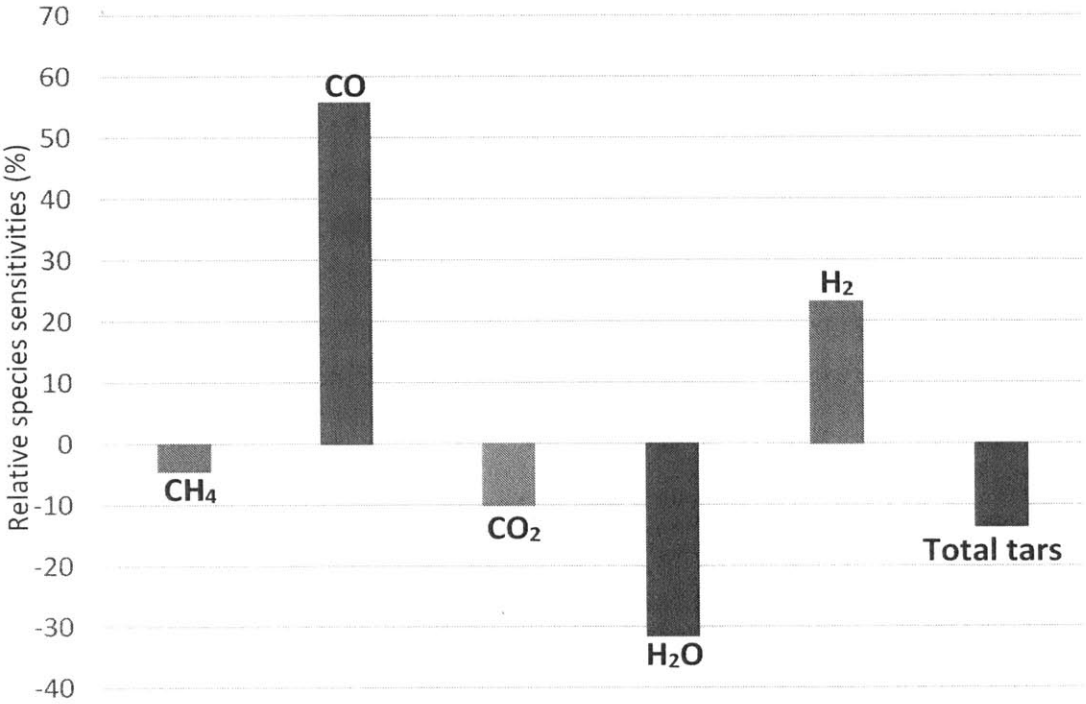

Figure 3-15: Relative sensitivities of the major gas species and total tar concentrations w.r.t to the char conversion. Char conversion model has the greatest impact on CO, H_2O and H_2, while its impact on CO_2 and total tars is much smaller

3.8.2 Sensitivity of the model outputs to primary tar concentrations

Different biomass feedstocks produce varying amounts of primary tars during devolatilization under different operating conditions and hence, it is crucial to understand the impact of this variation on the output gas composition. It is observed in Figure 3-16 that the primary tar concentration has the strongest impact on the secondary tar concentrations, while the impact on the major gases is relatively small. This is because the concentrations of the major gases are governed by other factors, such as the water-gas shift kinetics whereas the secondary tar concentration is almost completely dependent on the primary tars produced during devolatilization.

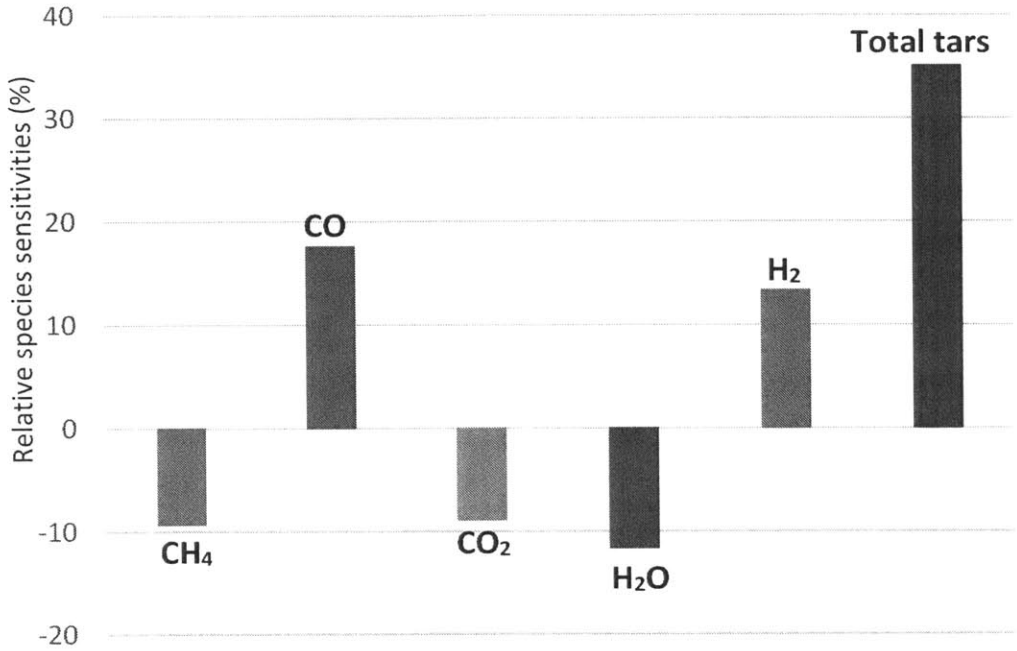

Figure 3-16: Relative sensitivities of the major gas species and total tar concentrations to the primary tar concentration. Total tar concentrations are the most sensitive to the primary tar concentrations, while its impact on the major gases is relatively weak

3.8.3 Sensitivity of the primary tar composition on the output gas composition

The impact of the primary tar composition on the major gas and tar concentrations to is important to understand, since the global models proposed in the previous sections are developed based on the primary tar composition. As described in Section 3.7, two different categories of primary tars are considered in the development of the global primary tar cracking reaction. The reaction parameters in the global cracking reaction depended on the relative mass fractions of the two primary tar categories produced during devolatilization. The effect of the variation in the primary tar composition on the output gas composition is plotted in Figure 3-17. It can be seen that the primary tar composition has the highest impact on the secondary tar concentrations. On the other hand, the impact of the primary tar composition on the major gas species concentrations is negligible.

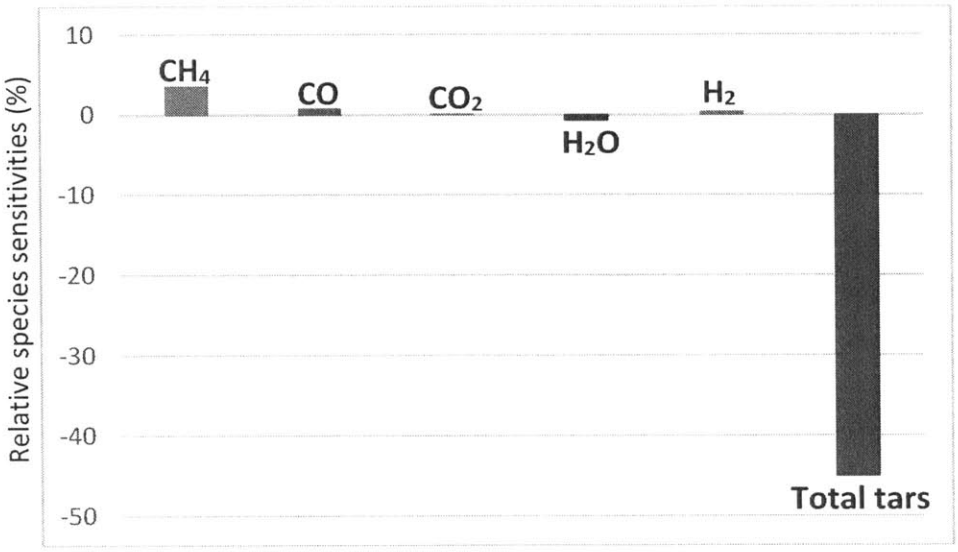

Figure 3-17: Relative sensitivities of the major gas species and total tar concentrations on the primary tar composition. Total tars have the greatest sensitivity to the primary tar composition; its impact on the major gases is negligible

3.8.4 Sensitivity of water-gas shift kinetics on model outputs

While the kinetics of the WGS reaction has been observed to be affected by the catalytic effects of the bed material and char, there is still significant uncertainty in literature on the quantification of these catalytic effects on WGS kinetics. A number of different WGS reaction kinetics have been proposed for specific set of operating conditions (i.e. bed material). In this section, two different water-gas shift kinetic models that have been proposed by Biba [97] and Gomez-Barea [23] are considered and the impact of these different kinetics on the output gas composition is plotted in Figure 3-18. It can be clearly seen that the effect of the WGS kinetic model on the major gas concentrations is significant, while its impact on the total tar concentrations is negligible.

Figure 3-18: Comparison of the Major Gas species and total tar concentration predictions using the Gomez-Barea (GB) and Biba water-gas shift kinetics for NREL gasification conditions. Major gas concentrations vary significantly with the choice of WGS kinetics; total tar concentrations have very little dependence on WGS kinetics

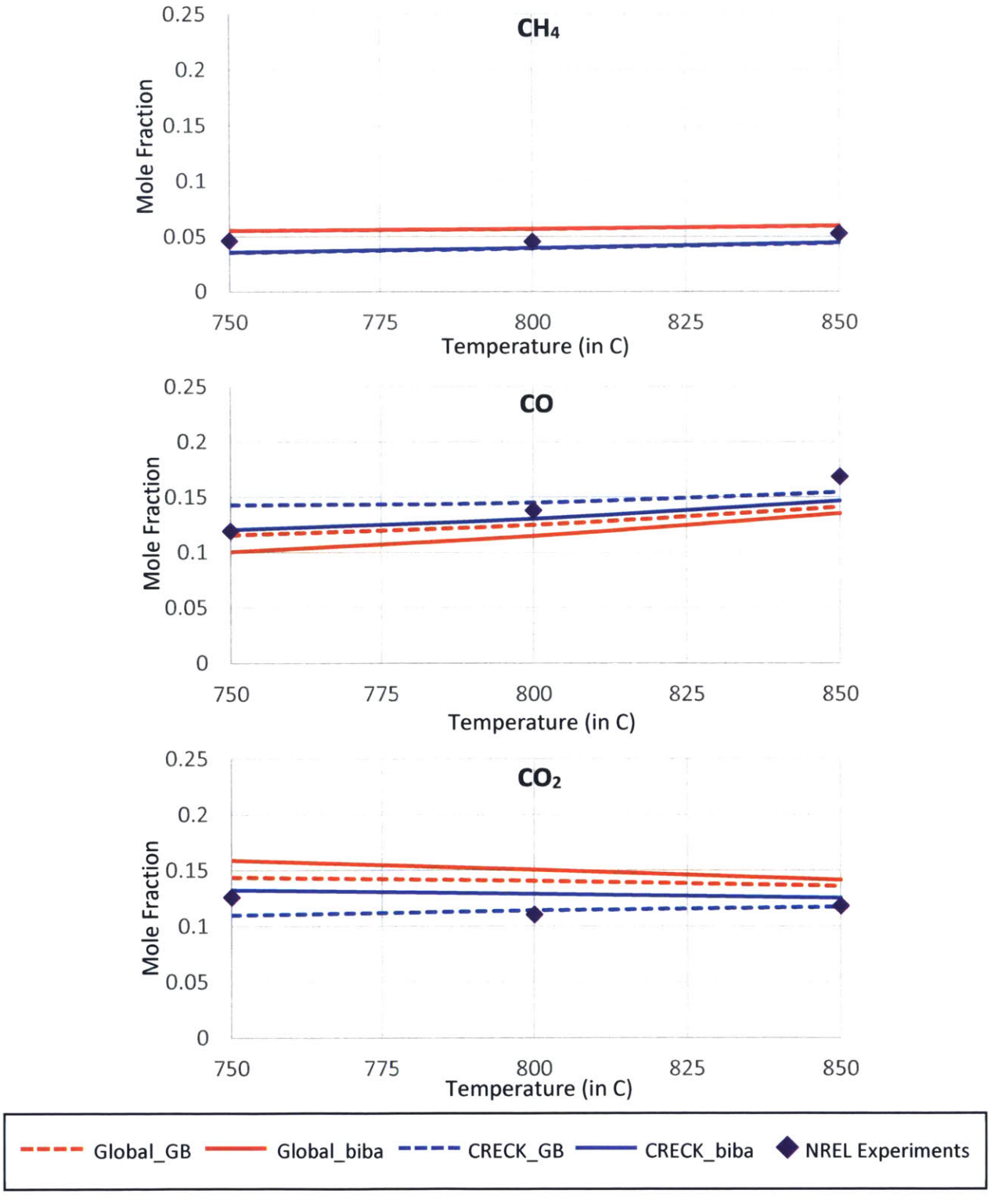

Figure 3-18 (contd.): Comparison of the Major Gas species and total tar concentration predictions using the Gomez-Barea (GB) and Biba water-gas shift kinetics for NREL gasification conditions. Major gas concentrations vary significantly with the choice of WGS kinetics; total tar concentrations have very little dependence on WGS kinetics

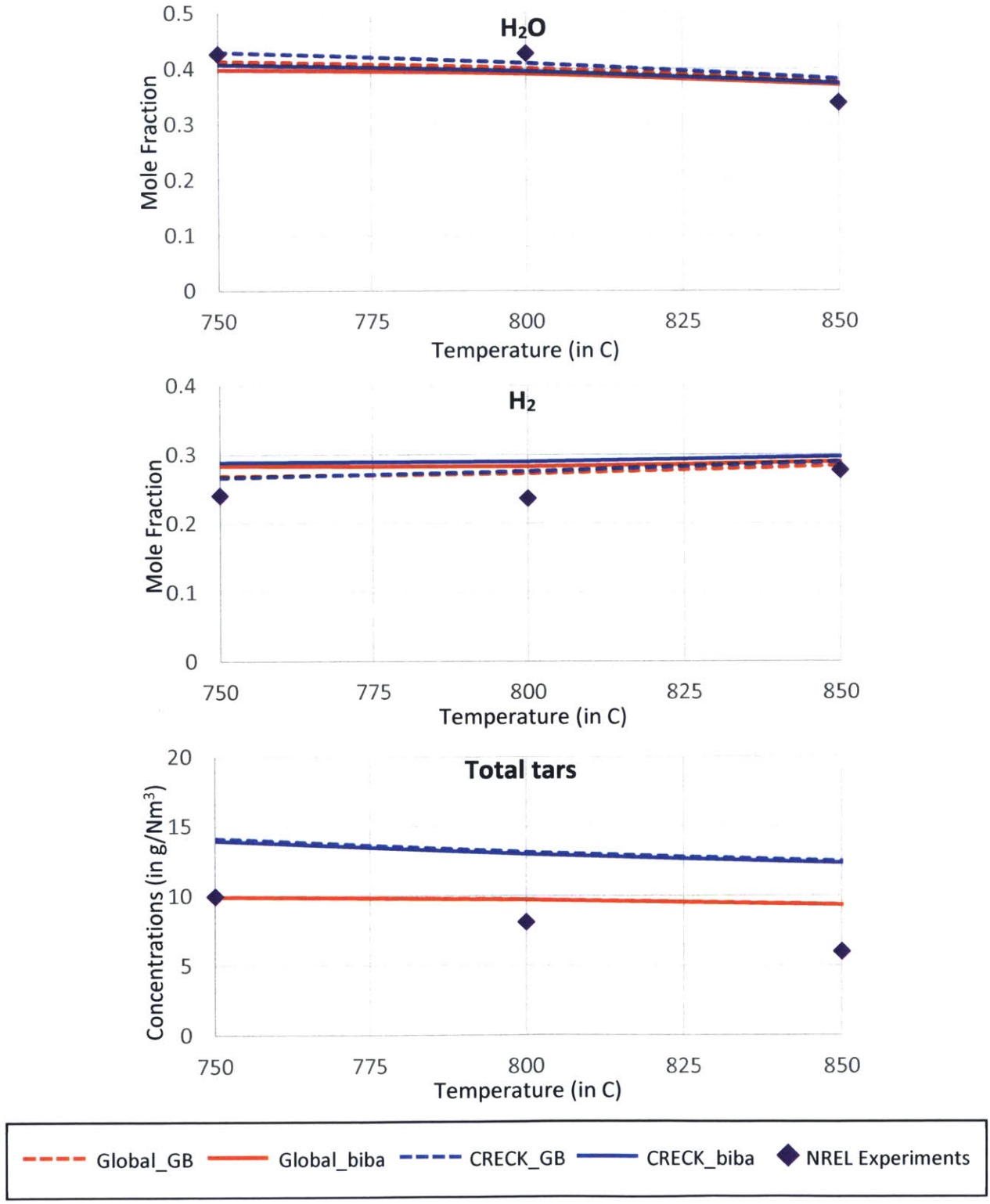

3.8.5 Sensitivity of model outputs to biomass feedstock characteristics

In this section, the major gas and tar concentrations predicted using the global model and the CRECK kinetic mechanism for other biomass feedstocks employed in the NREL experiments are examined. The three biomass feedstocks considered are: hybrid poplar, tulip poplar and Blend 2 (hybrid poplar, clean pine and whole pine).

It can be seen from Figure 3-19 that the predictions using both the global model and the detailed CRECK kinetic mechanism do not seem to depend on the feedstock properties. This is because the reactor network simulations do not take into account the catalytic effects of the various inorganic elements (i.e. aluminum, potassium and silicon) in the ash produced during biomass devolatilization. The impact of these inorganic materials on the char gasification rates have been observed in experiments [101].

In addition, the char conversion model employed in these simulations was originally developed for Oak hardwood and its application to other types of biomass feedstocks could result in erroneous predictions of char conversion. Depending on whether the biomass feedstock is herbaceous, hardwood or softwood, different amounts of char would be gasified since the attrition characteristics of the char particles are dependent on the biomass feedstock [98].

Figure 3-19: Comparison of the Major Gas species and total tar concentration predictions for different biomass feedstock: Hybrid poplar (red), tulip poplar (blue) and Blend2 (green) under NREL gasification conditions using CRECK mechanism (solid lines) and the proposed global model (dashed lines). Experiments are represented by symbols. There is little variation in the model predictions with the biomass feedstock

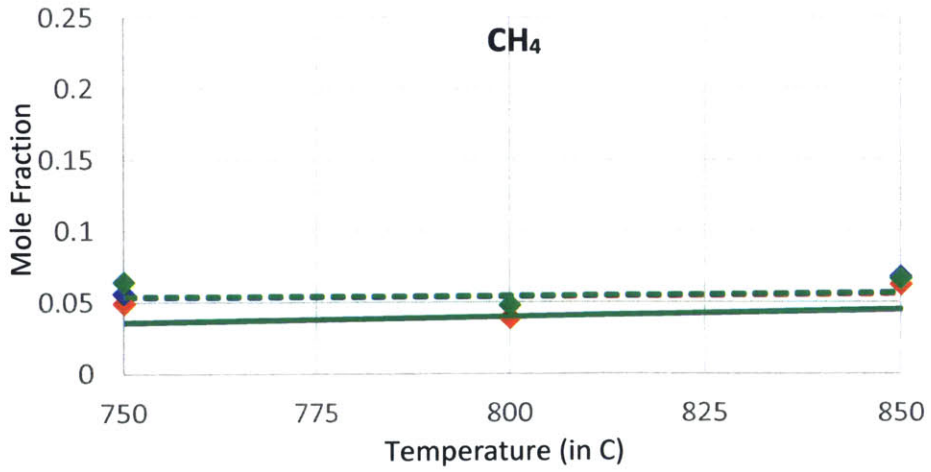

Figure 3-19 (contd.): Comparison of the Major Gas species and total tar concentration predictions for different biomass feedstock: Hybrid poplar (red), tulip poplar (blue) and Blend2 (green) under NREL gasification conditions using CRECK mechanism (solid lines) and the proposed global model (dashed lines). Experiments are represented by symbols. There is little variation in the model predictions with the biomass feedstock

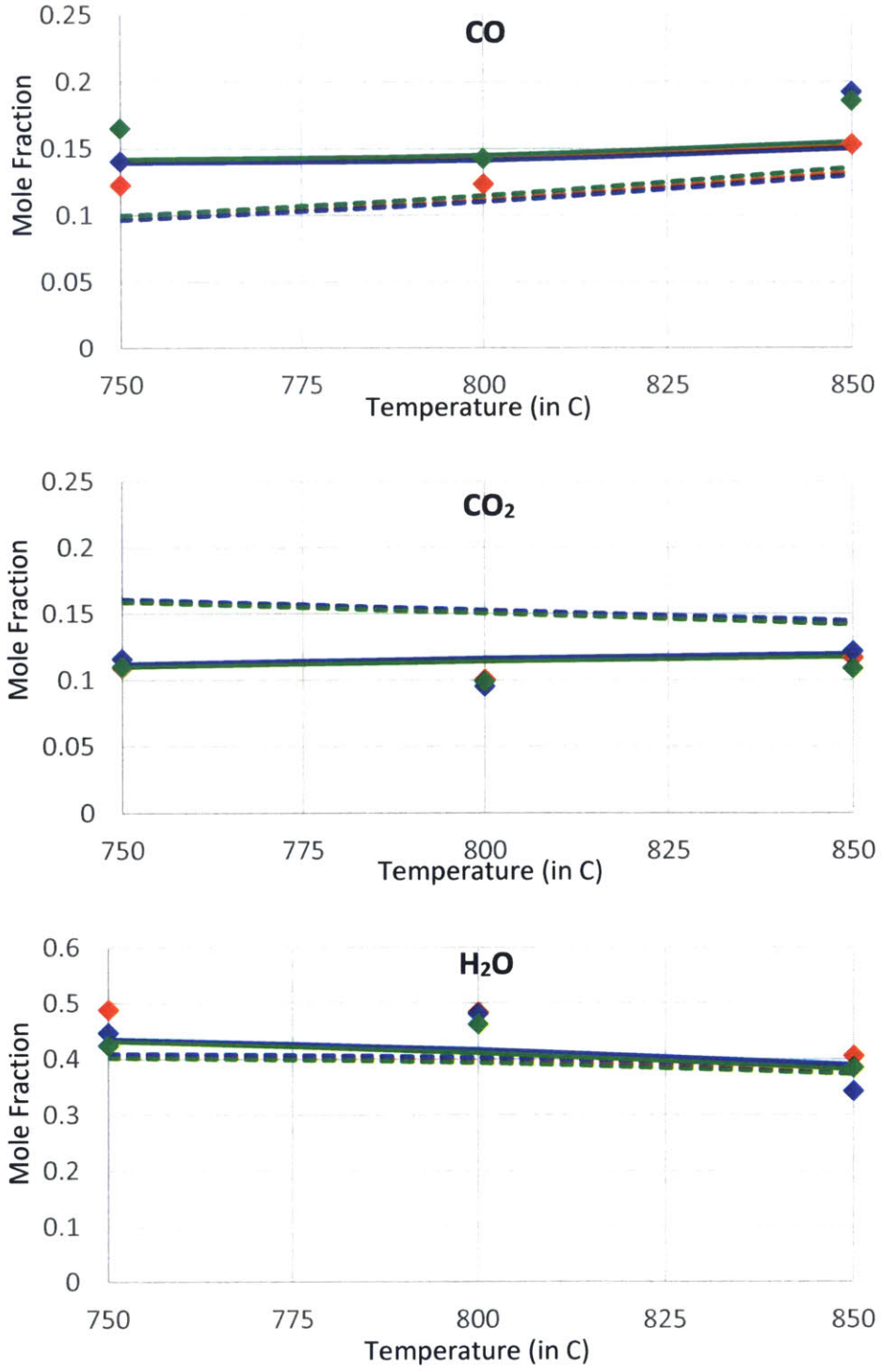

Figure 3-19 (contd.): Comparison of the Major Gas species and total tar concentration predictions for different biomass feedstock: Hybrid poplar (red), tulip poplar (blue) and Blend2 (green) under NREL gasification conditions using CRECK mechanism (solid lines) and the proposed global model (dashed lines). Experiments are represented by symbols. There is little variation in the model predictions with the biomass feedstock

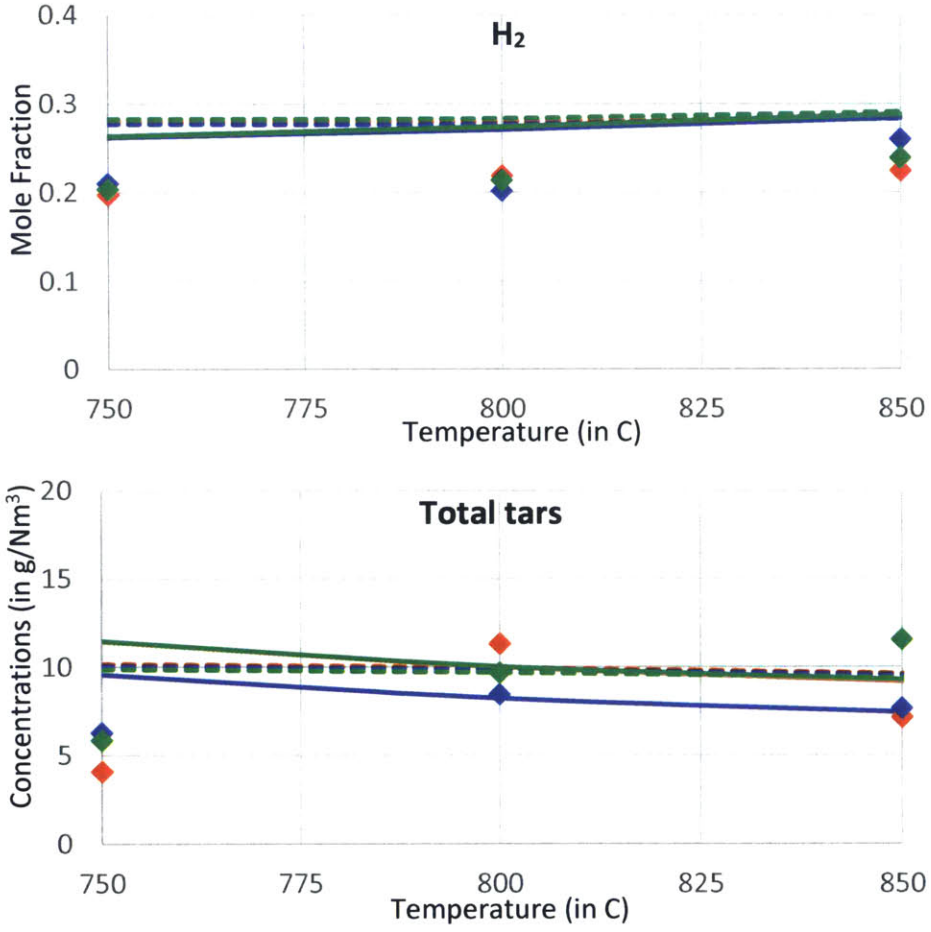

3.9 Conclusions

This chapter gave a detailed discussion of the methodology and development of two new global chemistry models for biomass gasification under air-blown and steam-blown gasification conditions. After a brief discussion of each of the different sub-models involved, an existing global chemistry model developed by Stark for CFD studies of biomass gasification was presented. The Stark global chemistry model was assembled from a set of empirically developed global reactions and in particular, it was found to significantly over-estimate the total tar concentrations compared to experimental results. Hence, a new global chemistry model was developed separately for steam-

blown and air-blown gasification including a new global primary tar cracking reaction formulated based on the decomposition pathways of the major primary tars present inside the gasifier under the given conditions.

Levoglucosan was found to be the major primary tar in the devolatilization products of beech wood employed in the air gasification experiments. Hence, the global primary tar cracking reaction was formulated based on the decomposition product composition of levoglucosan in the presence of air. The detailed CRECK kinetic scheme was used in conjunction with the Reactor Network model of the gasifier to ensure that the decomposition pathways of levoglucosan under the given reactor conditions were accurately captured. In the case of the NREL steam gasification experiments, it was found that there were also significant amounts of other volatiles (notably HMFU), in the devolatilization products of Oak wood employed in the experiments. It was determined that HMFU decomposition produced significantly higher amounts of secondary tars than levoglucosan decomposition. Hence, a new global primary tar cracking reaction, incorporating the decomposition characteristics of levoglucosan and HMFU in the presence of steam, was developed.

The predictive accuracy of these new global models was examined by comparing the predicted major gas species and tar concentrations with the corresponding predictions obtained using the detailed CRECK mechanism as well as the experimental values. For the air-blown gasification conditions, the global model predictions were found to be in very good agreement with the CRECK model predictions and experiments for all the major gas species (except H_2O) and total tar concentrations. The error in the predictions of the steam concentration by both the global model and the CRECK mechanism could potentially be attributed to the significant uncertainties over the measurement techniques employed in the experiments. Similarly, for the steam-blown gasification conditions, both the global model and the CRECK model predictions were shown to be in very good agreement with the experimental values for the major gas species concentrations. It was also shown that the total tars concentration predicted by both the detailed and global model were in good agreement with the experiments.

Finally, the impact of the different sub-models on the final product composition was studied. It was shown that the major gases (except methane) were particularly sensitive to the char conversion model employed in the simulations. In addition, the choice of water-gas shift kinetics used in the model were also shown to have a considerable impact on the major gas species

concentrations. It is important to note that the catalytic effects of the bed material on water-gas shift kinetics are still well understood yet, resulting in significant uncertainty in the WGS modeling. The total tar concentration at the gasifier outlet was strongly dependent on both the total primary tar concentration and composition, indicating the importance of using an accurate devolatilization model to be able to accurately predict the primary tar formation.

4 Reactor Network Modeling of Bubbling Fluidized Bed Biomass Gasification

In Chapter 3, a simplified reactor network model of the biomass gasifier was discussed. The reactor network model used a set of ideal chemical reactors to describe both the hydrodynamic mixing and chemical processes inside the biomass gasifier. While the freeboard region of the gasifier was modeled as a plug flow reactor, the bubbling bed region below the freeboard was represented as a continuously well stirred reactor, with the assumption that the bed is well mixed with small bubbles. While this assumption is valid at moderate superficial gas velocities ($1<U/U_{mf}<8$), it is overly simplistic and does not hold true for beds with high superficial gas velocities ($U/U_{mf}>8$). At these superficial velocities, the bubbles are no longer small, and a significant amount of the gasifying agent bypasses the bed inside these bubbles.

Stark [3] reported that the bubbling regime for a fluidized bed gasifier extended between $1<U/U_{mf}<8$, after which a large amount of the gasifying agent by-passed the bed through slugs. This resulted in the formation of two distinct regions/phases inside the bubbling bed: the emulsion (or dense) phase and the bubble phase. While the bubble phase is typically considered to be made of gases only, the emulsion phase represents the solids (i.e. biomass particles, char and bed material) along with the gases present in the inter-particle voidage. This approach of considering two distinct phases in a bubbling fluidized bed is known as the two-phase theory of fluidization and was proposed originally by Davidson [102].

When the biomass feedstock is fed to the gasifier, it devolatilizes primarily within the emulsion phase, releasing volatiles to the emulsion (dense) phase. Under moderate fluidization velocities ($1<U/U_{mf}<8$), when the bubbles are still small, the mass transfer resistances between the emulsion and bubble phases are small. Therefore, both the devolatilization gases and the gasifying agent are uniformly mixed inside the bed across both the emulsion and bubble phases. However, at high fluidization velocities ($U/U_{mf}>8$), the well mixed assumption for the fluidized bed does not hold and severe inhomogeneities arise in the bed. Significant amounts of the fluidization gas bypass the emulsion phase through slugs formed by bubble coalescence.

The gas bypass has a major impact on both the major gas species concentrations and tar growth within the gasifier. While the reduction in solids-gas contact times due to gas bypass affects the reaction rates of a number of important reactions inside the bed (e.g. water-gas shift reaction), the

relatively rich region within the emulsion phase due to gas bypass could potentially increase PAH formation in the gasifier ([3], [23]). While the influence of mixing and oxygen availability on the formation of PAH compounds in the gasifier has not been conclusively proven yet, it had been observed that the relative availabilities of O_2 and C_2H_2 locally in the gasifier could have a significant effect on PAH growth [3]. It was reported that PAH growth increased non-linearly with increasing C_2H_2:O_2 ratios, resulting in the formation of several 2+ ring PAH compounds. Once the PAH compounds are formed, it is very difficult to oxidize these compounds due to the slower oxidation kinetics, especially under lean conditions.

In this chapter, the reactor network model described in the previous chapter is extended to include a more detailed network of chemical reactors to represent the fluidized bed, factoring in mass transfer considerations to better capture the mixing inefficiencies.

4.1 Reactor Network model development

Reactor network models are widely used in biomass gasification simulations because they present a good balance between the overly simplistic global black box models and the computationally expensive Computational Fluid Dynamics (CFD) models. While reactor network models avoid the complex computations associated with CFD models, they are still able to capture a reasonable level of detail on the hydrodynamics using semi-empirical correlations.

Based on the two-phase theory of fluidization, reactor models represent the bubbling bed to be composed of two distinct regions with different flow patterns. While all the solid particles and some of the gas (including both the devolatilization product gases and the gasifying agent) are assumed to be perfectly mixed in the emulsion phase, the remaining gas (predominantly the gasifying agent) is modeled to be in a plug flow.

Reactor models employing the two-phase theory, had been widely used for a number of different gasifier applications ([89], [103]–[110]). Feng et al. [103] developed a reactor network model for the jet fluidized bed coal gasifier using CHEMKIN. While the freeboard was modeled as a PFR, the jetting zone and the annulus dense phase region at the bottom of the bed were modeled separately as CSTRs, with material transfer and heat exchange interactions occurring between the different regions. El Asri et al. [106] used a series of plug flow reactors to describe both the bubble and emulsion phases in their ASPEN Plus simulations of a bubbling fluidized bed

biomass gasifier. The mass transfer occurring between the two phases and bubble growth inside the bubbling bed were represented using standard correlations available in literature.

In addition to reactor models, several mathematical equation-based models have also been developed for fluidized bed applications. Kaushal et al. [89] developed a one dimensional model of a bubbling fluidized bed biomass gasifier. Employing the two-phase theory, the model consisted of several elemental CSTRs in series to represent both the phases. Reactions were assumed to occur only inside the emulsion phase and mass transfer between the phases were represented using bubble mass transfer correlations from literature. A comprehensive review of the different reactor/mathematical models available in literature was presented in Gomez-Barea et al. [23].

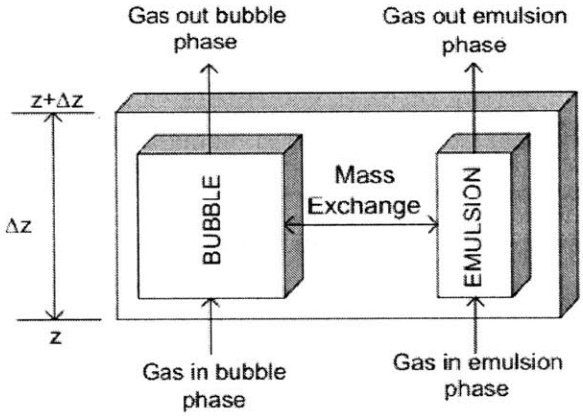

Figure 4-1: Schematic of the reactor network model of the bubbling fluidized bed, as presented in Kaushal [89]

A number of different correlations are used in reactor models to describe the various parameters required to define the individual reactor properties. Empirically derived correlations have been proposed for evaluating the division of incoming gas flow between the phases, the volume fractions of the two phases, the velocity and size of the bubbles and the gas velocity inside the bubbles ([23], [102], [111], [112]).

The validity of reactor network models depends strongly on the applicability of the employed correlations to the operating conditions under consideration. Given the critical role played by correlations in defining the model, reactor network models cannot be applied widely and caution must be exercised, especially while modeling a system with different properties than those for which the correlations were formulated.

A number of empirical correlations exist in literature for describing the mass exchange coefficient between the emulsion and bubble phases [23]. Davidson's model assumed that mass exchange between the two phases occurred only due to convective flow through the bubble [102]. Kunii and Levenspiel [111] developed a three-phase interaction theory for mass exchange by including a bubble cloud phase at the interface between the bubble and emulsion phases. In this model, mass transfer was assumed to occur between the bubble and cloud, and between the emulsion and cloud phase, individually. Thus, the total mass transfer resistance was written as a sum of the individual resistances between the two pairs of phases. A third approach, proposed by Rowe et al. [112] to describe the mass exchange between the phases, was based on the analogy of a liquid droplet rising in another liquid. On comparison with experiments, it was observed that the approaches that considered only the convective flow mass transfer significantly over-estimated the experimental values. On the other hand, purely molecular diffusion-based models under-estimated gas exchange, especially in the instances of strong bubble interactions. As a result, empirical correlations that included both the effects of convective mass transfer and molecular diffusion had been proposed and were found to agree better with experiments [15].

In this study, the bubbling bed is modeled using the two-phase theory, employing an ideal isothermal continuously stirred reactor and an ideal isothermal plug flow reactor in parallel to represent the emulsion and bubble phases, respectively. The outlet gases exiting the two reactors are then combined and used as input to the plug flow reactor describing the freeboard.

The evolution of each chemical species inside the bed depends on a number of different modeling parameters employed in the reactor network model. Reactor geometries representing the individual reactor volumes and mass flow rate of the incoming gases into each individual reactor are the most critical input parameters to the reactor network model.

Individual reactor volumes are evaluated using the bubble growth correlations employed in Kaushal et al. [89] to describe the volume fraction of the bubbles in the fluidized bed. Bubble coalescence is considered in these correlations.

The mass flow rate and composition of the incoming gases entering each reactor is modeled using four different cases, encompassing the entire spectrum of incoming gas flow conditions encountered in the gasifier. The inter-phase mass transfer between the two phases at each level of the bed is determined based on the bubble properties at that level.

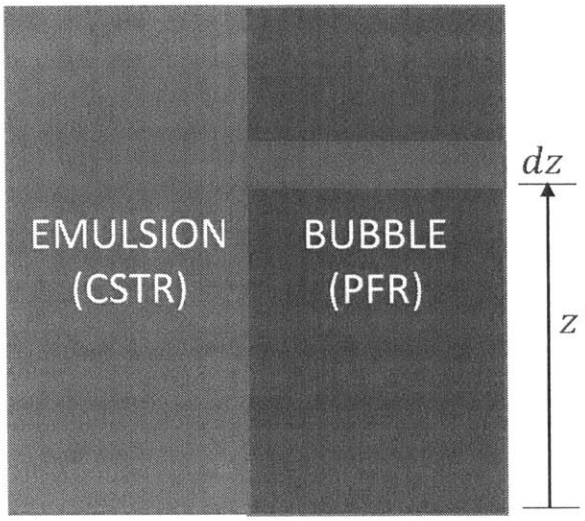

Figure 4-2: Schematic of the bubbling fluidized bed, modeled as a combination of isothermal CSTR and isothermal PFR

The interphase mass transfer between each reactor for species j is calculated as,

$$dM_j(z) = K_{BE}(z)dV_B(C_{j,B}(z) - C_{j,E}(z))$$

Where dM_j is the elemental mass transfer of species j between the reactors, K_{BE} is the mass transfer coefficient, $C_{j,B}$ and $C_{j,E}$ are the concentrations of species j in the bubble and emulsion phases respectively. dV_B is the elemental bubble volume obtained from the elemental bed volume dV and bubble fraction ϵ_B at the bed height z.

$$dV_B = \epsilon_B(z)dV$$

A detailed discussion of the different conservations equations employed in the reactor network model and the solution procedure used for evaluating the gas evolution inside the gasifier is given in Appendix I.

4.2 Air-blown gasification simulations

The improved reactor network model presented in the previous section is used to study the product gas composition for the air blown gasification conditions studied in the van Paasen and Kiel experiments [13]. While the devolatilization product composition evaluated using Stark's particle scale devolatilization model is used as the input to the reactor network model of the bed, the mass flow rate and composition of the incoming gas (devolatilization gases and the gasifying

agent) entering each individual reactor needs to be evaluated. While CFD simulations could be used to provide information on the incoming gas mass flow rate and composition entering the two phases, simple assumptions are used in this study to model these quantities. The different cases used to model the incoming gas mass flow rate and composition entering the two reactors are,

1. Case 1 – Equal amounts of the incoming gas (devolatilization gases and the gasifying agent) are assumed to enter the emulsion and bubble phases
2. Case 2 – Devolatilization gases are assumed to be released solely within the emulsion phase at the entry of the CSTR, while the entire amount of the gasifying agent is modeled to enter only the PFR (bubble phase)
3. Case 3 – While the entire amount of gasifying agent is assumed to enter the CSTR (emulsion phase), devolatilization gases from the particle scale model serve as the input to the PFR (bubble phase)

The simulation results using the improved reactor network model for the three cases are compared with a fourth case representing the original reactor network model

4. Case 4 – Original reactor network model; entire bed is modeled as a single CSTR

It is important to note that the Case 3 scenario, in which all the devolatilization gases are assumed to enter the bubble phase, may not be physically realistic; however, it helps us to represent the entire spectrum of incoming gas flow scenarios in order to understand their impact on the syngas product composition.

The output gases exiting the two individual reactors are then weighted by mass and combined to evaluate the input product composition to the freeboard.

The detailed CRECK kinetic mechanism is employed in the improved reactor network model to predict the concentrations of the major gas species and the various tar classes for the different incoming gas flow cases.

Different water-gas shift kinetics are used for the different regions of the gasifier. To account for the catalytic effects of the bed material, the CSTR model of the emulsion phase employed the faster WGS kinetics proposed by Biba [97]. On the other hand, the PFR models of the freeboard and the bubble phase used the original WGS kinetics employed in the CRECK mechanism.

In addition, heterogeneous char oxidation and gasification reactions are not included in the simulations, based on Stark et al. [8]. The average residence time of the char particles under the given reactor conditions was found to be much shorter than the characteristic time for the gasification reactions. While the characteristic residence time for the wood-chip char particles was estimated to be around 110s, the characteristic time for gasification at 800 °C was found to be almost an order of magnitude higher (~1100-4000 seconds) [100]. In addition, they also observed that the influence of char oxidation reactions on carbon conversion was negligible. This observation was justified by the good agreement between the reported carbon conversion (93%) and the char yield calculated from the particle scale devolatilization model. Details on the simulation conditions employed in the study are described below.

Table 4-1: Simulation conditions representing the van Paasen and Kiel experiments [13]

Simulation conditions	
Biomass feedstock	Beech wood (0.75-2mm)
Fluidizing medium	Silica sand (270 μm)
Fluidizing agent	Air
Bed diameter (in m)	0.074
Biomass feed rate (in kg/hr)	1
Bed temperature (in K)	973-1273
Pressure (in atm)	1
Air equivalence ratio	0.25
Ratio of incoming superficial velocity to minimum fluidization velocity	14.5

Figure 4-3: Schematic of the simulation conditions used in the improved RNM simulations for the van Paasen and Kiel air blown gasification conditions

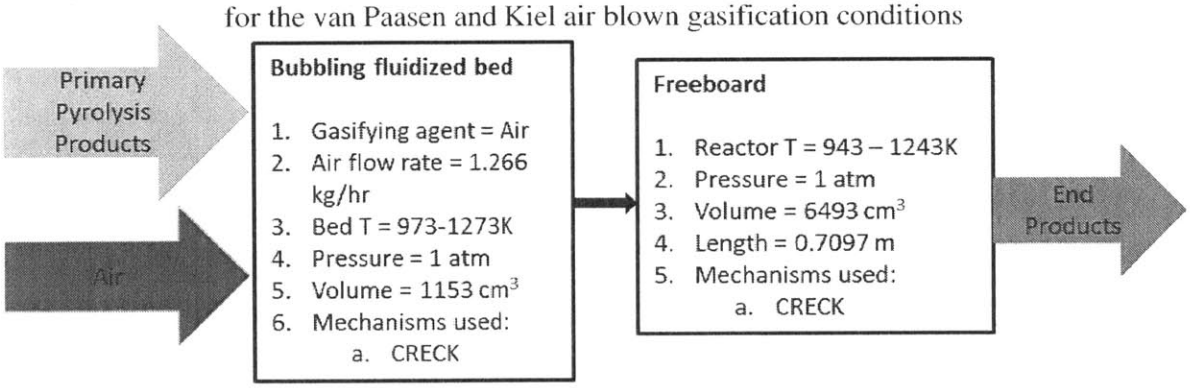

A list of the various bubble growth parameter values employed in the reactor network model is presented in Table 4-2.

Table 4-2: Bubble growth and inter-phase mass transfer correlations employed for the van Paasen and Kiel gasifier conditions

Quantity (Units)	**Value (given or calculated from correlations used in Kaushal et al. [89])**
Bubbling bed height (m)	0.268
Minimum Fluidization velocity, U_{mf} (m/s)	0.026
Incoming superficial velocity, U_0 (m/s)	0.38
Cross-sectional area of the bed, A (m^2)	0.0043
Bubble Diameter, $d_B(z)$ (m) (z is location along the bed height)	$0.54(U_0\text{-}U_{mf})^{0.4} g^{-0.2} \left(z + 4\sqrt{\frac{A}{100}} \right)^{0.8}$
Bubble rise velocity, U_{br} (m/s)	$0.711\sqrt{g d_B}$
Bubble velocity, U_b (m/s)	$U_0 - U_{mf} + U_{br}$
Diffusivity, D (m^2/s)	0.00001
Voidage at minimum fluidization velocity, ε_{mf}	0.3
Bed particle diameter (m)	270 μm
Bed particle density (kg/m^3)	2600
Bubble phase fraction	$\frac{U_0 - U_{mf}}{U_b - U_{mf}}$
Mass transfer coefficient, K_{BE} (m/s)	$K_{BE} = \frac{U_{mf}}{4} + \sqrt{\frac{4\varepsilon_{mf} D U_B}{\pi d_B}}$

4.2.1 Results and Discussion

The model predictions of the major gas species and the different tar class concentrations for the different gasification temperatures obtained using the improved reactor network model is plotted in Figures 4-4 to 4-6. It can be clearly seen that the different cases used to model the incoming gas flow result in widely varying predictions of the major gas species and the various tar class concentrations.

The extreme conditions considered in cases 2 and 3, in which the entire amount of devolatilization gases is assumed to enter a single phase (emulsion or bubble), give rise to significantly higher tar concentrations than cases 1 and 4. The locally rich regions of devolatilization products that are formed in these cases, result in the production of large tars and PAHs (represented by tar classes 3, 4 and 5). Because the characteristic operating temperatures of fluidized bed biomass gasifiers are not high enough to crack down these PAHs once they are formed, PAH concentrations continue to increase inside the gasifier and significant amounts of PAHs are seen at the outlet of the gasifier. While class 2 tar predictions are considerably higher than the experimental observations for all the cases, the reduction in their amounts with increasing temperature is correctly captured. In cases 2 and 3, the total tar concentrations exhibit a bell-shaped dependence on the operating temperatures. This is due to the significantly higher amounts of class 4 and class 5 tars observed at higher temperatures in these cases, as explained earlier. Figure 4-7 considers the evolution of Class 3 tar concentration at two temperatures (T = 973K and 1273K), for the different cases. The impact of these different cases on the tar concentrations is small at low temperatures; on the other hand, there is a significant variation in the tar concentration at high temperatures. This is because, at high temperatures, the phenol consumption reactions occur at a faster rate to produce class 3 tars, especially in the locally rich regions.

While the impact of the incoming gas flow assumptions on the methane concentrations is minimal, the other major gases (CO, CO_2, H_2 and H_2O) are significantly affected. This is mainly due to the interplay between the choice of the water-gas shift kinetics and the initial concentrations of these species in the two phases. As described earlier, slow WGS kinetics is employed for the bubble phase and fast WGS kinetics is employed in the emulsion phase to account for the catalytic effects of the bed material and char.

Figure 4-4: Different tar class concentrations predicted for the van Paasen and Kiel air gasification conditions using the improved reactor network model. Cases 2 and 3 predict significantly high tar concentrations (close to experiments) than cases 1 and 4

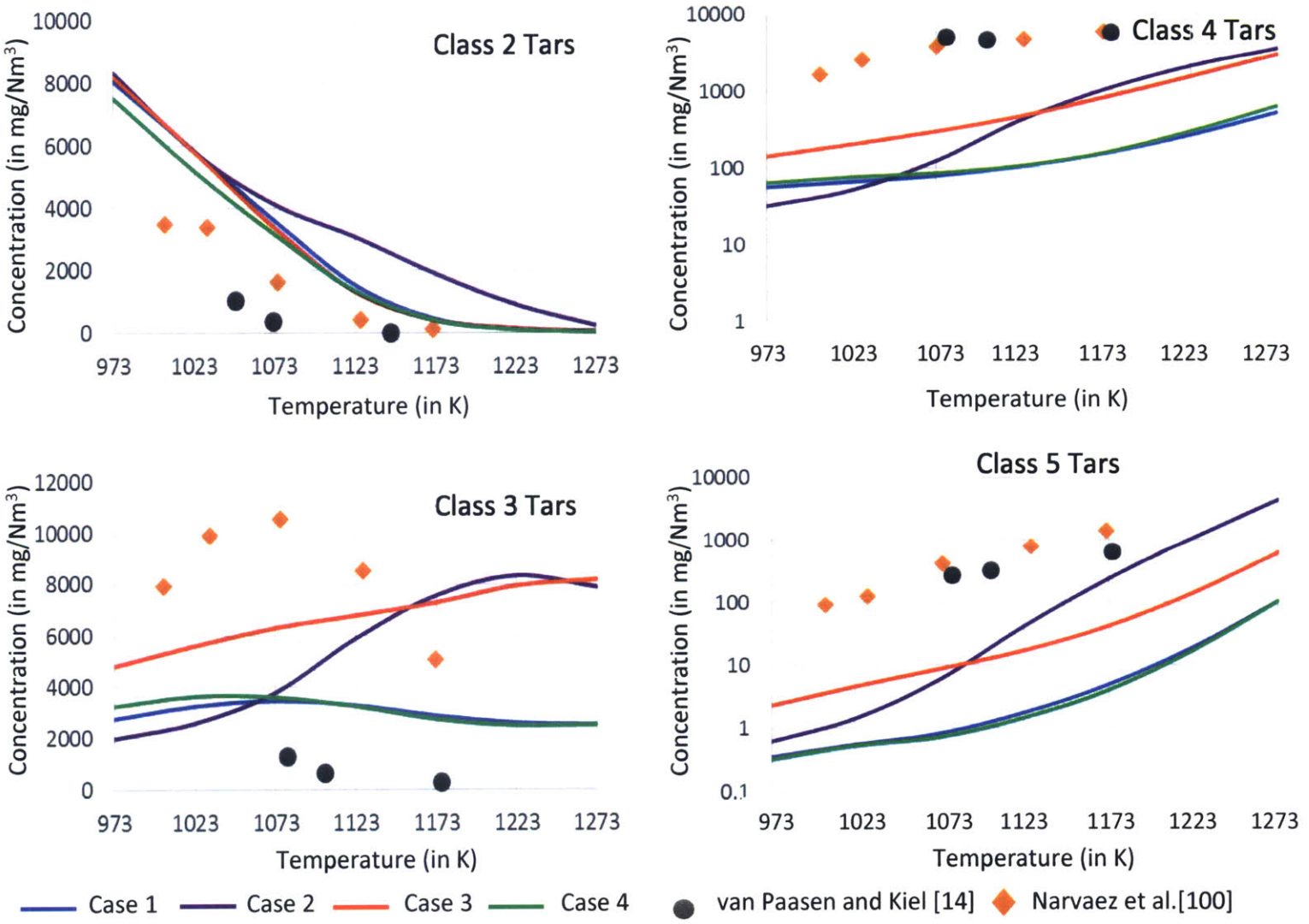

Figure 4-5: Major Gas species concentrations predicted for the van Paasen and Kiel air gasification conditions using the improved reactor network model. There are significant variations in the CO and CO_2 concentrations with the choice of the incoming gas flow cases

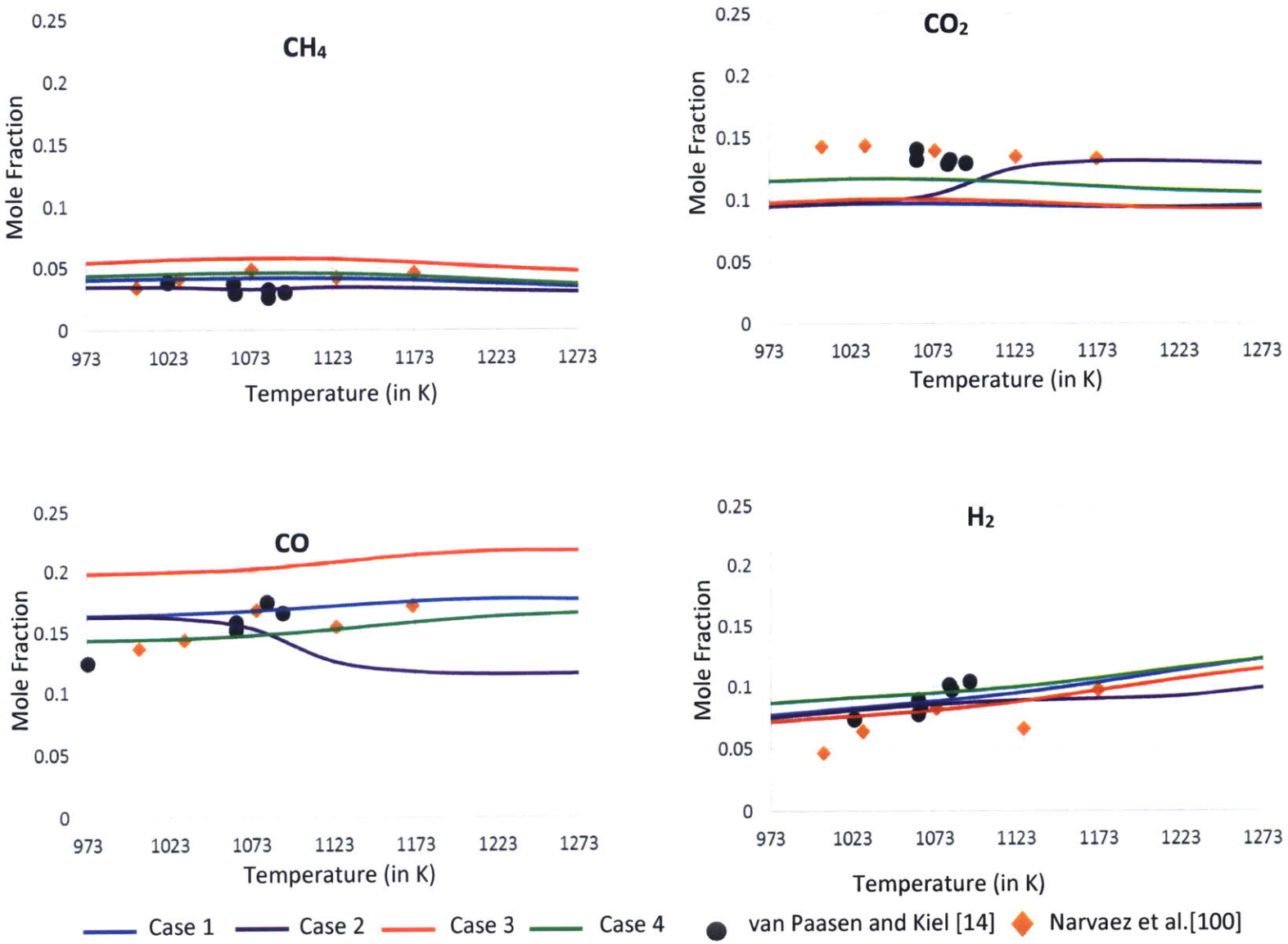

Figure 4-6: Steam and total tar concentration predicted for the van Paasen and Kiel air gasification conditions using the improved reactor network model. Cases 2 and 3 accurately predict the steam concentrations, while the total tar concentrations are in very good agreement with experiments for all cases (except Case 2)

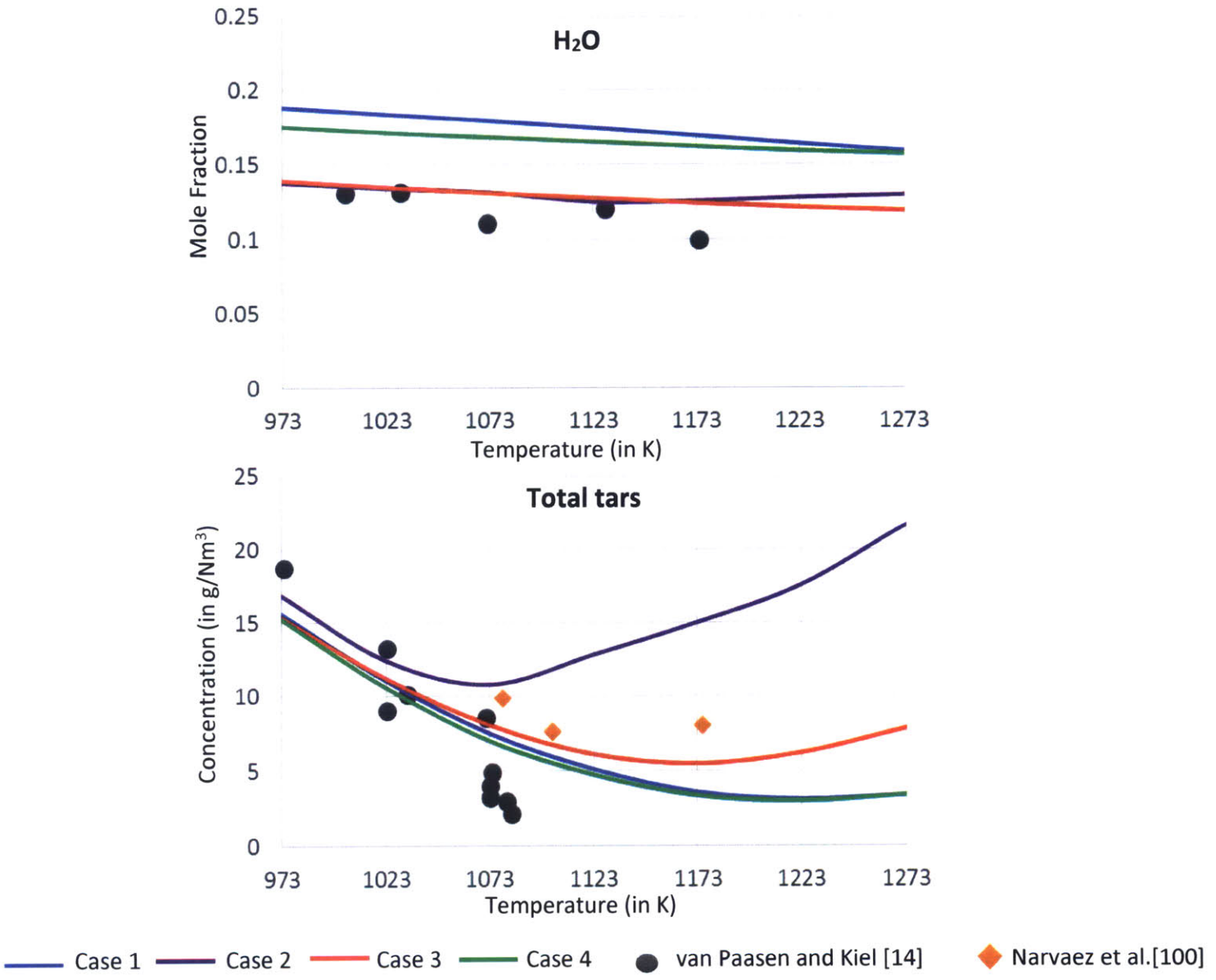

Figure 4-7: Evolution of the Class 3 tar concentrations inside the gasifier, evaluated using the improved reactor network model at two different temperatures (973K and 1273K). Significant variation in the tar concentration is observed for different incoming gas flow cases at 1273K, but there is negligible difference at 973K. Within the bed region, dashed lines indicate the species evolution within PFR and dotted lines represent the CSTR concentrations

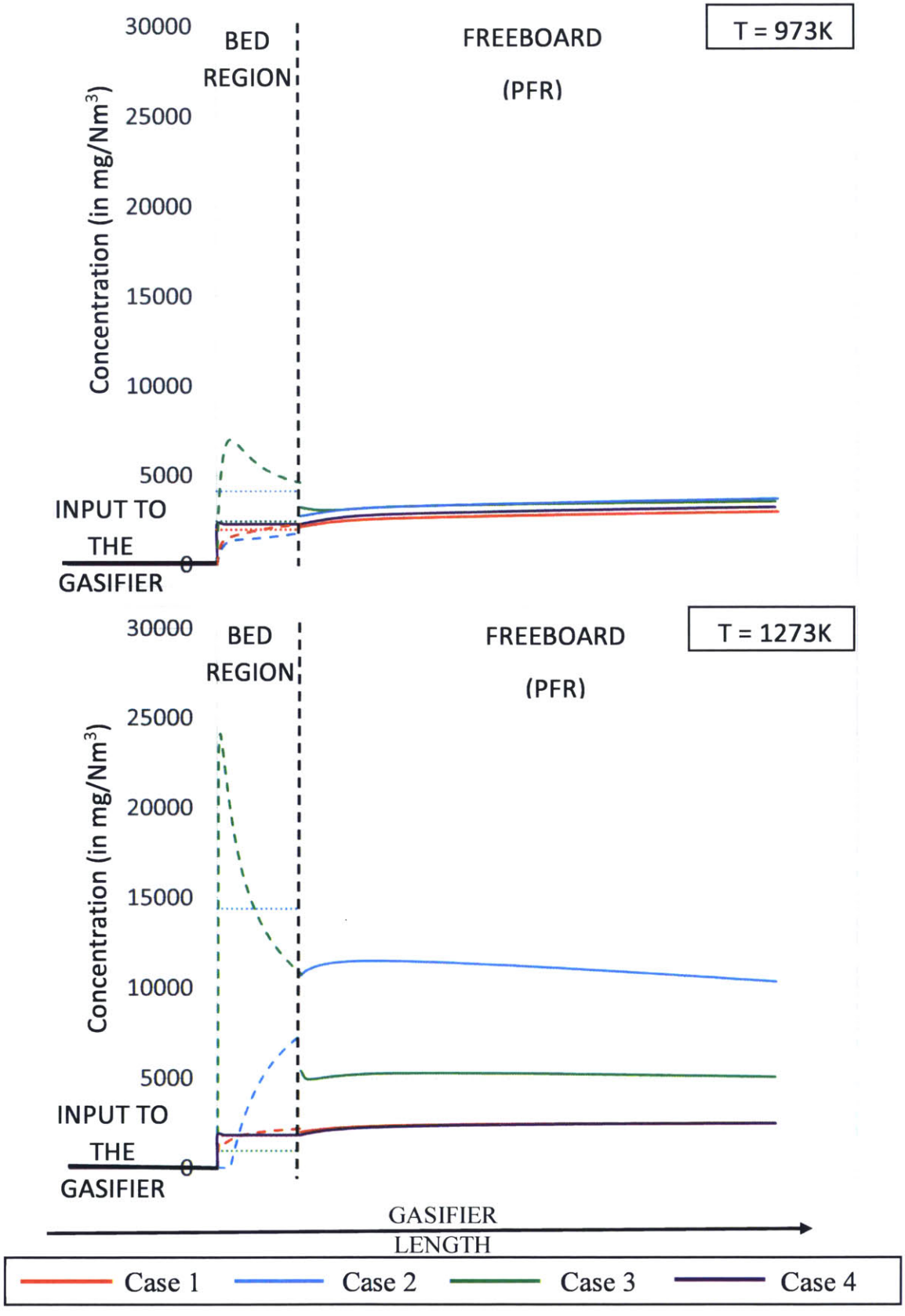

A distinct change in the CO and CO_2 concentrations is observed between 1073K and 1123K. This is due to two complementary factors: 1) The CO oxidation reaction is much faster at 1123K, and 2) The water-gas shift reaction is also significantly faster at 1123K compared to that at 1073K. The combined effect of these two reactions at 1123K results in noticeably smaller concentrations of CO than the CO concentration at 1073K. CO_2 concentrations experience the exactly opposite due to the larger conversion of CO at 1123K both due to the CO oxidation reaction and water-gas shift reaction. Figure 4-8 clearly shows a much faster rate of consumption of O_2 both due to CO oxidation and H_2 oxidation.

However, the same phenomenon is not observed in the other extreme incoming gas flow case (Case 3). This is because, in Case 3, a large fraction of CO and CO_2 is still contained within the bubble phase where the slow WGS kinetics are employed and the impact on the water-gas shift reaction on these species concentrations is much smaller. Figure 4-9 represents the impact of the choice of the WGS kinetics on CO and CO_2 concentrations. The effect of the water-gas shift reaction is explained by studying the evolution of CO and CO_2 for Case 2 mixing at 1123K employing two different WGS kinetics in the emulsion phase: 1) the faster WGS kinetics proposed by Biba et al [97] and 2) the slower WGS kinetics from the original CRECK mechanism. It is observed that the faster kinetics results in a significantly smaller concentration of CO. In both the cases, the slow WGS kinetics is used for the bubble phase and the CO oxidation rates remained constant.

To conclude, it can be stated that there are significant differences in the predictions for the major gas and tar concentrations using the different incoming gas flow cases. While Cases 2 and 3 are able to better predict the different tar classes than Cases 1 and 4, their major gas predictions have significant disagreements with experiments. While an accurate char conversion model could help us better predict the major gas concentrations, a more detailed reactor network that better captures the mixing inhomogeneities inside the bed might improve the tar predictions.

Figure 4-8: Evolution of the major gas species concentrations inside the bubbling bed at two different temperatures (1073K and 1123K) for Case 2 mixing. Solid lines indicate the species evolution within PFR and dashed lines represent the CSTR concentrations. Oxygen consumption is much faster at 1123K than 1073K

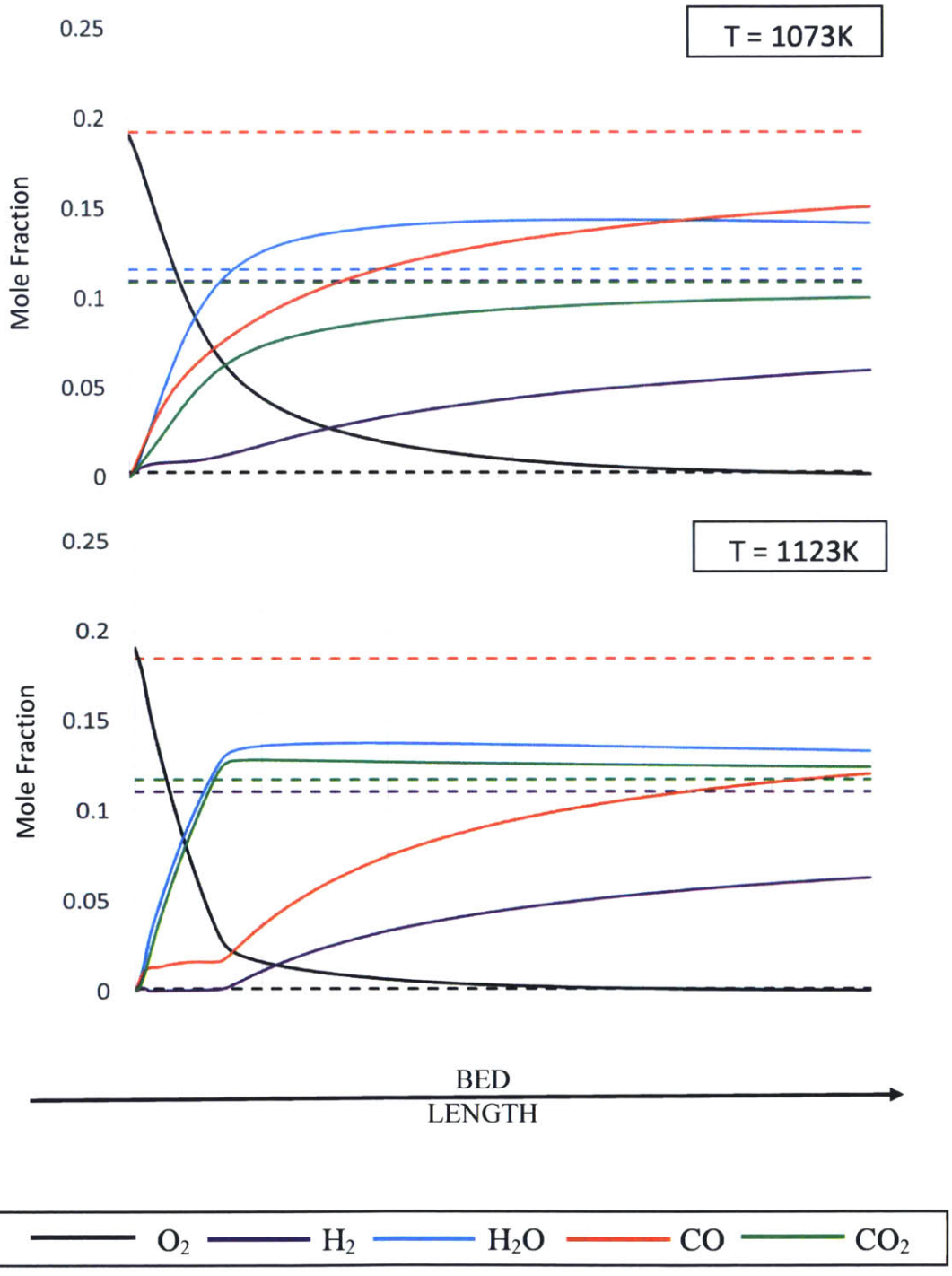

Figure 4-9: Impact of water-gas shift kinetics on the evolution of CO, CO_2 and O_2 concentrations inside the PFR (above) and CSTR (below) regions of the bubbling bed for Case 2 mixing at 1123K. Solid lines represent the case of slow WGS kinetics and dashed lines represent the case of fast WGS kinetics from Biba [97]. Larger CO conversion into CO2 is observed for the faster WGS kinetics case, even though the CO oxidation rates stayed constant

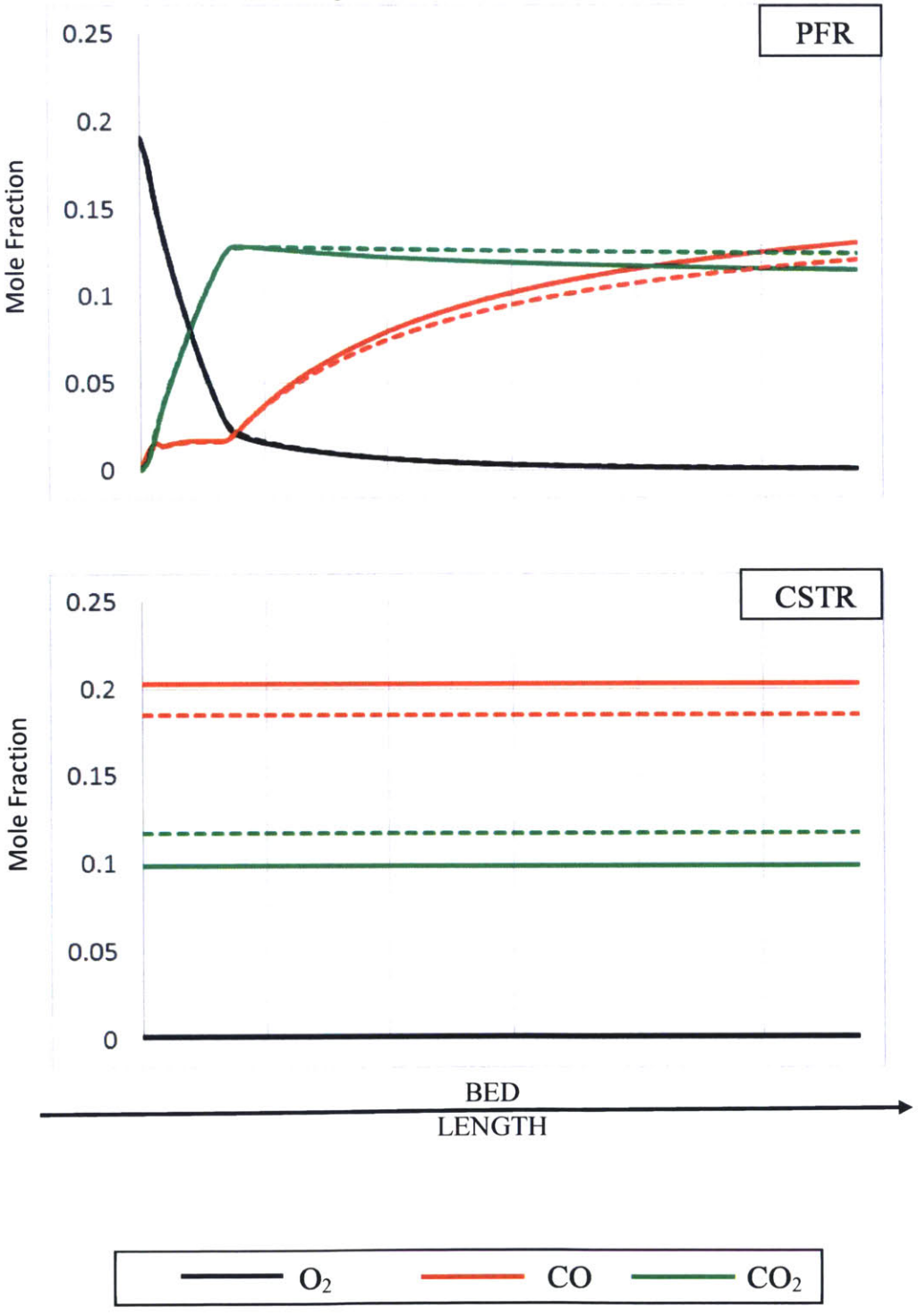

4.3 Steam Gasification conditions

In this section, the improved reactor network model is implemented for the NREL steam gasification conditions using the detailed CRECK kinetic scheme. The particle scale model developed by Stark [3] is used to evaluate the devolatilization gas composition, which is then used as the input to the Reactor Network model of the gasifier. The fluidized bed is modeled using an isothermal continuously stirred reactor (CSTR) and an isothermal plug flow reactor (PFR) in parallel, with the emulsion (dense) phase being modeled as the CSTR and the bubble phase modeled as the PFR. Similar to the previous section, four different cases for modeling the incoming gas flow rate and composition into the two phases are considered (Table 4-3). The NREL steam gasification conditions used in the simulations are presented in Table 4-4. The different correlations used to describe bubble growth inside the fluidized bed as well as the mass transfer correlations to describe the interphase exchange between the bubble and emulsion phases are tabulated in Table 4-5.

The catalytic effect of the bed material on the water-gas shift reaction kinetics is accounted for, by the use of the fast WGS kinetics proposed by Gomez Barea [23], for the emulsion phase. In addition, the char conversion model, described in Section 3.5, is used to represent the effects of char gasification on the production/consumption of CO, H_2, H_2O and CO_2 inside the emulsion phase.

Table 4-3: Different cases for the incoming gas flow conditions considered in the improved Reactor Network Model

	Emulsion phase (CSTR)	Bubble phase (PFR)
Case 1	Half of the devolatilization gases and gasifying agent	Half of the devolatilization gases and gasifying agent
Case 2	The entire amount of devolatilization gases enters the emulsion phase	The entire amount of gasifying agent enters the bubble phase
Case 3	The entire amount of gasifying agent enters the emulsion phase	The entire amount of devolatilization gases enters the bubble phase
Case 4	Entire bed modeled as a single CSTR	

Table 4-4: Simulation conditions representing the NREL experiments

Simulation conditions	
Biomass feedstock	Hybrid poplar (0.75-2mm)
Fluidizing medium	Olivine sand (270 μm)
Fluidizing agent	Steam
Bed diameter (in m)	0.102
Biomass feed rate (in kg/hr)	0.8
Bed temperature (in K)	1023-1123
Pressure (in atm)	1.154
Steam Biomass ratio	1
Ratio of incoming superficial velocity to minimum fluidization velocity	4.1

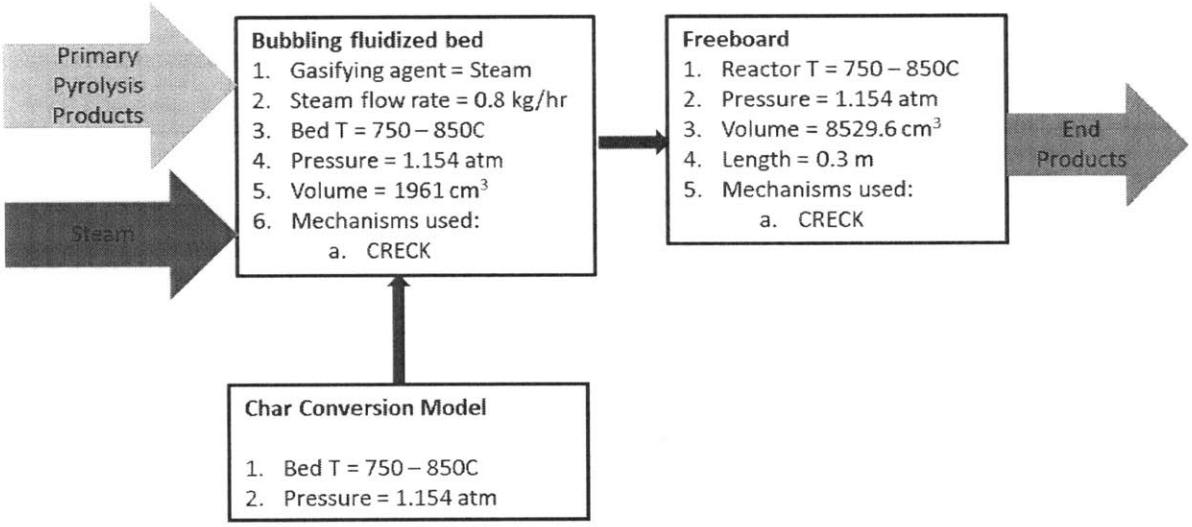

Figure 4-10: Schematic of the simulation conditions used in the improved RNM simulations for the NREL steam blown gasification conditions

Table 4-5: Bubble growth and inter-phase mass transfer correlations employed for the NREL steam blown gasifier conditions

Quantity (Units)	**Value** (given or calculated from correlations used in Kaushal et al. [90])
Bubbling bed height (m)	0.24
Minimum Fluidization velocity, U_{mf} (m/s)	0.034
Incoming superficial velocity, U_0 (m/s)	0.1394
Cross-sectional area of the bed, A (m^2)	0.0082
Bubble Diameter, $d_B(z)$ (m) (z is location along the bed height)	$0.54(U_0\text{-}U_{mf})^{0.4} g^{-0.2} \left(z + 4\sqrt{\frac{A}{100}} \right)^{0.8}$
Bubble rise velocity, U_{br} (m/s)	$0.711\sqrt{g d_B}$
Bubble velocity, U_b (m/s)	$U_0 - U_{mf} + U_{br}$
Diffusivity, D (m^2/s)	0.00001
Voidage at minimum fluidization velocity, ε_{mf}	0.5
Bed particle diameter (m)	270 μm
Bed particle density (kg/m^3)	2500
Bubble phase fraction	$\frac{U_0 - U_{mf}}{U_b - U_{mf}}$
Mass transfer coefficient (m/s)	$K_{BE} = \frac{U_{mf}}{4} + \sqrt{\frac{4\varepsilon_{mf} D U_B}{\pi d_B}}$

4.3.1 Results and Discussion

The major gas species concentrations and the individual tar class concentrations for the different gasification temperatures are plotted in Figures 4-11 and 4-12, for the steam gasification conditions. Unlike the case of air-blown gasification, the choice of the incoming gas flow case does not have a very significant impact on the concentrations of the major gas species and the individual tar classes. The original assumption of the bed being well mixed (Case 4) is found to be accurate in predicting both the major gas species concentration as well as the individual tar classes. This could be attributed to the moderate superficial gas velocities (U_0/U_{mf} = 4.1) in the NREL steam gasification experiments. Under these conditions, the bubbles are small and the mixing is vigorous, hence the assumption that the fluidized bed is well mixed holds and the CSTR assumption is valid.

Similar to air gasification, the extreme condition represented by Case 3, in which all the devolatilization gases are assumed to enter the bubble phase, results in the production of higher amounts of tars and PAH's, implying the positive effect of locally rich regions on PAH growth.

However, in the other extreme condition (Case 2), the total tar amounts at the gasifier outlet are smaller than the other cases. This could be attributed to the inhibition effect of hydrogen on tar growth and PAH formation reactions in the emulsion phase. This is possible because, unlike air gasification, there is a significantly large concentration of hydrogen under steam gasification conditions. Subsequently, hydrogen concentration at the gasifier outlet is smaller in Case 2 than the other cases.

Methane concentration is affected only to a negligible extent for the different incoming gas flow cases considered. The concentrations of the other major gases are largely affected by the choice of the water-gas shift kinetics and the difference in the predictions for the different cases is mainly due to the difference in the relative contributions of the emulsion phase (faster WGS kinetics) and the bubble phase (slower WGS kinetics) to the final product composition.

To conclude, it can be stated that there are not significant variations in the major gas and tar predictions for the different incoming gas flow cases. The original assumption of a well-mixed bed is found to be accurate.

Figure 4-11: Different tar class concentrations predicted for the NREL steam blown gasification conditions using the improved reactor network model for the different incoming gas flow cases. The variation in the tar concentrations with the gasification temperature is similar for all the incoming gas flow cases

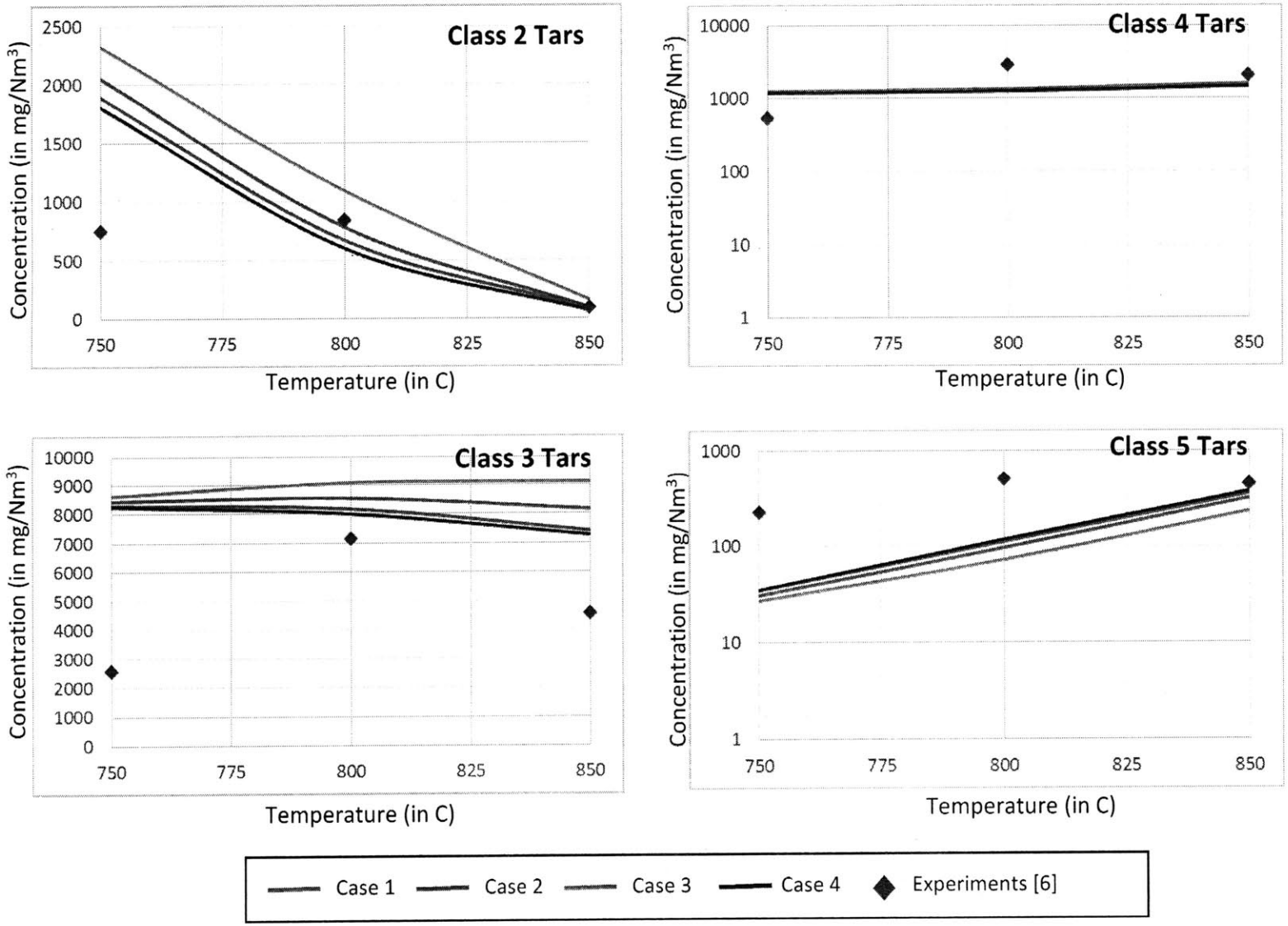

Figure 4-12: Major gas species and total tar concentrations predicted for the NREL steam blown gasification conditions using the improved reactor network model for the different incoming gas flow cases. The model predictions are in good agreement for all the incoming gas flow cases.

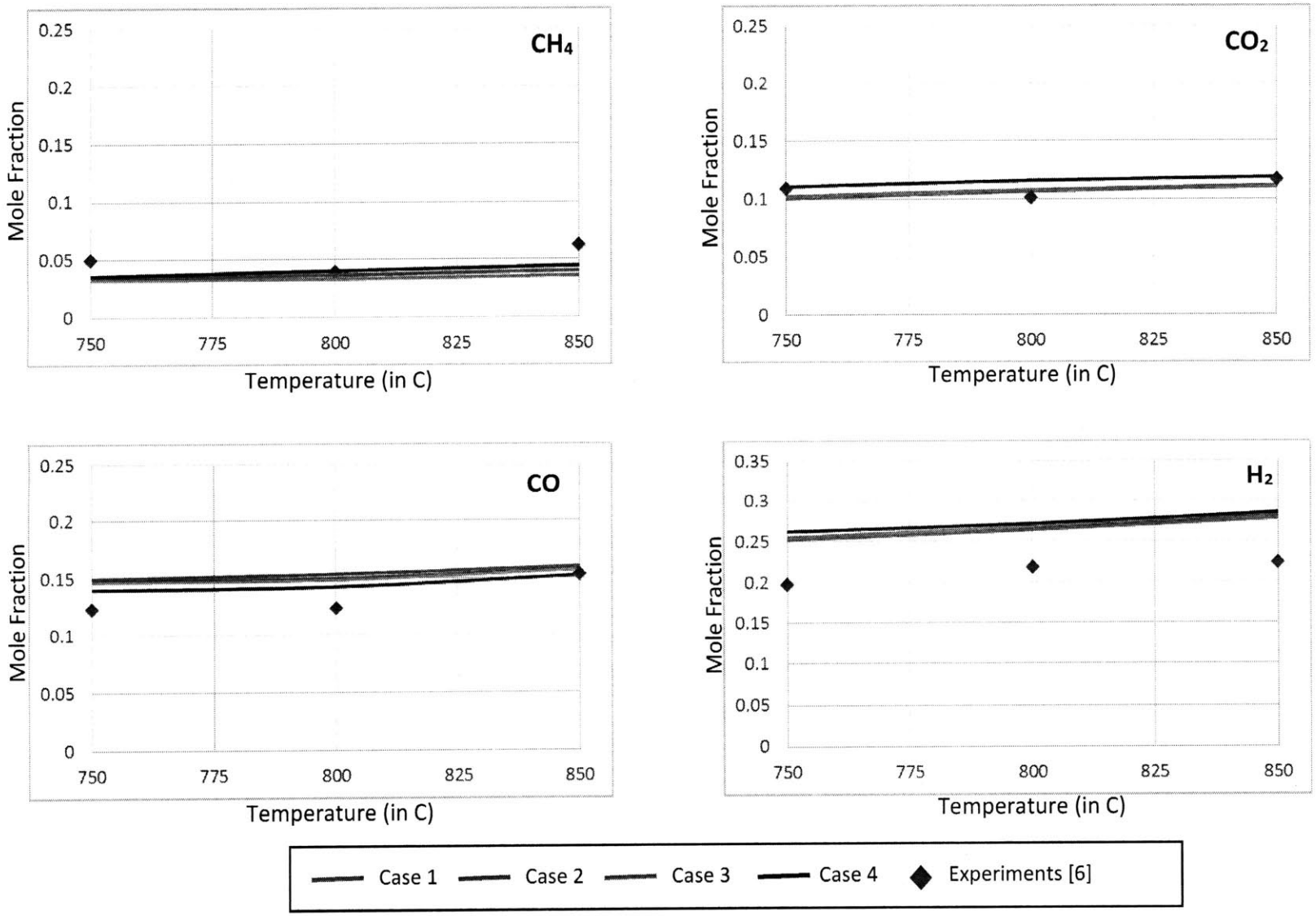

Figure 4-12 (contd.): Major gas species and total tar concentrations predicted for the NREL steam blown gasification conditions using the improved reactor network model for the different incoming gas flow cases. The model predictions are in good agreement for all the incoming gas flow cases.

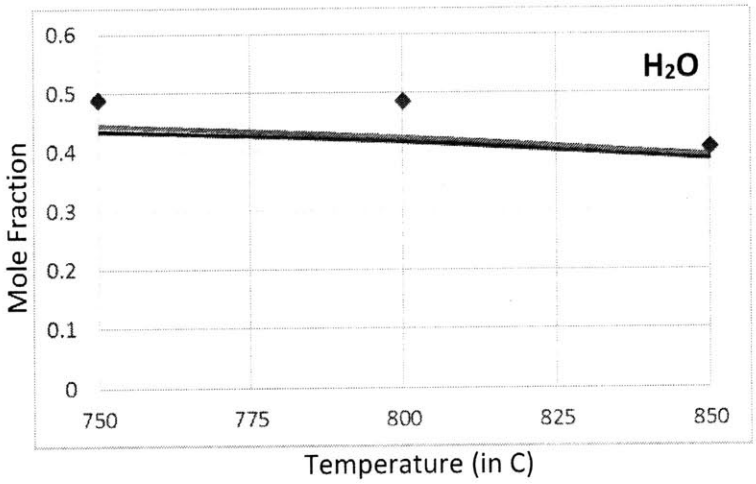

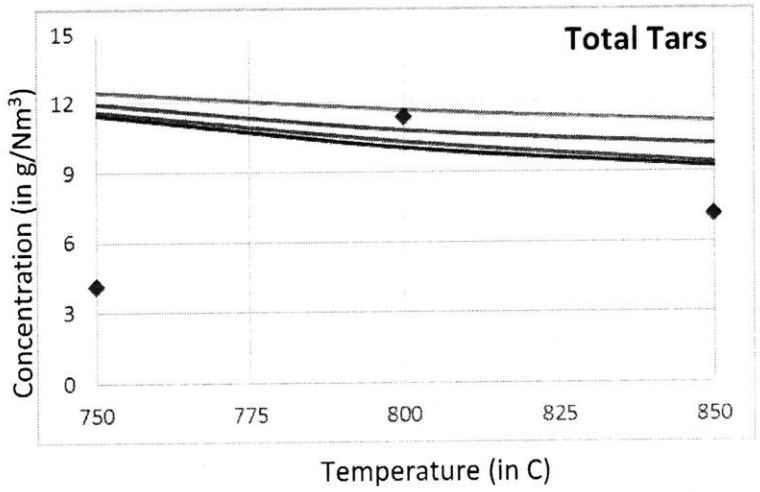

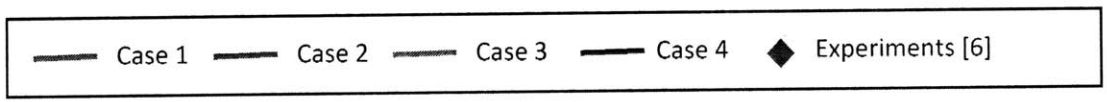

Figures 4-13 and 4-14 depict the evolution of hydrogen, carbon monoxide and class 3 tars along the gasifier bed at a bed temperature of 800°C, for the different incoming gas flow cases. It can be seen that the impact of these incoming gas flow cases on the class 3 tar concentration is weak compared to air gasification. This is because, in the absence of oxygen, tar concentrations are affected only by the slow steam reforming reactions and PAH growth reactions at these low temperatures. Similarly, the outlet concentrations of carbon monoxide and hydrogen are largely dominated by the water-gas shift kinetics employed and the influence of the different incoming gas flow cases is small.

Figure 4-13: Evolution of the hydrogen concentrations inside the gasifier, evaluated using the improved reactor network model at 1073K. There is negligible difference in the hydrogen concentrations for the different incoming gas flow cases. Within the bed region, dashed lines indicate the species evolution within PFR and dotted lines represent the CSTR concentrations

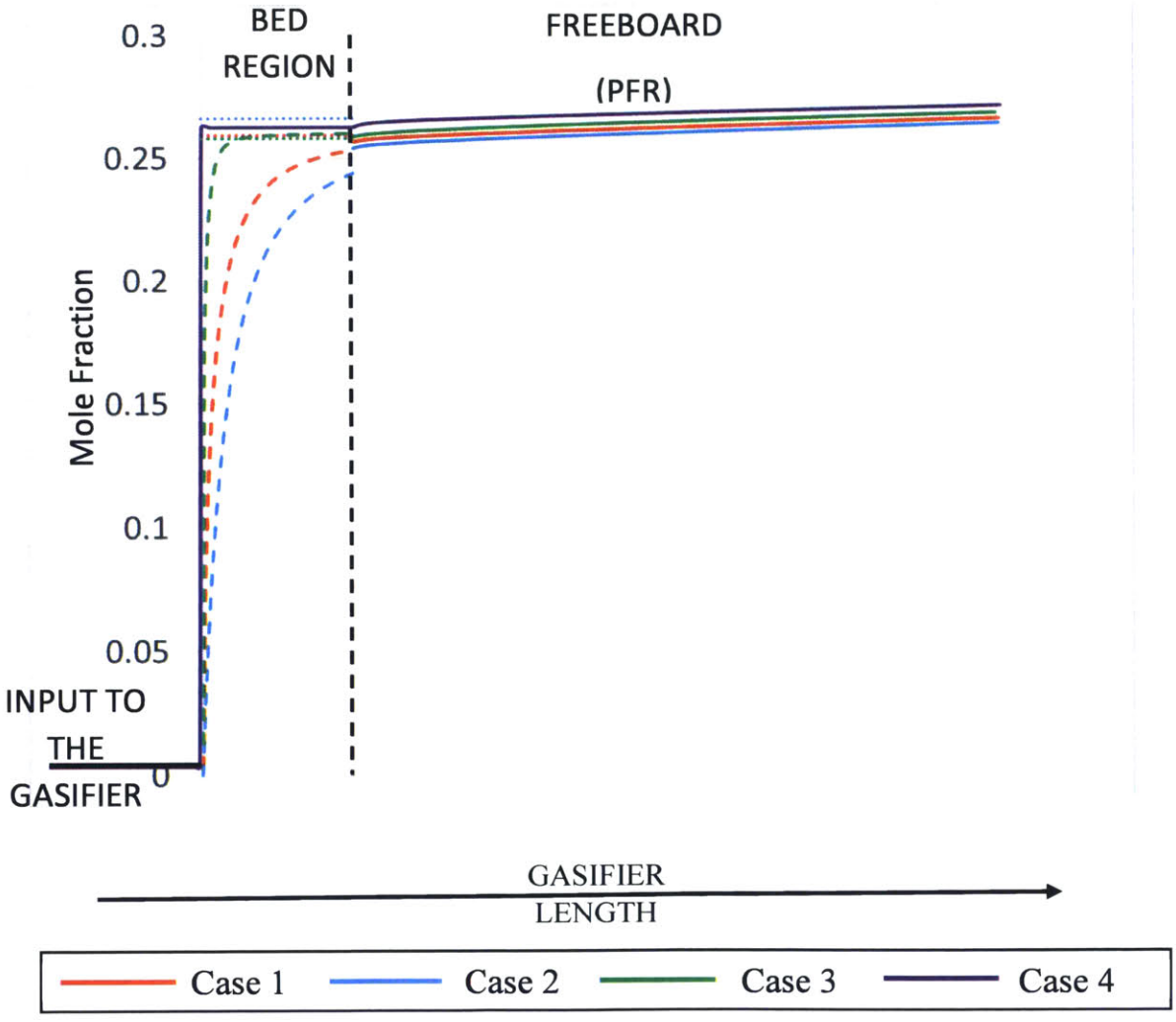

Figure 4-14: Evolution of the CO (above) and Class 3 tar (below) concentrations inside the gasifier, evaluated using the improved reactor network model at 1073K. The difference in both the concentrations is not very significant for the different incoming gas flow cases. Within the bed region, dashed lines indicate the species evolution within PFR and dotted lines represent the CSTR concentrations

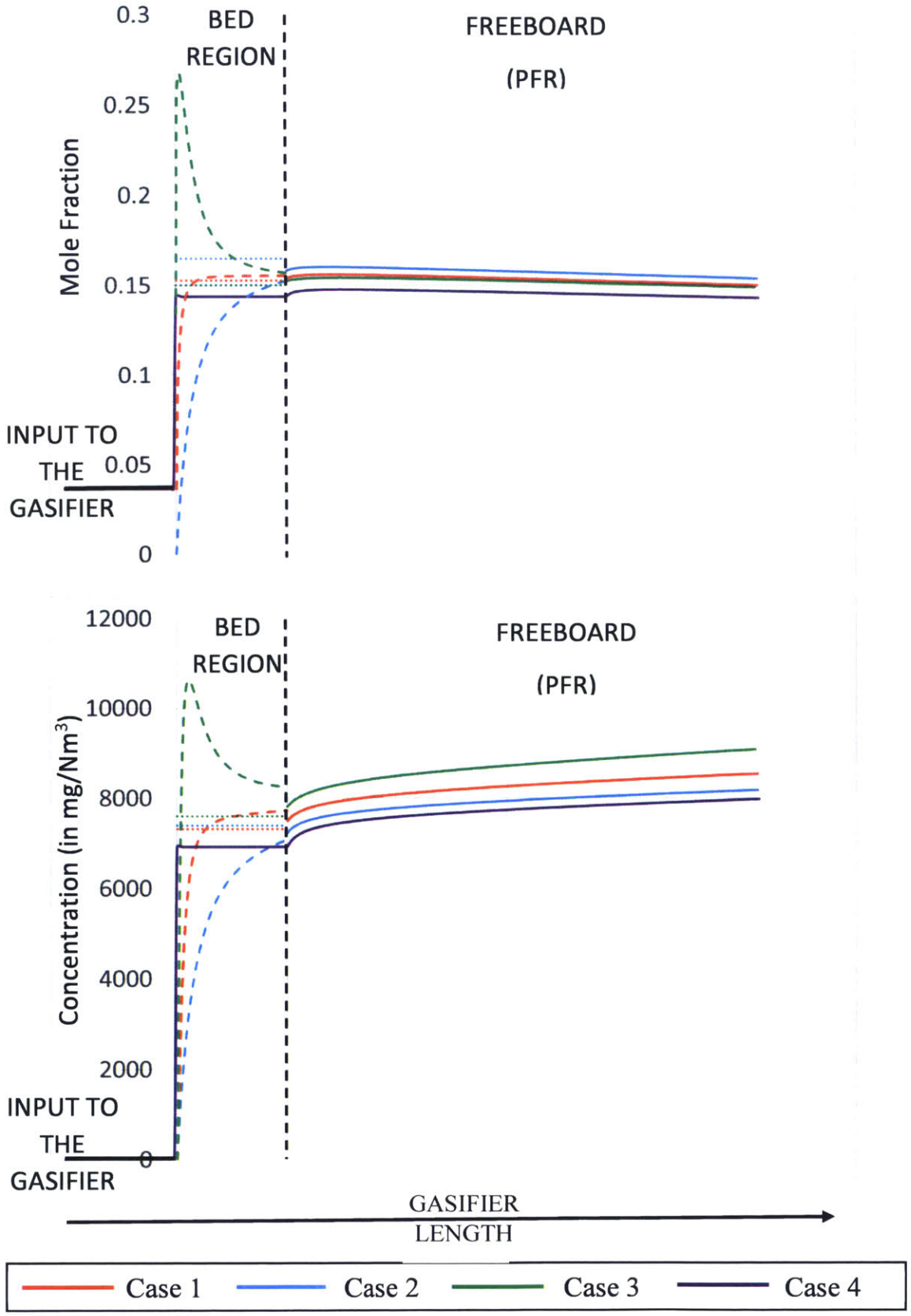

4.4 Conclusions

In this chapter, an improved reactor network model based on the two-phase theory was developed for fluidized bed biomass gasification. The fluidized bed was represented using a single stage reactor network model consisting of a continuously well stirred reactor (CSTR) for the emulsion phase and a plug flow reactor (PFR) for the bubble phase. The reactor geometries were evaluated using standard bubble property correlations available in literature and the interphase mass exchange between the reactors was modeled using available mass transfer correlations. The division of the incoming gas flow into each of the reactors was modeled using simple assumptions on the incoming gas flow conditions and the impact of these assumptions on the major gas and tar concentrations was studied.

Employing the detailed CRECK kinetic mechanism, the improved reactor network model was implemented for the air-blown gasification conditions considered in the van Paasen and Kiel experiments, as well as for the steam gasification conditions used in the NREL experiments. In the case of air gasification, it was observed that the extreme incoming gas flow cases, representing the case of severe inhomogoeneities in the bed, over-predicted the various tar classes and Polycyclic Aromatic Hydrocarbons (PAH) supporting the hypothesis that locally rich regions in the bed could potentially result in the presence of large amounts of PAHs in the synthetic gas. However, in the case of steam gasification, the well mixed CSTR assumption was found to be accurate and the predictions for the major gas species and tar concentrations were in very good agreement with experimentally measured values.

5 Conclusions

A comprehensive review of the various chemistry models available for biomass gasification was presented. Starting with the thermodynamic-based models used to model the chemical processes in biomass gasification, different kinetic models of varying complexity were discussed. The simplest kinetic models were the global reaction models that were developed empirically from experiments and considered a small set of chemical species and global reactions to describe the gasification process. With the advent of computers and developments in automatic generation of chemical mechanisms, large chemical kinetic mechanisms consisting of a few hundred species and thousands of reactions have been developed. While the global models are very restrictive in terms of applicability, these large kinetic mechanisms can, in theory, be applied to a wide variety of operating conditions. However, the huge computational demands associated with solving these detailed kinetic mechanisms necessitated the development of compact reaction mechanisms using various mechanism reduction techniques. Compact mechanisms present an ideal balance between the accuracy of the large kinetic mechanisms and the smaller computational requirements of global chemistry models. After a brief discussion of the different mechanism reduction techniques, two compact mechanisms for biomass gasification from the literature were presented.

With the aim to be used in CFD simulations, two global chemistry models incorporating a global primary tar cracking reaction was presented for air-blown and steam-blown gasification conditions. After a brief overview of the different sub-models used in the reactor network simulations of biomass gasification, a detailed discussion on the development of the new global chemistry models was presented. The predictive accuracy of the global models were then examined on comparison with the experimental observations, as well as the predictions using the detailed CRECK mechanism. The sensitivity of the different sub-models employed in the simulation on the synthetic gas composition were also studied.

In the final chapter, an improved reactor network model, based on the two-phase theory of fluidization, was developed. The improved reactor network model employed a single stage of ideal chemical reactors to describe the bubbling fluidized bed. The impact of the incoming gas flow conditions inside the bubbling bed on the major gas species evolution and tar growth was examined for air gasification and steam gasification conditions. The reactor geometries as well as the interphase mass exchange were modeled using standard bubble property correlations available in literature. In the case of van Paasen and Kiel experiments with very high fluidization velocities, it

was observed that the well mixed assumption for the bed predicted significantly smaller tar class (classes 3, 4 and 5) concentrations than experimental observations [13]. The extreme cases of incoming gas flow conditions were able to explain some of these under-predictions, implying that the large PAH concentrations observed in the experiments were potentially due to mixing inhomogeneities in the bed. On the other hand, the well mixed assumption for the bubbling bed was found to be quite accurate in predicting the tar concentrations and major gas species concentrations for the NREL steam gasification experiments which employed moderate superficial gas velocities [101].

5.1 Future Work

An even more detailed modeling of the bubbling bed could help us better capture the mixing inhomogeneities in the bed, and could potentially answer some of the important questions on the impact of incomplete mixing and biomass segregation on the major gas and different tar class concentrations in the gasifier. A schematic of a more detailed reactor network model, consisting of multiple stages of CSTR and PFR interacting with each other, to model the bubbling fluidized bed is depicted in Figure 5-1.

A number of different inputs and model parameters would be required to be able to represent the reactor geometries and flow characteristics in this reactor network model. The gas flow division at each stage of the gasifier as well as the volume of the individual reactors at each stage could be evaluated based on correlations obtained from experiments. While the bubble property correlations would provide information on the individual reactor volumes, the information on the gas slow division to each reactor could be obtained from CFD simulations of the gasifier. In this case, the CFD simulation could employ a simple global chemistry model, with a small number of chemical species and reactions, just to evaluate the flow characteristics inside the gasifier.

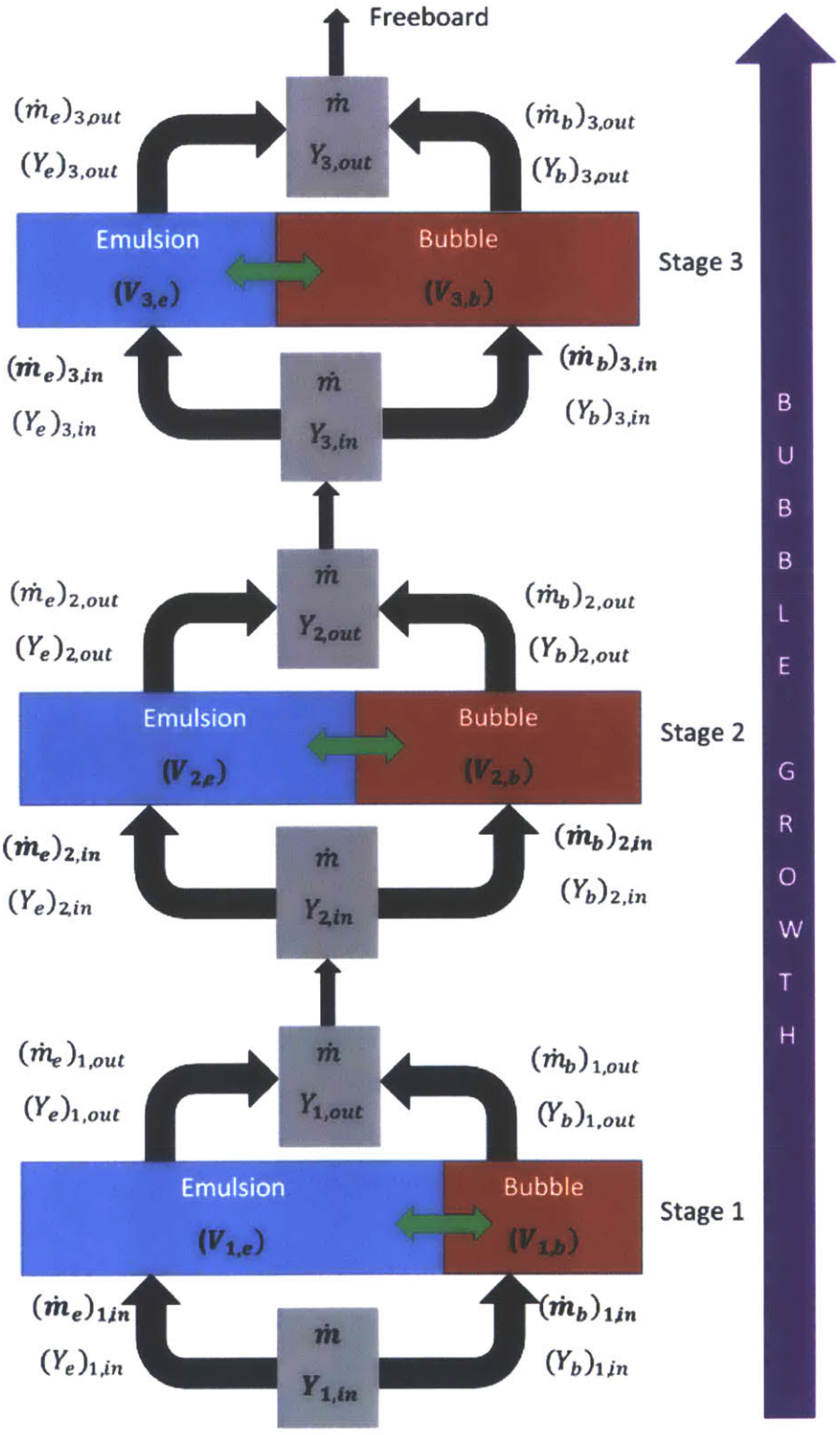

Figure 5-1: Schematic of the detailed Reactor network model for the bubbling fluidized bed (Y is the composition of the gas, V is the volume of the reactor and $\dot{m}$ is the mass flow rate into/out of each of the reactors

Bibliography

[1] C. McGlade and P. Ekins, "The geographical distribution of fossil fuels unused when limiting global warming to 2 °C," *Nature*, vol. 517, no. 7533, pp. 187–190, Jan. 2015.

[2] A. Demirbaş, "Biomass resource facilities and biomass conversion processing for fuels and chemicals," *Energy Convers. Manag.*, vol. 42, no. 11, pp. 1357–1378, Jul. 2001.

[3] A. K. Stark, "Multi-Scale Chemistry Modeling of the Thermochemical Conversion of Biomass in a Fluidized Bed Gasifier," PhD thesis, Massachusetts Institute of Technology, 2015.

[4] K. T. Tan, K. T. Lee, and A. R. Mohamed, "Role of energy policy in renewable energy accomplishment: The case of second-generation bioethanol," *Energy Policy*, vol. 36, no. 9, pp. 3360–3365, 2008.

[5] P. McKendry, "Energy production from biomass (part 1): overview of biomass," *Bioresour. Technol.*, vol. 83, no. 1, pp. 37–46, May 2002.

[6] T. A. Milne, N. Abatzoglou, and R. J. Evans, *Biomass gasifier" tars": Their nature, formation, and conversion*, vol. 570. National Renewable Energy Laboratory Golden, CO, 1998.

[7] C. Li and K. Suzuki, "Tar property, analysis, reforming mechanism and model for biomass gasification—An overview," *Renew. Sustain. Energy Rev.*, vol. 13, no. 3, pp. 594–604, Apr. 2009.

[8] A. K. Stark, R. B. Bates, Z. Zhao, and A. F. Ghoniem, "Prediction and Validation of Major Gas and Tar Species from a Reactor Network Model of Air-Blown Fluidized Bed Biomass Gasification," *Energy Fuels*, vol. 29, no. 4, pp. 2437–2452, Apr. 2015.

[9] E. Ranzi, A. Cuoci, T. Faravelli, A. Frassoldati, G. Migliavacca, S. Pierucci, and S. Sommariva, "Chemical Kinetics of Biomass Pyrolysis," *Energy Fuels*, vol. 22, no. 6, pp. 4292–4300, Nov. 2008.

[10] M. Puig-Arnavat, J. C. Bruno, and A. Coronas, "Review and analysis of biomass gasification models," *Renew. Sustain. Energy Rev.*, vol. 14, no. 9, pp. 2841–2851, Dec. 2010.

[11] M. Balat, "Mechanisms of Thermochemical Biomass Conversion Processes. Part 2: Reactions of Gasification," *Energy Sources Part Recovery Util. Environ. Eff.*, vol. 30, no. 7, pp. 636–648, Mar. 2008.

[12] C. Di Blasi, "Modeling chemical and physical processes of wood and biomass pyrolysis," *Prog. Energy Combust. Sci.*, vol. 34, no. 1, pp. 47–90, Feb. 2008.

[13] S. V. B. van Paasen and J. H. A. Kiel, "Tar formation in a fluidised bed gasifier," Energy Research Center of the Netherlands, ECN-C--04-013, 2004.

[14] Z. A. Zainal, R. Ali, C. H. Lean, and K. N. Seetharamu, "Prediction of performance of a downdraft gasifier using equilibrium modeling for different biomass materials," *Energy Convers. Manag.*, vol. 42, no. 12, pp. 1499–1515, Aug. 2001.

[15] S. Jarungthammachote and A. Dutta, "Thermodynamic equilibrium model and second law analysis of a downdraft waste gasifier," *Energy*, vol. 32, no. 9, pp. 1660–1669, Sep. 2007.

[16] R. D. Philippe Mathieu, "Performance analysis of a biomass gasifier," *Energy Convers. Manag.*, pp. 1291–1299, 2002.

[17] S. Jarungthammachote and A. Dutta, "Equilibrium modeling of gasification: Gibbs free energy minimization approach and its application to spouted bed and spout-fluid bed gasifiers," *Energy Convers. Manag.*, vol. 49, no. 6, pp. 1345–1356, Jun. 2008.

[18] W. Gumz, *Gas Producers and Blast Furnaces: Theory Ad Metods of Calculation*. John Wiley & Sons, 1950.

[19] D. W. Bacon, J. Downie, J. C. Hsu, and J. Peters, "Modelling of Fluidized Bed Wood Gasifiers," in *Fundamentals of Thermochemical Biomass Conversion*, R. P. Overend, T. A. Milne, and L. K. Mudge, Eds. Springer Netherlands, 1985, pp. 717–732.

[20] M. J. Prins, K. J. Ptasinski, and F. J. J. G. Janssen, "From coal to biomass gasification: Comparison of thermodynamic efficiency," *Energy*, vol. 32, no. 7, pp. 1248–1259, Jul. 2007.

[21] A. Villanueva, A. Gomez-Barea, E. Revuelta, M. Campoy, and P. Ollero, "Guidelines for selection of gasifiers modelling strategies," in *16th European biomass conference and exhibition*, 2008.

[22] G. Schuster, G. Löffler, K. Weigl, and H. Hofbauer, "Biomass steam gasification – an extensive parametric modeling study," *Bioresour. Technol.*, vol. 77, no. 1, pp. 71–79, Mar. 2001.

[23] A. Gomez-Barea and B. Leckner, "Modeling of biomass gasification in fluidized bed," *Prog. Energy Combust. Sci.*, vol. 36, no. 4, pp. 444–509, Aug. 2010.

[24] M. Ruggiero and G. Manfrida, "An equilibrium model for biomass gasification processes," *Renew. Energy*, vol. 16, no. 1–4, pp. 1106–1109, Jan. 1999.

[25] X. T. Li, J. R. Grace, C. J. Lim, A. P. Watkinson, H. P. Chen, and J. R. Kim, "Biomass gasification in a circulating fluidized bed," *Biomass Bioenergy*, vol. 26, no. 2, pp. 171–193, Feb. 2004.

[26] A. Melgar, J. F. Pérez, H. Laget, and A. Horillo, "Thermochemical equilibrium modelling of a gasifying process," *Energy Convers. Manag.*, vol. 48, no. 1, pp. 59–67, Jan. 2007.

[27] D. Baruah and D. C. Baruah, "Modeling of biomass gasification: A review," *Renew. Sustain. Energy Rev.*, vol. 39, pp. 806–815, Nov. 2014.

[28] S. Gerber, F. Behrendt, and M. Oevermann, "An Eulerian modeling approach of wood gasification in a bubbling fluidized bed reactor using char as bed material," *Fuel*, vol. 89, no. 10, pp. 2903–2917, Oct. 2010.

[29] B. V. Babu, "Biomass pyrolysis: a state-of-the-art review," *Biofuels Bioprod. Biorefining*, vol. 2, no. 5, pp. 393–414, 2008.

[30] Fred Shafizadeh and Peter P. S. Chin, "Thermal Deterioration of Wood," in *Wood Technology: Chemical Aspects*, vol. 43, 0 vols., American Chemical Society, 1977, pp. 57–81.

[31] R. J. Evans and T. A. Milne, "Molecular characterization of the pyrolysis of biomass. 2. Applications," *Energy Fuels*, vol. 1, no. 4, pp. 311–319, 1987.

[32] W. S.-L. Mok and M. J. Antal Jr., "Effects of pressure on biomass pyrolysis. I. Cellulose pyrolysis products," *Thermochim. Acta*, vol. 68, no. 2–3, pp. 155–164, Oct. 1983.

[33] M. J. Antal, "Biomass pyrolysis: A review of the literature. Part II- Lignocellulose pyrolysis," *Adv. Sol. Energy*, pp. 175–253, 1985.

[34] M. L. Boroson, J. B. Howard, J. P. Longwell, and W. A. Peters, "Product yields and kinetics from the vapor phase cracking of wood pyrolysis tars," *AIChE J.*, vol. 35, no. 1, pp. 120–128, 1989.

[35] P. Morf, P. Hasler, and T. Nussbaumer, "Mechanisms and kinetics of homogeneous secondary reactions of tar from continuous pyrolysis of wood chips," *Fuel*, vol. 81, no. 7, pp. 843–853, May 2002.

[36] J. Rath and G. Staudinger, "Cracking reactions of tar from pyrolysis of spruce wood," *Fuel*, vol. 80, no. 10, pp. 1379–1389, Aug. 2001.

[37] A. N. García, R. Font, and A. Marcilla, "Kinetic study of the flash pyrolysis of municipal solid waste in a fluidized bed reactor at high temperature," *J. Anal. Appl. Pyrolysis*, vol. 31, pp. 101–121, Feb. 1995.

[38] R. S. Miller and J. Bellan, "A generalized biomass pyrolysis model based on superimposed cellulose hemicellulose and lignin kinetics," NASA Jet Propulsion Laboratory, Pasadena,CA, 91109-8099, 1996.

[39] C. Di Blasi, "Heat, momentum and mass transport through a shrinking biomass particle exposed to thermal radiation," *Chem. Eng. Sci.*, vol. 51, no. 7, pp. 1121–1132, Apr. 1996.

[40] C. Di Blasi, "Influences of physical properties on biomass devolatilization characteristics," *Fuel*, vol. 76, no. 10, pp. 957–964, Aug. 1997.

[41] C. Di Blasi, "Physico-chemical processes occurring inside a degrading two-dimensional anisotropic porous medium," *Int. J. Heat Mass Transf.*, vol. 41, no. 24, pp. 4139–4150, Oct. 1998.

[42] K. M. Bryden, K. W. Ragland, and C. J. Rutland, "Modeling thermally thick pyrolysis of wood," *Biomass Bioenergy*, vol. 22, no. 1, pp. 41–53, Jan. 2002.

[43] K. M. Bryden and M. J. Hagge, "Modeling the combined impact of moisture and char shrinkage on the pyrolysis of a biomass particle☆," *Fuel*, vol. 82, no. 13, pp. 1633–1644, Sep. 2003.

[44] J. Saastamoinen and J.-R. Richard, "Simultaneous drying and pyrolysis of solid fuel particles," *Combust. Flame*, vol. 106, no. 3, pp. 288–300, Aug. 1996.

[45] S. Shrestha, S. Cramer, and R. White, "Time temperature profiles across a lumber section exposed to pyrolytic temperatures," *Fire Mater.*, vol. 18, no. 4, pp. 211–220, 1994.

[46] R. Bilbao, J. F. Mastral, J. Ceamanos, and M. E. Aldea, "Modelling of the pyrolysis of wet wood," *J. Anal. Appl. Pyrolysis*, vol. 36, no. 1, pp. 81–97, Apr. 1996.

[47] R. Difelice, G. Coppola, S. Rapagna, and N. Jand, "Modeling of biomass devolatilization in a fluidized bed reactor," *Can. J. Chem. Eng.*, vol. 77, no. 2, pp. 325–332, 1999.

[48] B. V. Babu and A. S. Chaurasia, "Heat transfer and kinetics in the pyrolysis of shrinking biomass particle," *Chem. Eng. Sci.*, vol. 59, no. 10, pp. 1999–2012, May 2004.

[49] A. Marongiu, Politechnico di Milano, Italy, 2005.

[50] E. Ranzi, M. Dente, A. Goldaniga, G. Bozzano, and T. Faravelli, "Lumping procedures in detailed kinetic modeling of gasification, pyrolysis, partial oxidation and combustion of hydrocarbon mixtures," *Prog. Energy Combust. Sci.*, vol. 27, no. 1, pp. 99–139, Jan. 2001.

[51] A. Stagni, A. Cuoci, A. Frassoldati, T. Faravelli, and E. Ranzi, "Lumping and Reduction of Detailed Kinetic Schemes: an Effective Coupling," *Ind. Eng. Chem. Res.*, vol. 53, no. 22, pp. 9004–9016, Jun. 2014.

[52] C. Chevalier, J. Warnatz, and H. Melenk, "Automatic Generation of Reaction Mechanisms for the Description of the Oxidation of Higher Hydrocarbons," *Berichte Bunsenges. Für Phys. Chem.*, vol. 94, no. 11, pp. 1362–1367, 1990.

[53] K. M. Van Geem, M.-F. Reyniers, G. B. Marin, J. Song, W. H. Green, and D. M. Matheu, "Automatic reaction network generation using RMG for steam cracking of n-hexane," *AIChE J.*, vol. 52, no. 2, pp. 718–730, 2006.

[54] L. J. Broadbelt, S. M. Stark, and M. T. Klein, "Computer Generated Pyrolysis Modeling: On-the-Fly Generation of Species, Reactions, and Rates," *Ind. Eng. Chem. Res.*, vol. 33, no. 4, pp. 790–799, Apr. 1994.

[55] L. P. Hillewaert, J. L. Dierickx, and G. F. Froment, "Computer generation of reaction schemes and rate equations for thermal cracking," *AIChE J.*, vol. 34, no. 1, pp. 17–24, 1988.

[56] S. E. Prickett and M. L. Mavrovouniotis, "Construction of complex reaction systems—I. Reaction description language," *Comput. Chem. Eng.*, vol. 21, no. 11, pp. 1219–1235, 1997.

[57] S. E. Prickett and M. L. Mavrovouniotis, "Construction of complex reaction systems—II. Molecule manipulation and reaction application algorithms," *Comput. Chem. Eng.*, vol. 21, no. 11, pp. 1237–1254, 1997.

[58] S. E. Prickett and M. L. Mavrovouniotis, "Construction of complex reaction systems—III. An example: alkylation of olefins," *Comput. Chem. Eng.*, vol. 21, no. 12, pp. 1325–1337, 1997.

[59] M. S. Okino and M. L. Mavrovouniotis, "Simplification of Mathematical Models of Chemical Reaction Systems," *Chem. Rev.*, vol. 98, no. 2, pp. 391–408, Apr. 1998.

[60] H. Rabitz, M. Kramer, and D. Dacol, "Sensitivity Analysis in Chemical Kinetics," *Annu. Rev. Phys. Chem.*, vol. 34, no. 1, pp. 419–461, Oct. 1983.

[61] Y. Reuven, M. D. Smooke, and H. Rabitz, "Sensitivity analysis of boundary value problems: application to nonlinear reaction-diffusion systems," *J. Comput. Phys.*, vol. 64, no. 1, pp. 27–55, May 1986.

[62] T. Lu and C. K. Law, "A directed relation graph method for mechanism reduction," *Proc. Combust. Inst.*, vol. 30, no. 1, pp. 1333–1341, Jan. 2005.

[63] T. Lu and C. K. Law, "On the applicability of directed relation graphs to the reduction of reaction mechanisms," *Combust. Flame*, vol. 146, no. 3, pp. 472–483, Aug. 2006.

[64] P. Pepiot-Desjardins and H. Pitsch, "An efficient error-propagation-based reduction method for large chemical kinetic mechanisms," *Combust. Flame*, vol. 154, no. 1–2, pp. 67–81, Jul. 2008.

[65] W. Sun, Z. Chen, X. Gou, and Y. Ju, "A path flux analysis method for the reduction of detailed chemical kinetic mechanisms," *Combust. Flame*, vol. 157, no. 7, pp. 1298–1307, Jul. 2010.

[66] S. H. Lam and D. A. Goussis, "The CSP method for simplifying kinetics," *Int. J. Chem. Kinet.*, vol. 26, no. 4, pp. 461–486, 1994.

[67] T. Lu, Y. Ju, and C. K. Law, "Complex CSP for chemistry reduction and analysis," *Combust. Flame*, vol. 126, no. 1–2, pp. 1445–1455, Jul. 2001.

[68] U. Maas and S. B. Pope, "Simplifying chemical kinetics: Intrinsic low-dimensional manifolds in composition space," *Combust. Flame*, vol. 88, no. 3–4, pp. 239–264, Mar. 1992.

[69] H. Huang, M. Fairweather, J. F. Griffiths, A. S. Tomlin, and R. B. Brad, "A systematic lumping approach for the reduction of comprehensive kinetic models," *Proc. Combust. Inst.*, vol. 30, no. 1, pp. 1309–1316, Jan. 2005.

[70] S. M. Jacob, B. Gross, S. E. Voltz, and V. W. Weekman, "A lumping and reaction scheme for catalytic cracking," *AIChE J.*, vol. 22, no. 4, pp. 701–713, 1976.

[71] T. T. Alison S. Tomlin, "Chapter 4 Mathematical tools for the construction, investigation and reduction of combustion mechanisms."

[72] L. E. Whitehouse, A. S. Tomlin, and M. J. Pilling, "Systematic reduction of complex tropospheric chemical mechanisms, Part II: Lumping using a time-scale based approach," *Atmospheric Chem. Phys.*, vol. 4, no. 7, pp. 2057–2081, Oct. 2004.

[73] P. Pepiot-Desjardins and H. Pitsch, "An automatic chemical lumping method for the reduction of large chemical kinetic mechanisms," *Combust. Theory Model.*, vol. 12, no. 6, pp. 1089–1108, Nov. 2008.

[74] J. Wei and J. C. W. Kuo, "Lumping Analysis in Monomolecular Reaction Systems. Analysis of the Exactly Lumpable System," *Ind. Eng. Chem. Fundam.*, vol. 8, no. 1, pp. 114–123, Feb. 1969.

[75] J. C. W. Kuo and J. Wei, "Lumping Analysis in Monomolecular Reaction Systems. Analysis of Approximately Lumpable System," *Ind. Eng. Chem. Fundam.*, vol. 8, no. 1, pp. 124–133, 1969.

[76] G. Li and H. Rabitz, "A general analysis of exact lumping in chemical kinetics," *Chem. Eng. Sci.*, vol. 44, no. 6, pp. 1413–1430, 1989.

[77] G. Li and H. Rabitz, "A general analysis of approximate lumping in chemical kinetics," *Chem. Eng. Sci.*, vol. 45, no. 4, pp. 977–1002, 1990.

[78] G. Li and H. Rabitz, "New approaches to determination of constrained lumping schemes for a reaction system in the whole composition space," *Chem. Eng. Sci.*, vol. 46, no. 1, pp. 95–111, 1991.

[79] G. Li, H. Rabitz, and J. Tóth, "A general analysis of exact nonlinear lumping in chemical kinetics," *Chem. Eng. Sci.*, vol. 49, no. 3, pp. 343–361, 1994.

[80] G. Li, A. S. Tomlin, H. Rabitz, and J. Tóth, "A general analysis of approximate nonlinear lumping in chemical kinetics. I. Unconstrained lumping," *J. Chem. Phys.*, vol. 101, no. 2, pp. 1172–1187, Jul. 1994.

[81] A. S. Tomlin, G. Li, H. Rabitz, and J. Tóth, "A general analysis of approximate nonlinear lumping in chemical kinetics. II. Constrained lumping," *J. Chem. Phys.*, vol. 101, no. 2, pp. 1188–1201, Jul. 1994.

[82] G. Li and H. Rabitz, "Determination of constrained lumping schemes for nonisothermal first-order reaction systems," *Chem. Eng. Sci.*, vol. 46, no. 2, pp. 583–596, 1991.

[83] G. Li and H. Rabitz, "The direct lumping approach: an application to a catalytic reforming model," *Chem. Eng. Sci.*, vol. 48, no. 10, pp. 1903–1909, 1993.

[84] T. Lu and C. K. Law, "Strategies for mechanism reduction for large hydrocarbons: n-heptane," *Combust. Flame*, vol. 154, no. 1–2, pp. 153–163, Jul. 2008.

[85] C. Font Palma, "A model for biomass gasification including tar formation and evolution," *Energy Fuels*, Apr. 2013.

[86] K. Malhotra, P. Pepiot, and M. Nimlos, "A novel approach for the development of global kinetic models for biomass gasification," 2013.

[87] C. Font Palma, "Modelling of tar formation and evolution for biomass gasification: A review," *Appl. Energy*, vol. 111, pp. 129–141, Nov. 2013.

[88] E.-J. Shin, M. R. Nimlos, and R. J. Evans, "Kinetic analysis of the gas-phase pyrolysis of carbohydrates," *Fuel*, vol. 80, no. 12, pp. 1697–1709, Oct. 2001.

[89] P. Kaushal, J. Abedi, and N. Mahinpey, "A comprehensive mathematical model for biomass gasification in a bubbling fluidized bed reactor," *Fuel*, vol. 89, no. 12, pp. 3650–3661, Dec. 2010.

[90] C. Di Blasi and C. Branca, "Kinetics of Primary Product Formation from Wood Pyrolysis," *Ind. Eng. Chem. Res.*, vol. 40, no. 23, pp. 5547–5556, Nov. 2001.

[91] V. Seebauer, J. Petek, and G. Staudinger, "Effects of particle size, heating rate and pressure on measurement of pyrolysis kinetics by thermogravimetric analysis," *Fuel*, vol. 76, no. 13, pp. 1277–1282, Oct. 1997.

[92] M. L. de Souza-Santos, *Solid fuels combustion and gasification : modeling, simulation, and equipment operation / Marcio L. de Souza-Santos.* New York: Marcel Dekker, 2004.

[93] J. C. Wurzenberger, S. Wallner, H. Raupenstrauch, and J. G. Khinast, "Thermal conversion of biomass: Comprehensive reactor and particle modeling," *AIChE J.*, vol. 48, no. 10, pp. 2398–2411, 2002.

[94] C. Di Blasi, F. Buonanno, and C. Branca, "Reactivities of some biomass chars in air," *Carbon*, vol. 37, no. 8, pp. 1227–1238, Jan. 1999.

[95] A. Gómez-Barea and B. Leckner, "Estimation of gas composition and char conversion in a fluidized bed biomass gasifier," *Fuel*, vol. 107, pp. 419–431, May 2013.

[96] E. M. Suuberg, I. Milosavljevic, and V. Oja, "Two-regime global kinetics of cellulose pyrolysis: The role of tar evaporation," *Symp. Int. Combust.*, vol. 26, no. 1, pp. 1515–1521, 1996.

[97] V. Biba, J. Macak, E. Klose, and J. Malecha, "Mathematical Model for the Gasification of Coal under Pressure," *Ind. Eng. Chem. Process Des. Dev.*, vol. 17, no. 1, pp. 92–98, Jan. 1978.

[98] R. B. Bates, C. Altantzis, and A. F. Ghoniem, "Bubbling fluidizd bed biomass gasification: Modeling of char gasification and attrition kinetics," presented at the 9th U.S. National Combustion Meeting, Cincinnati, Ohio, 2015.

[99] I. Narváez, A. Orío, M. P. Aznar, and J. Corella, "Biomass Gasification with Air in an Atmospheric Bubbling Fluidized Bed. Effect of Six Operational Variables on the Quality of the Produced Raw Gas," *Ind Eng Chem Res*, vol. 35, no. 7, pp. 2110–2120, 1996.

[100] C. Dupont, T. Nocquet, J. A. Da Costa Jr., and C. Verne-Tournon, "Kinetic modelling of steam gasification of various woody biomass chars: Influence of inorganic elements," *Bioresour. Technol.*, vol. 102, no. 20, pp. 9743–9748, Oct. 2011.

[101] A. Garg, J. Barton, R. Chen, W. Jablonski, D. L. Carpenter, and R. P. Field, "Assessment of Feedstocks and Operating Conditions on Gasification Products," National Renewable Energy Laboratory, Golden, CO, MIT David H. Koch School of Chemical Engineering Practice.

[102] Fluidised particles, J. F. Davidson and D. Harrison, Cambridge University Press, New York (1963). .

[103] J. Feng, X. Hou, X. Chen, Y. Jia, and W. Li, "Thermochemical Process Study on a Jet-Fluidized-Bed Gasifier Reaction System by an Equivalent Chemical Reactor Network," *Energy Fuels*, vol. 25, no. 9, pp. 4063–4069, Aug. 2011.

[104] M. Mancini, P. Schwöppe, R. Weber, and S. Orsino, "On mathematical modelling of flameless combustion," *Combust. Flame*, vol. 150, no. 1–2, pp. 54–59, Jul. 2007.

[105] D. Fiaschi and M. Michelini, "A two-phase one-dimensional biomass gasification kinetics model," *Biomass Bioenergy*, vol. 21, no. 2, pp. 121–132, Aug. 2001.

[106] R. El Asri, A. A. Konnov, and J. De Ruyck, "Reactor Network Modeling of a Biomass Dedicated Swirling Combustor and a Fluidized Bed Gasifier," in *Progress in Thermochemical Biomass Conversion*, Blackwell Science Ltd, 2001, pp. 599–613.

[107] E. D. Gordillo and A. Belghit, "A two phase model of high temperature steam-only gasification of biomass char in bubbling fluidized bed reactors using nuclear heat," *Int. J. Hydrog. Energy*, vol. 36, no. 1, pp. 374–381, Jan. 2011.

[108] R. Radmanesh, J. Chaouki, and C. Guy, "Biomass gasification in a bubbling fluidized bed reactor: Experiments and modeling," *AIChE J.*, vol. 52, no. 12, pp. 4258–4272, 2006.

[109] M. B. Nikoo and N. Mahinpey, "Simulation of biomass gasification in fluidized bed reactor using ASPEN PLUS," *Biomass Bioenergy*, vol. 32, no. 12, pp. 1245–1254, Dec. 2008.

[110] S. S. Sadaka, A. E. Ghaly, and M. A. Sabbah, "Two phase biomass air-steam gasification model for fluidized bed reactors: Part I—model development," *Biomass Bioenergy*, vol. 22, no. 6, pp. 439–462, Jun. 2002.

[111] D. Kunii and O. Levenspiel, *Fluidization engineering*, 2nd ed. Stoneham, MA: Butterworth-Heinemann, 1991.

[112] P. N. Rowe, "Particle-to-liquid mass transfer in fluidised beds," *Chem. Eng. Sci.*, vol. 30, no. 1, pp. 7–9, Jan. 1975.

Appendix I – Conservation Equations for isothermal CSTR and PFR

This section details the various conservation equations and the associated assumptions involved in the solution of species evolution inside the ideal continuously stirred reactors (CSTR) and plug flow reactors (PFR) used in the improved reactor network model. As described in Chapter 4, the emulsion phase in the bubbling fluidized bed is modeled using a CSTR and the bubble phase was assumed to be in a plug flow.

The following assumptions are involved in the solution of CSTR,

1. The reactor is assumed to be isothermal and isobaric.
2. The mass transfer occurring between the emulsion and bubble phases is calculated as,

$$M_j = k\ (\Delta C_j)$$

where M_j is the number of moles of species j transferred between the two phases, k is the mass transfer coefficient and ΔC_j is the concentration gradient of species j across the two phases.

The species conservation equation for each of the j species is written as,

Species conservation (N species and equations)

$$V_e \frac{dC_j}{dt} + \dot{V}_{out} C_j - \dot{V}_{in} C_{j,in} = r_j V_e + M_j\ (mol/s)$$

The continuity equation for the mass flow through the reactor is given by,

Continuity (1 equation)

$$V_e \frac{dC_{tot}}{dt} + \dot{V}_{out} C_{tot} - \dot{V}_{in} C_{tot} = \sum_{j=1}^{N} r_j V_e + \sum_{j=1}^{N} M_j$$

where N is the total number of chemical species in the system.

When the reactor is isothermal, isobaric, and constant volume,

$$\frac{dC_{tot}}{dt} = 0$$

Solving for the outlet volumetric flow rate, we obtain

$$\dot{V}_{out} = \frac{\sum_{j=1}^{N} (r_j V_e + M_j)}{C_{tot}} + \dot{V}_{in}$$

Substituting the expression for the outlet volumetric flow rate into the species conservation equation for species j,

$$V_e \frac{dC_j}{dt} + \frac{\sum_{j=1}^{N}(r_j V_e + M_j)}{C_{tot}} C_j + \dot{V}_{in} C_j - \dot{V}_{in} C_{j,in} = r_j V_e$$

$$V \frac{dC_j}{dt} = (\dot{V}_{in} C_{j,in} - \dot{V}_{in} C_j) - \frac{\sum_{j=1}^{N}(r_j V_e + M_j)}{C_{tot}} C_j + r_j V_e$$

$$V_e \frac{dC_j}{dt} = \dot{V}_{in} C_{j,in} - \dot{V}_{out} C_j + r_j V_e + M_j$$

The bubble phase is modeled as a plug flow type reactor, with the following assumptions:

1. The reactor is assumed to be isothermal, isobaric.
3. As in the case of CSTR, mass transfer is calculated as,

$$M_j = k\,(\Delta C_j)$$

The differential form of the species conservation equations are written as,

$$\frac{d}{dz}(C_j A_c u) = R_j A_c + \frac{dM_j}{dz} \left[\frac{mol}{m\,sec}\right]$$

where the last term denotes the differential amount of moles entering the PFR through mass transfer. It can be calculated as,

$$dM_j = k_{BE} A_c (C_j - C_{j,CSTR})\, dz$$

Substituting the expression for dM_j in the species conservation equations,

$$\frac{d}{dz}(C_j A_c u) = R_j A_c + k_{BE} A_c (C_j - C_{j,CSTR}) \left[\frac{mol}{m\,sec}\right]$$

$$C_j \left(A_c \frac{du}{dz} + u \frac{dA_c}{dz}\right) + A_c u \frac{dC_j}{dz} = R_j A_c + k_{BE} A_c (C_j - C_{j,CSTR})$$

The differential form of the continuity equation is written as,

$$\frac{d}{dz}(C_{tot} A_c u) = A_c \sum_j \left(R_j + k_{BE}(C_j - C_{j,CSTR})\right)$$

$$C_{tot} A_c \frac{du}{dz} + C_{tot} u \frac{dA_c}{dz} + A_c u \frac{dC_{tot}}{dz} = A_c \sum_j \left(R_j + k_{BE}(C_j - C_{j,CSTR})\right)$$

Since the reactor is assumed to be isothermal and isobaric,

$$\frac{dC_{tot}}{dz} = 0$$

Substituting this in the continuity equation,

$$C_{tot}\left(A_c\frac{du}{dz} + u\frac{dA_c}{dz}\right) = A_c\sum_j\left(R_j + k_{BE}\left(C_j - C_{j,CSTR}\right)\right)$$

Rearranging,

$$\left(A_c\frac{du}{dz} + u\frac{dA_c}{dz}\right) = \frac{A_c}{C_{tot}}\sum_j\left(R_j + k_{BE}\left(C_j - C_{j,CSTR}\right)\right)$$

Substituting this in the species conservation equation, we obtain

$$\frac{C_j}{C_{tot}}A_c\sum_j\left(R_j + k_{BE}A_c\left(C_j - C_{j,CSTR}\right)\right) + A_c u\frac{dC_j}{dz} = R_j A_c + k_{BE}\left(C_j - C_{j,CSTR}\right)$$

Using $dz = ud\tau$,

$$u\frac{dC_j}{dz} = \frac{dC_j}{d\tau}$$

$$\frac{C_j}{C_{tot}}A_c\sum_j\left(R_j + k_{BE}A_c\left(C_j - C_{j,CSTR}\right)\right) + A_c\frac{dC_j}{d\tau} = R_j A_c + k_{BE}\left(C_j - C_{j,CSTR}\right)$$

Rearranging,

$$\frac{dC_j}{d\tau} = R_j + k_{BE}\left(C_j - C_{j,CSTR}\right) - \frac{C_j}{C_{tot}}\sum_j\left(R_j + k_{BE}\left(C_j - C_{j,CSTR}\right)\right)$$

Solution procedure for solving the CSTR and PFR equations for the improved reactor network model:

- Step 1 – Solve the conservation equations for each reactor, assuming no interaction between the phases
- Step 2 – Calculate the mass transfer source term based on the species concentrations in the reactors from the previous iteration and solve the conservation equations again
- Continue (go to Step 2) until the convergence criteria is satisfied

Convergence criteria: User-defined

1. Select the major species of interest
2. Check Conv value for the CSTR concentrations of the species of interest
3. Continue until the largest value of Conv is within tolerance

$$Conv = \frac{Conc(j, e, i+1) - Conc(j, e, i)}{Conc(j, e, i)}$$

Convergence means we have achieved an accurate estimate for the mass transfer occurring inside the bed, and hence an accurate representation of the species evolution within each individual reactor.

A nomenclature of the different symbols employed in the analysis is given below,

Symbol	Explanation	Units
M_j	Moles of species j transferred between the two phases	moles
k_{BE}	Bubble mass transfer coefficient	1/s
C_j	Concentration of species j	moles/m^3
V_e	Volume of the emulsion phase	m^3
$\dot{V}_{out}$	Volumetric flow rate out of CSTR	m^3/s
$\dot{V}_{in}$	Volumetric flow rate into CSTR	m^3/s
r_j	Production rate of species j due to the reactions inside CSTR	moles/m^3/s
C_{tot}	Total concentration of the gas in CSTR	moles/m^3
N	Total Number of chemical species	
A_c	Cross-sectional area of the bubble phase	m^2
u	Flow velocity inside the bubble	m/s
$C_{j,CSTR}$	Concentration of species j in CSTR	moles/m^3
dM_j	Differential moles of species j transferred between the two phases	moles/s
R_j	Production rate of species j due to the reactions in the PFR	moles/m^3/s
$Conc(j,e,i)$	Steady state concentration of species j in the emulsion phase during iteration i	moles/m^3

Appendix II - Primary tar decomposition pathways

The primary tar decomposition pathways for the major volatile species produced in the biomass devolatilization process is considered in this section.

Levoglucosan, produced from the decomposition of cellulose, forms a major part of the primary pyrolysis gases, and its decomposition pathway is of particular interest in accurately predicting the major gas concentration. Levoglucosan is almost completely converted into the major light gases (CO, H_2, CO_2, H_2O and CH_4) through a set of intermediate species such as formaldehyde and the radical $\bullet CH_2CHO$ obtained from hydrogen abstraction of acetaldehyde.

Hemicellulose decomposition produces xylofuranose, which undergoes a similar decomposition pathway as levoglucosan to produce a mixture of the light gases through formaldehyde.

The major production pathway for tars in biomass gasification is from the decomposition of lignin. Phenol is a major product of lignin decomposition and it plays an important role in the subsequent evolution of the different tar species inside the gasifier. Lignin initially decomposes into synapoyl aldehyde ($C_{11}H_{12}O_4$), syringol ($C_8H_{10}O_3$) and pCoumaryl ($C_9H_{10}O_2$), all of which share a phenolic base structure, which subsequently break down into phenol and light gases. While synapoyl aldehyde produces a mixture of light gases on cracking, syringol decomposition results in phenol.

Phenol undergoes subsequent cracking reactions to produce light gases, depending on the operating temperature. Cyclopentadiene and its hydrogen abstracted radical play an important role in this process. While phenol decomposition accelerates at high temperatures, the PAH growth reactions through phenol and phenolic radical ($\bullet C_6H_5O$) become significant as well. While benzene is formed from phenol through a set of radical reactions involving the benzyl radical (C_6H_5), the benzyl radicals could also combine with unsaturated hydrocarbons such as acetylene and other aromatics such as naphthalene to produce larger PAH's. The PAH growth reactions are encouraged at the higher temperatures especially due to the faster kinetics of radical formation at these temperatures.

A schematic of levoglucosan decomposition and synapoyl aldehyde decomposition is depicted in the Figures 1 and 2.

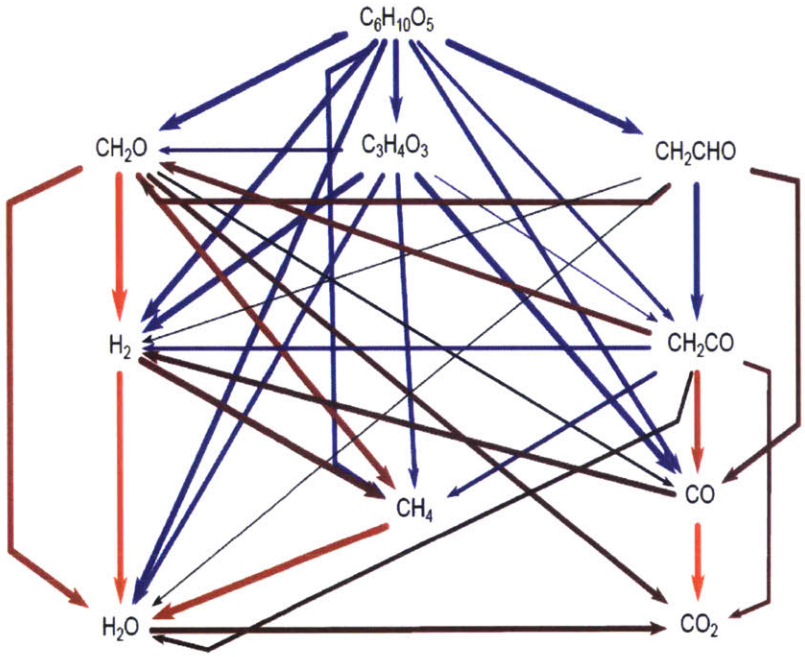

Figure 1: Levoglucosan decomposition reaction pathways produces CO, CO_2 and H_2O predominantly [3]

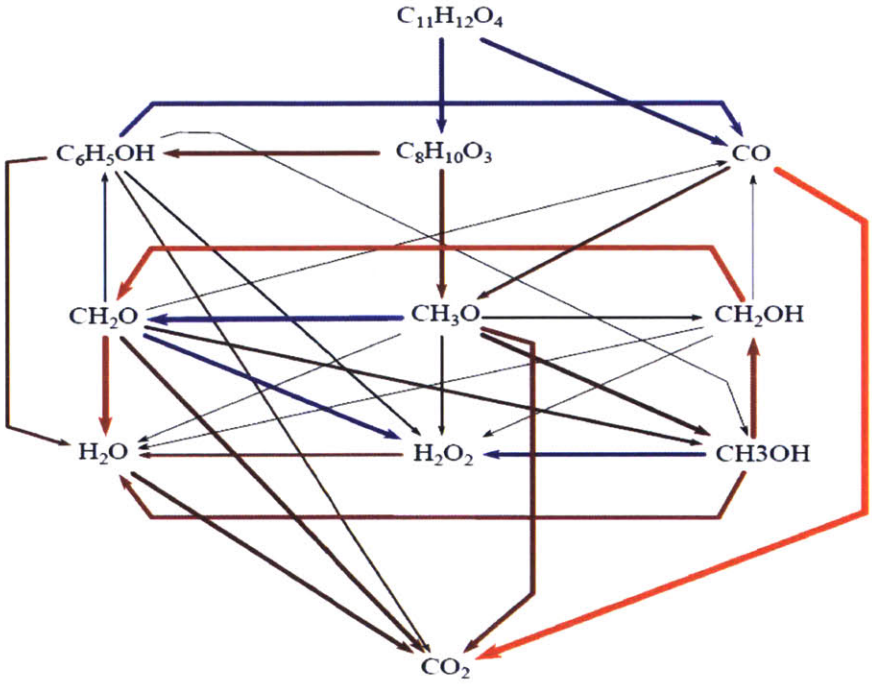

Figure 2: Synapoyl aldehyde decomposition reaction pathways produces CO, CO_2 and H_2O and also significant amounts of phenol [3]